

AD-A208 740

NAVAL POSTGRADUATE SCHOOL

Monterey, California



THESIS

Particle Sizing in Solid Rocket Motors

by

DOUGLAS LYLE HOVLAND

March 1989

Thesis Advisor

D. W. Netzer

Approved for public release; distribution is unlimited.

SDTIC
ELECTE
JUN 09 1989
H

89 6 09 022

Unclassified

SECURITY CLASSIFICATION OF THIS PAGE

REPORT DOCUMENTATION PAGE

1a REPORT SECURITY CLASSIFICATION Unclassified			1b RESTRICTIVE MARKINGS		
2a SECURITY CLASSIFICATION AUTHORITY			3 DISTRIBUTION/AVAILABILITY OF REPORT Approved for public release; distribution is unlimited.		
2b DECLASSIFICATION/DOWNGRADING SCHEDULE					
4. PERFORMING ORGANIZATION REPORT NUMBER(S)			5 MONITORING ORGANIZATION REPORT NUMBER(S)		
6a. NAME OF PERFORMING ORGANIZATION Naval Postgraduate School		6b OFFICE SYMBOL (If applicable) Code 67	7a. NAME OF MONITORING ORGANIZATION Naval Postgraduate School		
6c. ADDRESS (City, State, and ZIP Code) Monterey, California 93943-5000			7b. ADDRESS (City, State, and ZIP Code) Monterey, California 93943-5000		
8a. NAME OF FUNDING / SPONSORING ORGANIZATION Air Force Astronautics Laboratory		8b OFFICE SYMBOL (If applicable)	9 PROCUREMENT INSTRUMENT IDENTIFICATION NUMBER		
8c. ADDRESS (City, State, and ZIP Code) Edwards Air Force Base, California 93523-5000			10 SOURCE OF FUNDING NUMBERS		
PROGRAM ELEMENT NO.		PROJECT NO F04611- 88-X-0021		TASK NO	WORK UNIT ACCESSION NO.
11. TITLE (Include Security Classification) PARTICLE SIZING IN SOLID ROCKET MOTORS					
12. PERSONAL AUTHOR(S) Hovland, Douglas Lyle					
13a. TYPE OF REPORT Engineer's Thesis		13b TIME COVERED FROM TO		14. DATE OF REPORT (Year, Month, Day) 1989 March	
15 PAGE COUNT 110					
16. SUPPLEMENTARY NOTATION The views expressed in this thesis are those of the author and do not reflect the official policy or position of the Department of Defense or the U.S. Government.					
17. COSATI CODES			18 SUBJECT TERMS (Continue on reverse if necessary and identify by block number)		
FIELD	GROUP	SUB-GROUP	Particle sizing; solid propellant rocket motors; light scattering, <i>theses, (magn)</i>		
19. ABSTRACT (Continue on reverse if necessary and identify by block number)					
<p>Particle size distribution measurements were made with a Malvern 2600c forward laser light diffraction system across the exhaust nozzle entrance and exhaust plume of a small two-dimensional rocket motor. The solid propellants tested were GAP propellants containing 2.0% and 4.69% aluminum. Surface agglomeration of the aluminum, indicated by the in-motor results, was found to decrease as the motor chamber pressures were increased. At low pressures, increasing the aluminum loading with fixed total solids decreased the mean particle size at the nozzle entrance. Exhaust plume particle size was practically independent of nozzle inlet particle diameters, supporting the critical Weber number particle breakup theory. Initial validation of the Malvern 2600c measurements was accomplished by favorable comparison to exhaust plume particle distribution results obtained using a particle collection probe.</p>					
20. DISTRIBUTION/AVAILABILITY OF ABSTRACT <input checked="" type="checkbox"/> UNCLASSIFIED/UNLIMITED <input type="checkbox"/> SAME AS RPT <input type="checkbox"/> DTIC USERS			21 ABSTRACT SECURITY CLASSIFICATION Unclassified		
22a NAME OF RESPONSIBLE INDIVIDUAL D. W. Netzer			22b TELEPHONE (Include Area Code) 408-645 2980		22c OFFICE SYMBOL Code 67Nt

Approved for public release; distribution is unlimited.

Particle Sizing in Solid Rocket Motors

by

Douglas Lyle Hovland
Lieutenant Commander, United States Navy
B.S., United States Naval Academy, 1977

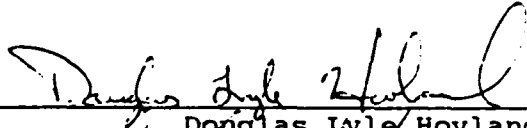
Submitted in partial fulfillment of the
requirements for the degree of

AERONAUTICAL ENGINEER

from the

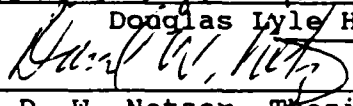
NAVAL POSTGRADUATE SCHOOL
March 1989

Author:

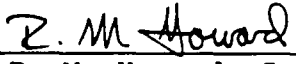


Douglas Lyle Hovland

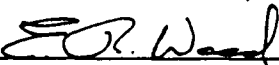
Approved By:




D. W. Netzer, Thesis Advisor



R. M. Howard, Second Reader



E. Roberts Wood, Chairman,
Department of Aeronautics and Astronautics



Gordon E. Schacher
Dean of Science and Engineering

ABSTRACT

Particle size distribution measurements were made with a Malvern 2600c forward laser light diffraction system across the exhaust nozzle entrance and exhaust plume of a small two-dimensional rocket motor. The solid propellants tested were GAP propellants containing 2.0% and 4.69% aluminum. Surface agglomeration of the aluminum, indicated by the in-motor results, was found to decrease as the motor chamber pressures were increased. At low pressures, increasing the aluminum loading with fixed total solids decreased the mean particle size at the nozzle entrance. Exhaust plume particle size was practically independent of nozzle inlet particle diameters, supporting the critical Weber number particle breakup theory. Initial validation of the Malvern 2600c measurements was accomplished by favorable comparison to exhaust plume particle distribution results obtained using a particle collection probe.



Accession For	
NTIS GRA&I	<input checked="checked" type="checkbox"/>
DTIC TAB	<input type="checkbox"/>
Unannounced	<input type="checkbox"/>
Justification	
By	
Distribution/	
Availability Codes	
Dist	Avail and/or Special
A-1	

TABLE OF CONTENTS

I.	INTRODUCTION	1
II.	THEORETICAL BACKGROUND	5
	A. ALUMINIZED PROPELLANT COMBUSTION PROCESS	5
	B. PARTICLE SIZE PERFORMANCE EFFECTS	12
	C. LIGHT DIFFRACTION THEORY	12
	D. PARTICLE SIZE PARAMETERS	14
III.	EXPERIMENTAL APPARATUS	17
	A. ROCKET MOTOR	17
	B. LASER LIGHT DIFFRACTION PARTICLE SIZER	26
	C. DATA ACQUISITION AND CONTROL	33
	D. EXHAUST PARTICLE COLLECTION PROBE	36
IV.	RESULTS AND DISCUSSION	40
	A. INTRODUCTION	40
	B. SYSTEM CALIBRATION	45
	C. EXHAUST NOZZLE ENTRANCE RESULTS	48
	1. Test Conditions	48
	2. DD1 Results	51
	3. DD5 Results	59
	4. DD1 and DD5 Comparative Results	61
	D. MALVERN EXHAUST PLUME RESULTS	67
	1. Test Conditions	67
	2. DD1 Results	69

3.	DD5 Results	77
4.	DD1 and DD5 Comparative Results	78
E.	AFAL PROBE DATA	78
V.	CONCLUSIONS AND RECOMMENDATIONS	90
	APPENDIX A - HP BASIC 5.1 DATA ACQUISITION	
	CONTROLLING CODE	94
	APPENDIX B - 2-D ROCKET MOTOR FIRING CHECKLIST	96
	APPENDIX C - 2-D MOTOR FIRING SUMMARY	98
	APPENDIX D - CALIBRATION RETICLE FINAL DATA SHEET	100
	LIST OF REFERENCES	101
	INITIAL DISTRIBUTION LIST	103

ACKNOWLEDGMENT

I wish to express my sincere thanks to my thesis advisor, Professor David Netzer, for making the experience of conducting experimental research positive, worthwhile, and fun. Additionally, I would like to thank the Combustion Lab Technician, Harry Conner, for sharing his technical assistance, as well as his wonderful sense of humor. Finally, I express my deep gratitude to my wife, Mary, for her unfailing patience and support.

I. INTRODUCTION

The use of solid propellant rocket motors is widespread in military missile and space vehicle propulsion. Examples of military applications include the Minuteman and Poseidon strategic missiles, and a long list of tactical missiles. Solid propellant rockets are also used on the NASA Space Shuttle Solid Rocket Boosters (SRBs). Recent history has highlighted the safety aspects of these SRBs. Each of the shuttle's two SRBs contain a large Solid Rocket Motor (SRM) and eight small Booster Separation Motors (BSMs). The SRM uses PBAN-AP (Polybutadiene-acrylonitrile-acrylic acid-ammonium perchlorate) composite propellant with 16% powdered aluminum [Ref. 1]. The clusters of BSMs, which serve to separate the expended SRB from the Shuttle, use HTPB-AP (Hydroxy-terminated polybutadiene-ammonium perchlorate) composite propellant with 2.0% powdered aluminum [Ref. 1]. Both the aluminum loading and cross-sectional geometry of a BSM are similar to the two-dimensional solid propellant rocket used for this thesis study.

Solid propellants with metal fuel additives such as aluminum are of interest due to the high specific impulses and propellant densities that can be achieved. Aluminized propellants have the additional beneficial effect of

suppressing transverse modes of combustion oscillations. This can be attributed to the damping provided by the aluminum agglomerates in the combustion chamber. However, the effects of having large agglomerates in a rocket motor are not all positive. This is particularly true if the agglomerates remain as relatively large condensed particles in the nozzle exhaust expansion area. Large thrust losses will result from the velocity and thermal lags between the condensed particles and the expanding gas. Additional losses occur due to the fact that, unlike a gas, the condensed particles do not expand in the nozzle expansion area. These losses, called two-phase flow losses, are often the largest factor in the determination of the nozzle loss coefficient. Besides causing performance losses in the nozzle, the condensed Al_2O_3 particles will cause a primary exhaust plume. This has significance when missiles are designed for tactical purposes and plume signature is a critical issue. [Ref. 2]

Clearly the particle size distribution in a rocket nozzle and exhaust plume have great impact on the performance of the rocket and its visible exhaust signature. Presently, rocket performance predictive codes such as the Air Force Astronautics Laboratory SPP (Solid Propellant Performance Prediction Code) require particle size parameters, such as D_{50} or a particle size distribution at the nozzle entrance, for input. As of yet, there are no firmly established and

reliable means to obtain the required particle size distribution data. Values used are typically semi-empirical, based on collection of exhaust particles [Ref. 3]. Recent work at the Naval Postgraduate School has demonstrated promising potential in using forward laser light diffraction, holography, and high speed motion pictures as means to obtain particle size information inside the motor and exhaust nozzle.

The primary goal of the research work presented in this paper was to gain a better understanding of the behavior of combustion particulates in rocket motors. A two-dimensional solid rocket motor developed by Walker [Ref. 4] and Pruitt [Ref. 5] was used with propellants containing 2.0% and 4.69% aluminum. Particle size measurements were made in the converging section of the exhaust nozzle and just outside the exhaust nozzle exit. Data were collected at both locations using a Malvern 2600c laser diffraction particle sizer. Combustion chamber pressures were varied over a range from 100 to 600 psia in order to determine pressure effects on agglomerate formation and break-up for the two propellants. Additionally, particles from the exhaust were collected using a supersonic shock swallowing collection probe developed by the Air Force Astronautics Laboratory (AFAL) in order to verify the Malvern exhaust measurements [Ref. 6].

It should be noted, due to the small size of the 2-D motor, that direct application of the specific test results

to larger production motors would not be appropriate. However, the use of a small scale motor provided an economical means to examine the process of aluminized propellant combustion as well as particle sizing techniques that have potential direct application to large motors. The employment of a 2-D motor provided greater probability of obtaining successful laser scattering data than that of a 3-D motor. A 2-D motor allows for easier motor windowing and shorter optical paths than does a 3-D motor. Short optical paths serve to reduce obscuration problems and increase the detectable scattering angles for a given size window. Proper window designs allow data to be successfully collected at high motor operating pressures.

Besides the primary research goal described above, a secondary objective was validation of exhaust measurements by comparing Malvern exhaust plume data to the AFAL collection probe data. A favorable comparison of the exhaust plume data would also provide a preliminary increased confidence level in the in-motor data collected. Eventually the in-motor data will be compared against data collected under similar conditions from the other particle sizing techniques which are being used at the Naval Postgraduate School. Tertiary goals included determination of optimal usage of the Malvern 2600c Particle Sizer, assembly and employment of the AFAL collection probe, and determination of the advantages and disadvantages of using a two-dimensional motor for testing.

II. THEORETICAL BACKGROUND

A. ALUMINIZED PROPELLANT COMBUSTION PROCESS

The combustion process for aluminized propellants in the rocket motor environment is very complex. There are many factors that are believed to effect the degree to which aluminum will agglomerate within the combustion chamber and the degree to which the agglomerates will breakup in the exhaust nozzle. The size of the agglomerates leaving the surface of the propellant will affect the acoustic damping present in the combustion chamber. Within the nozzle, the initial size of the agglomerates and the amount of agglomerate breakup will impact on the amount of two-phase flow losses in the nozzle and the overall combustion efficiency. Prior research conducted by Gany and Caveny at Princeton University [Ref. 7] puts forth a model to account for the agglomeration and breakup process of particles in aluminized propellant rocket motors.

Before reviewing the Gany and Caveny model, a description of the physical properties of aluminum (Al) and aluminum oxide (Al_2O_3) is provided in Table II.1. It is important to note that the boiling point of aluminum oxide is higher than that of aluminum. This characteristic causes a gaseous diffusion

flame to form around burning particles. Also of importance is that the value of the estimated chamber temperature is often between the boiling points of pure aluminum and its oxide.

TABLE II.1. PHYSICAL PROPERTIES OF ALUMINUM.

Material	Melting Point, °K	Boiling Point, °K
Aluminum	933 [Ref. 8]	2750 [Ref. 8]
Aluminum Oxide	2320 [Ref. 8]	3253 [Ref. 8]

In the combustion model described by Gany and Caveny, a thin mobile layer on the surface of the burning propellant, called the reaction layer, is assumed. In this reaction layer, initial heating of the aluminum particles takes place. As the particle temperature approaches 700 °K, an adhesion process begins between aluminum particles in close proximity to one another. When the propellant temperature increases to 933 °K, the melting temperature of aluminum, the adhesion process of adjacent particles is enhanced by molten flows of aluminum emerging from cracks in the solid oxide shells surrounding the individual aluminum particles. The emerging molten aluminum acts as a bridge between adjacent aluminum particles. As the melting point of aluminum oxide is approached, the bridged particles are merged together to form large spheroid shaped agglomerates. However, it is also

possible that those individual particles exposed to intense heat will ignite prior to forming agglomerates. [Ref. 7]

Price [Ref. 8] presents a flow chart that summarizes the possible sequence of events for an aluminum particle during the combustion process. Aluminum particles can either emerge on the propellant burning surface as single particles or accumulated particles. These particles can then either leave the propellant surface unignited and eventually ignite in the gas flow or they can ignite on the propellant surface without detaching. The ignited particles remaining on the surface can continue to burn on the surface or can eventually detach into the flow. Those accumulates that remain on the surface may possibly agglomerate further before detaching. When the particles finally leave the surface, the small agglomerates and single particles will burnout quickly while the large agglomerates will burnout later and leave large residual oxides in the flow. A depiction and physical characteristics of an aluminum droplet after it has broken away from the propellant surface are shown in Figure II.1. The droplet temperature is approximately 2500 °K, which is just below the pure aluminum boiling temperature and just above the melting point of aluminum oxide. If the droplet temperature were to drop below 2320 °K, the aluminum oxide melting point, surface oxide would envelop the aluminum droplet and cause flame collapse. On the other hand, temperatures above the aluminum

boiling point would cause the droplet to be disrupted.

[Ref. 8]

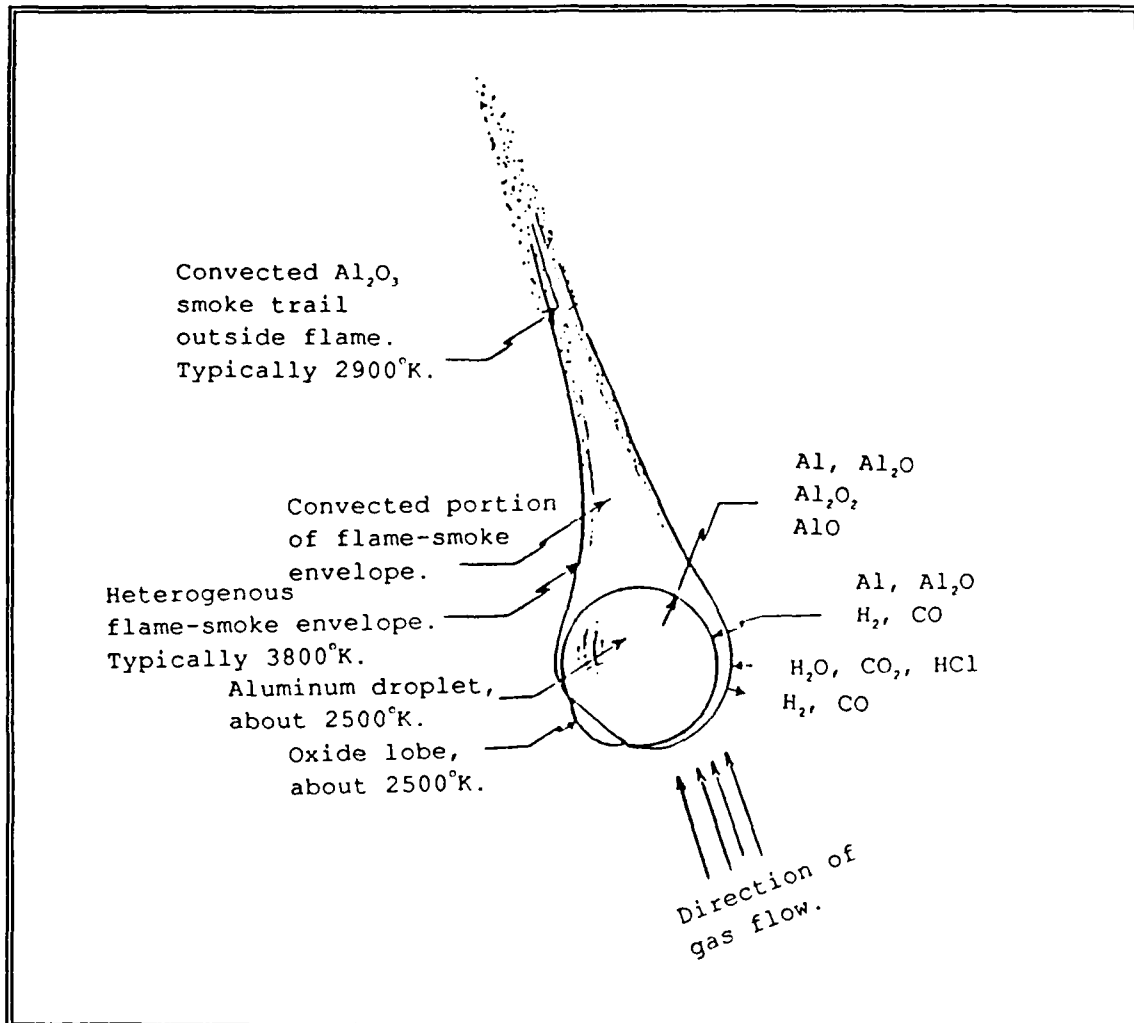


Figure II.1. Aluminum Droplet Burning in Mild Convective Flow [Ref. 9].

As stated earlier, the size of the agglomerates is a function of many factors. Gany and Caveny [Ref. 7] describe in detail the effect that the aluminum particle size within the propellant matrix has on agglomeration. Four particle size zones are outlined. Zone one includes very small

particles having diameters much less than the thickness of the reaction layer, typically less than one micron. Sub-micron aluminum particles, however, are not typically used in propellants. Zone two is the next larger size range with an upper bound on diameter equal to that of the reaction layer thickness. Agglomeration and ignition on the propellant surface are expected to be prominent for particles in this size band. Zone three is made up of particles with diameters just slightly larger than the thickness of the reaction layer. This size band of ten to 25 microns is typical of the aluminum particles that are used in propellants. In this zone the ignition time for individual particles rapidly becomes less than the minimum accumulation time required to guarantee agglomeration. Therefore, the particles tend to ignite individually on the surface of the propellant before agglomeration can occur. Zone four contains the large particles that are not considered small enough to be classified as being zone three. These large particles have diameters much larger than the reaction layer and thereby have very little chance of forming agglomerates. Additionally, in a strong crossflow environment, large particles may be swept from the propellant surface prior to ignition. [Ref. 7]

Oxidizer particle size will also affect the degree of aluminum agglomeration. Typically, ammonium perchlorate (AP) is used as the primary oxidizer in propellants due to its low

cost and its high availability. Often, propellants are mixed with multimodal size distributions of ammonium perchlorate particles. It has been found that by reducing the size of the ammonium perchlorate particles that the burning rate of the propellant will be increased and the agglomeration of aluminum will be reduced. A reduction in agglomeration can be expected due to the geometry of the closely packed AP particles. Tighter AP interstitial spacing reduces the size of "pockets" in which aluminum particles tend to be concentrated in the propellant matrix. [Ref. 10]

As described above, conditions that enhance surface ignition of the aluminum particles and accumulates will serve to reduce the average size of particulates leaving the propellant surface. Additional factors that will be favorable to ignition are higher chamber pressures and greater amounts of oxidizer content in the propellant. [Ref. 8]

Equally as important as understanding the process of the formation of agglomerates, is the understanding of their breakup process. Two-phase flow velocity lags of sufficient magnitude will cause the breakup of larger agglomerates in the exhaust nozzle. Gany and Caveny [Ref. 11] found the Weber Number to be a good correlation parameter for predicting breakup conditions. The Weber Number is defined as the ratio of inertial forces to surface tension forces:

$$We = d_{ag} \rho_g (u_g - u_{ag})^2 / \sigma$$

where d_{ag} = diameter of agglomerate (m)
 ρ_g = density of gas (kg/m^3)
 u_g = velocity of gas (m/s)
 u_{ag} = velocity of agglomerate (m/s)
 σ = surface tension (N/m)

Critical values of the Weber number were found to be between 20 and 30. This equates to larger particles breaking up near the entrance of the converging section of the exhaust nozzle at low Mach numbers and smaller particles breaking up further downstream, nearer the throat of the exhaust nozzle, at high Mach numbers. It is also possible that those particles that are sufficiently small in size will not breakup at all in the nozzle. [Ref. 11]

The breakup time of a particle which has exceeded the critical Weber Number is of importance as well. Particle breakup outside of the nozzle will not impact on combustion efficiency or two-phase flow losses. The breakup time of a droplet suddenly exposed to a gas stream can be approximated as:

$$t_b \approx d_{ag}(\rho_{ag}/\rho_g) / 2(u_a - u_{ag}) \quad [\text{Ref. 11}]$$

The nozzle size must be large enough (or the rate of change of Mach number slow enough) to allow particle residence times to exceed the time required for breakup in order for in-nozzle breakup to occur.

B. PARTICLE SIZE PERFORMANCE EFFECTS

Acoustic damping of pressure oscillations will be a direct function of the particle size distribution in the propellant chamber. For this reason, propellant composition is very important to the rocket motor design. Consideration of the factors affecting agglomeration which were described in the previous section must be given in order to realize maximum damping effects at the desired frequencies. For example, optimal damping provided for motor pressure oscillations at 2000 Hz would require the mean diameter of the chamber particles to be approximately six microns, while a mean diameter of approximately four microns would be required for optimal damping of 4000 Hz oscillations [Ref. 1]. Clearly, knowledge of the degree of expected agglomeration is required in order to make sound design decisions in terms of matching combustion chamber design to the propellant utilized.

Predictions of two-phase flow losses and combustion efficiency are even more complex. Knowledge of the particle size distribution at the exhaust nozzle entrance is not sufficient. In addition, the particle breakup location within the nozzle and the degree of breakup must be known.

C. LIGHT DIFFRACTION THEORY

Forward laser light scattering provides a viable means for obtaining particle size distribution information throughout

the solid rocket motor flow field. Its principal advantage is that it is an insitu, non-intrusive method for particle sizing.

Light scattering from particles larger than approximately one micron is a complex process which can be broken down into reflection, refraction, and diffraction. Light scattering theory greatly simplifies to Fraunhofer diffraction theory when the illuminated particles have diameters larger than the wavelength of the incident laser light and only small forward scattering angles are considered. In the case of a He-Ne laser ($\lambda = 0.6328$ microns), it has been demonstrated that Fraunhofer diffraction theory remains valid for measurement of particles as small as one micron [Ref. 12].

Fraunhofer diffraction can be described by considering an incident beam of constant wavelength, λ , on a sample volume of spherical particles of various radii, a . In the near forward, small-angle region, the light intensity, I , is a function of the scattering angle, θ , and can be expressed as:

$$I(\theta) = (I_0/k^3\theta^2) \int_0^\infty J_1^2(\alpha\theta)\alpha^2n(\alpha) d\alpha$$

where I_0 = intensity incident on the particles

α = $2\pi a/\lambda$ = size parameter

k = $2\pi/\lambda$ = wave number

J_1 = Bessel function of the first kind of order one

$n(\alpha)$ = size distribution function

θ = scattering angle measured from the incident beam propagation direction

This equation makes the small angle approximations of $\sin(\theta) \approx \theta$ and $(1 + \cos^2(\theta))/2 \approx 1$. The equation also assumes the effects of the refractive index, multiple scattering and vignetting to be insignificant. [Ref. 13]

The underlying principal of particle sizing using laser diffraction is to detect the diffraction signature, $I(\theta)$, and invert the Fraunhofer equation in order to determine the particle size distribution, $n(\alpha)$ [Ref. 13]. With the particle size distribution known, size parameters such as D_{43} and D_{32} can then be calculated.

D. PARTICLE SIZE PARAMETERS

Most of the previous rocket motor particle size data collected has been reported in terms of size parameters, namely D_{32} and D_{43} . This is due to the fact that earlier employed optical diagnostics led to direct determination of D_{32} , without providing the information necessary to calculate the particle size distribution. Additionally, a particle size parameter provides a compact descriptive means to compare data, whereas comparison of distribution data is more cumbersome.

The Sauter Mean Diameter, D_{32} , describes the mean volume of material in a sample which has a given mean surface area

[Ref. 14]. D_{32} can be calculated from either a discrete number or volume distribution as follows:

$$D_{32} = \frac{\sum (N(x_i)x_i^3)}{\sum (N(x_i)x_i^2)}$$

$$= \frac{\sum V(x_i)}{\sum (V(x_i)/x_i)}$$

D_{43} is defined in a similar manner:

$$D_{43} = \frac{\sum (N(x_i)x_i^4)}{\sum (N(x_i)x_i^3)}$$

$$= \frac{\sum (V(x_i)x_i)}{\sum V(x_i)}$$

where x_i = particle size in band i

$N(x_i)$ = particle number distribution

$V(x_i)$ = particle volume distribution

Both D_{32} and D_{43} will bias particle size towards the larger particles, which are of particular interest to the rocket motor combustion process. The following simple example demonstrates this biasing:

<u># OF PARTICLES</u>	<u>PARTICLE DIAMETER</u>
10	25 microns
10	50 microns
10	75 microns

MEAN DIAMETER = 50 microns

$$D_{43} = \sum (N(x_i)x_i^4) / \sum (N(x_i)x_i^3)$$

$$= 68.1 \text{ microns}$$

$$D_{32} = \sum (N(x_i)x_i^3) / \sum (N(x_i)x_i^2)$$

$$= 64.3 \text{ microns}$$

III. EXPERIMENTAL APPARATUS

A. ROCKET MOTOR

A two-dimensional solid rocket motor designed by Walker [Ref. 4] and Pruitt [Ref. 5] was used for all of the test firings. Figure III.1. is a photograph of the assembled motor and Figure III.2. shows the motor disassembled into its two main sections. The principal advantage of using this two-dimensional motor for light scattering measurements of particle size was that the optical path of the sampled flow was only 0.25 inches. This minimized the number of particles in the laser's optical path, thereby reducing obscuration and multiple scattering effects. The short optical path in conjunction with the forward tapered window insert diameter of 0.35 inches caused the detectable scattering angle to be limited only by the radius of the Malvern diode array and not the motor windowing. This allowed particles as small as 0.5 microns to be detected by the Malvern. As mentioned in the last chapter, Fraunhofer diffraction theory begins to break down in the sub-micron size range.

Secondary advantages of the two-dimensional motor were that the propellant was easy to cut, easy to load, and the motor was relatively easy to clean. Chamber pressures were

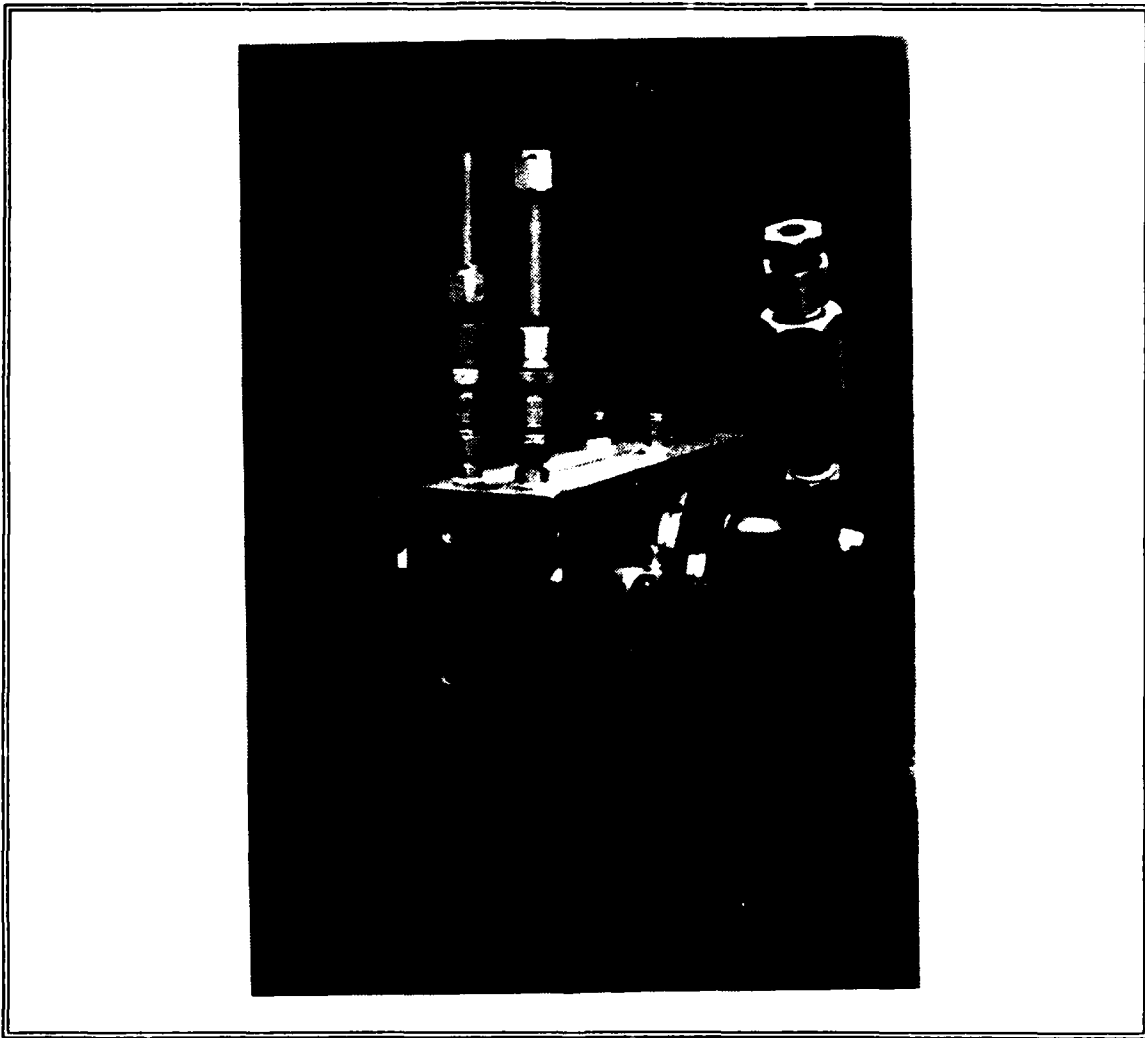


Figure III.1. NPS Two-Dimensional Solid Propellant Rocket Motor.

varied from run to run by simply changing the length of the propellant slabs that were loaded.

Figure III.3. shows the forward window assemblies. The bottom component on the left side of Figure III.3. is a tapered window insert which was a modification designed to reduce the mass flow rate of nitrogen required to keep the windows clean at high motor operating pressures. The center

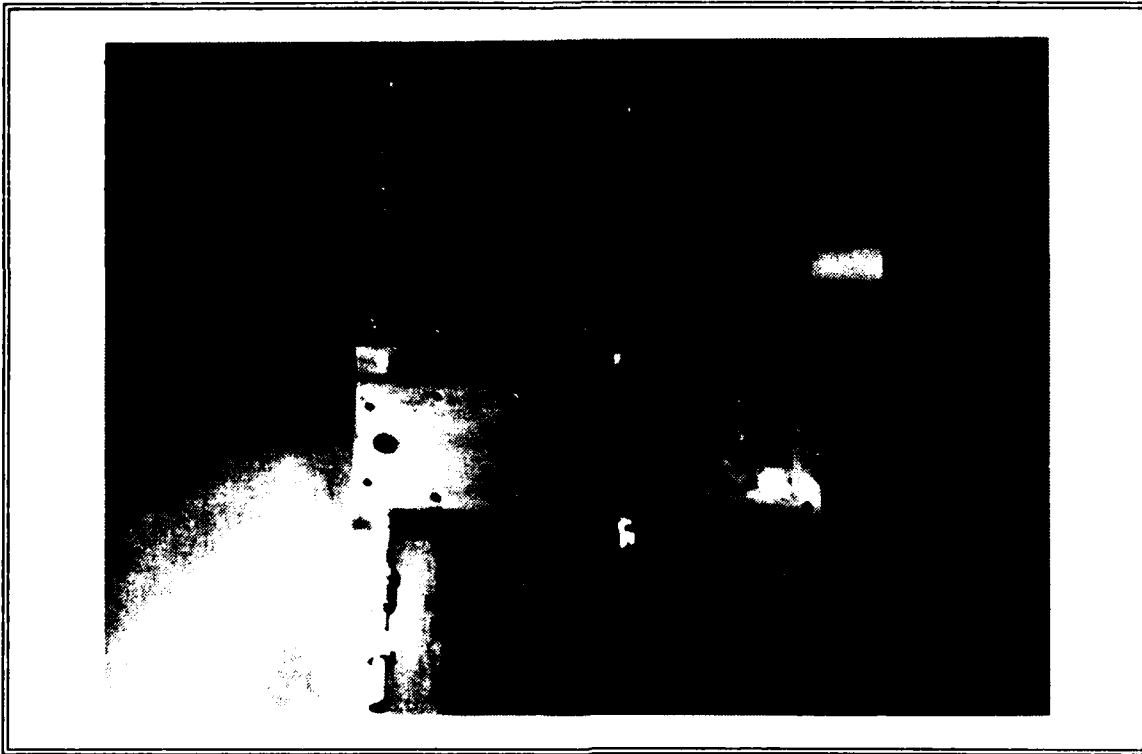


Figure III.2. Disassembled NPS Two-Dimensional Solid Propellant Rocket Motor.

component is a sintered bronze cylinder designed to diffuse the incoming nitrogen purge gas in order to provide a more even flow of purge gas around the window surface. The top component holds a one inch diameter and 0.25 inch thick fused silica window. The window is pressed and sealed in place by an O-ring contained in an outer cover plate.

Nitrogen purge gas was supplied to the window assemblies from one of three 2200 psig certified tanks via a pressure dome loader, solenoid valve, a flexible hose, and a 0.031 inch diameter sonic choke. The nitrogen pressure set by the dome loader was as a rule set to be twice the expected combustion chamber pressure plus 200 psig. The solenoid valve was

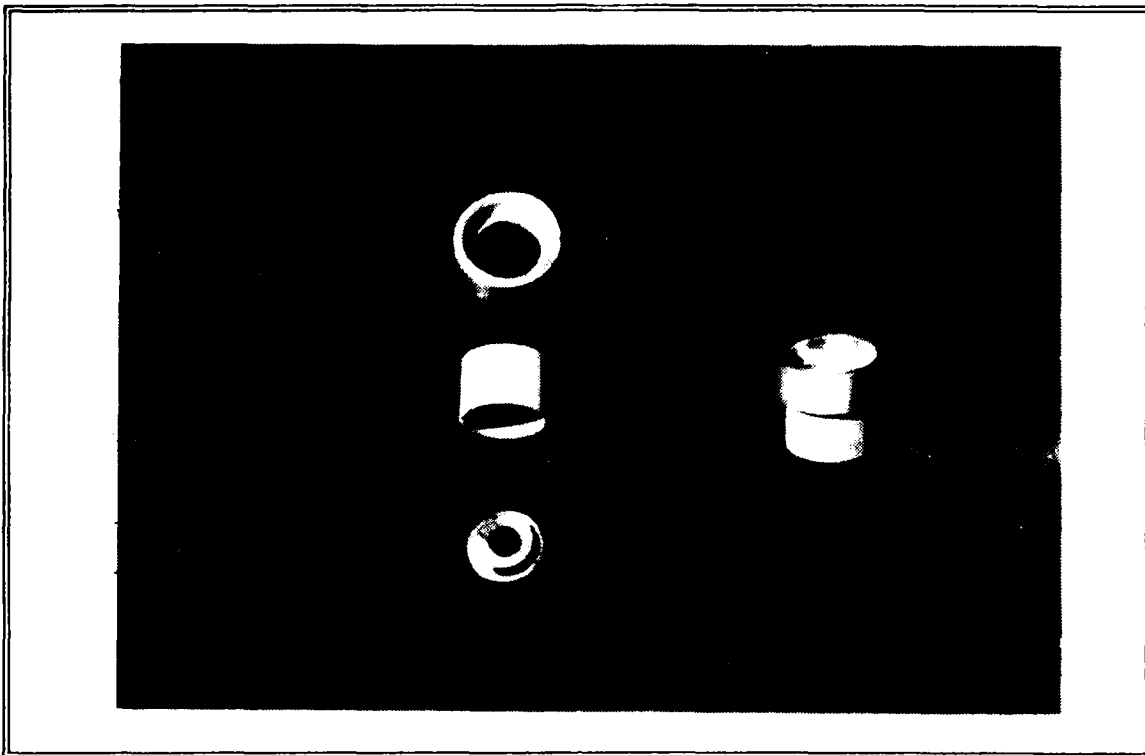


Figure III.3. Forward Window Assembly.

capable of being controlled either locally or remotely from the fire control room. Remote control was used in order to allow the nitrogen to be turned on just prior to rocket firing. One 0.031 inch sonic choke was placed in a line going to each window. Choked flow was guaranteed over the range of nitrogen pressures that would be required to be set in order to keep the windows clean. Mass flow rates were computed using the choked flow formula:

$$m = P_t A_{th} (\gamma g_c (2/\gamma + 1))^{((\gamma + 1)/(\gamma - 1))^{0.5}} / (T_t R)^{0.5}$$

where P_t = nitrogen pressure (psia)

A_{th} = sonic choke area (in²)

γ = 1.4

$$g_c = 32.174 \text{ lbf-ft/lbf-sec}^2$$

$$T = \text{nitrogen total temperature (500}^\circ \text{ R)}$$

$$R = 55 \text{ ft-lbf/lbm-}^\circ \text{R}$$

Typical values set in the nitrogen dome loader ranged from 1200 to 2200 psig. These pressures yielded a nitrogen purge mass flow rate range of 0.021 to 0.039 lbf/sec.

Figure III.4. is a sketch of the exhaust nozzle. The area ratios in the converging section were designed to be the same as a 30° conical, converging axisymmetric nozzle [Ref. 5]. Labeled stations 1, 2, and 3 are located across the 0.35 inch diameter forward window insert. This was the location where all in-motor data were taken. Station 4 is the nozzle throat, which had an area of 0.0336 square inches. The angle from the throat to the exhaust nozzle exit, labeled station 5, was 7°. Based on the area ratios and a PEPCODE estimated γ of 1.2, the isentropic calculations for the Mach number at each labeled station are presented in Figure III.4.

The dimensions of the motor chamber were approximately 10.5 inches by 2.3 inches by 0.25 inches. Two propellant slabs of 0.25 inch thickness and of a width of 0.75 inches were loaded in the end of the chamber nearest the ignitor. The propellant slab lengths were varied from 3.0 inches to 8.25 inches. This varied the burning area, which in turn varied the chamber pressure. The propellant slabs were bonded into the motor using 732-RTV self-vulcanizing silicone rubber.

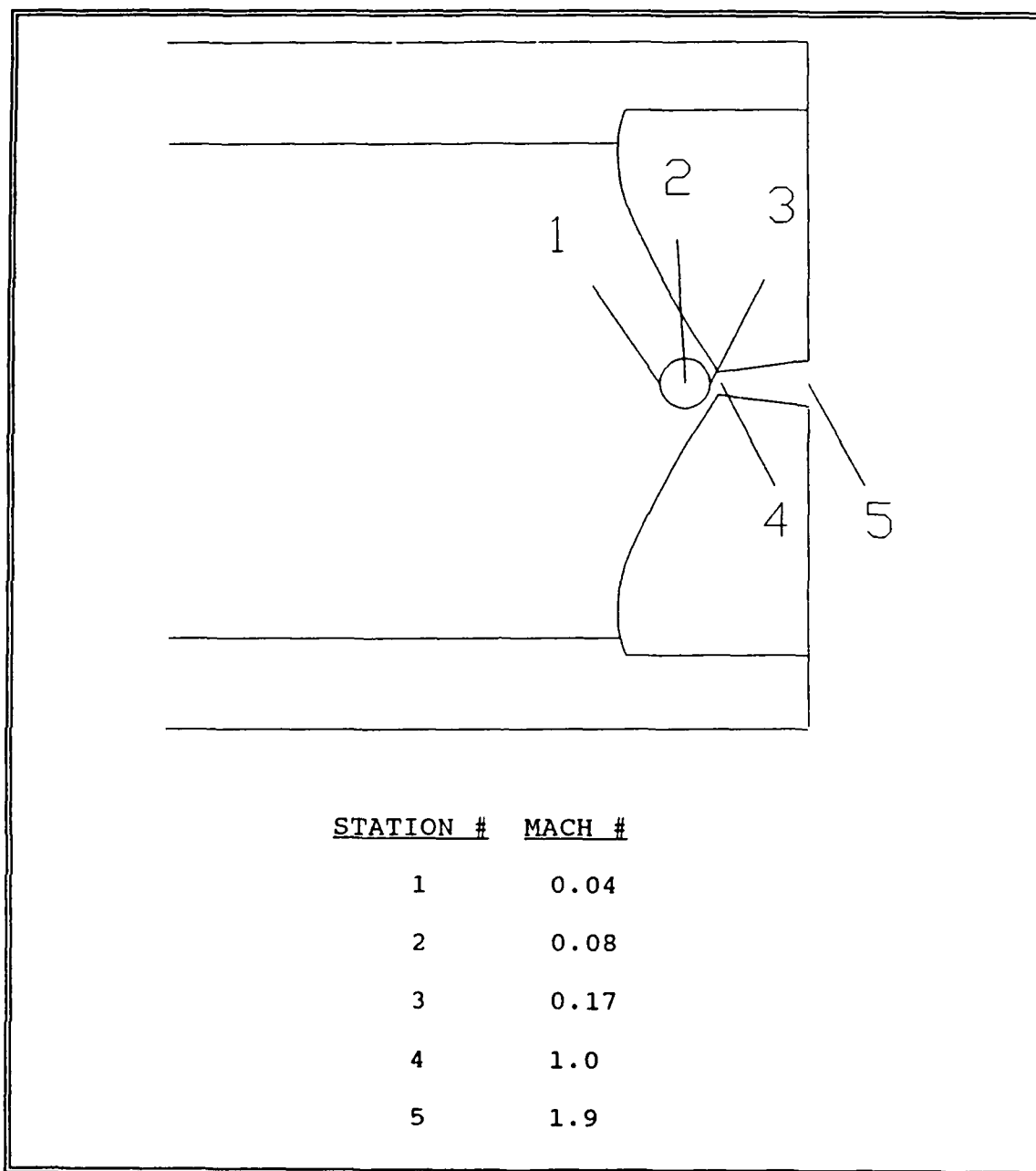


Figure III.4. Two-Dimensional Rocket Exhaust Nozzle.

The 732-RTV also served as a burning inhibitor. Initial runs were conducted by exposing only the lengthwise sides of each propellant slab in hopes of realizing neutral burns. This worked only at the lower pressures. Progressive burns were

observed at higher pressures. Additionally, it was thought that RTV from the ends of the propellant slabs was contaminating the exhaust flow, since there was no chamber surface on which the RTV could adhere. Therefore, it was decided that test runs would be conducted with RTV only on the propellant surfaces that were in direct contact with the walls of the combustion chamber. This meant the initial burning surface for each slab could be calculated by adding the length of the slab to the width and multiplying by the slab thickness.

Two GAP-AP propellants with aluminum fuel additives, designated DD1 and DD5, were tested. DD1 contained 2.0% mass loading of aluminum and DD5 had a content of 4.69% aluminum. Table III.1. lists all the ingredients of the two propellants. Note that the increased DD5 aluminum loading was at the expense of the ammonium perchlorate (AP) content. More specifically, the loading of 200 micron AP particles was reduced by 1.75% and the 25 micron AP particle composition was decreased by 0.94%.

Ignition of the propellant was accomplished by remotely switching a 12 volt DC source to an ignition plug located in the back of the rocket motor. The ignition plug consisted of a 0.2 inch diameter cavity filled with BKNO_3 . Nestled within the BKNO_3 was a nichrome filament which, when heated by application of the 12 volt DC source, caused the BKNO_3 to

TABLE III.1. DD1 AND DD5 PROPELLANT INGREDIENTS.

INGREDIENT	DD1	DD5
GAP (200-1)	14.67 %	14.67 %
TEGON (AK-17E)	8.49	8.49
ALUMINUM (C003)	2.00	4.69
TEPANOL (HX-878)	0.15	0.15
AP (200 micron)	47.45	45.70
AP (25 micron)	25.55	24.61
N-100 (MOBAY)	0.845	0.845
HDI	0.845	0.845

ignite. The hot gases and particles from the ignitor were directed to the surface of the propellant by a splitter plate (beveled post) located just downstream of the ignitor port. It was found that the splitter plate was not required for ignition of the DD1 and DD5 propellants. However, the enhancement the splitter plate provided to the ignition process was required for a reduced smoke, zirconium carbide propellant.

Safety was built into the NPS two-dimensional motor in the form of an elbow joint burst disk assembly. The burst disks used were rated at 1000 psi. This provided insurance against possible window "blow out" due to unexpected high combustion chamber pressures. Inadvertent high pressures could be caused

by exhaust nozzle blockage or excessive propellant surface area exposure. Excessive surface area exposure could occur due to cracks in the propellant grain or failure of the 732 RTV inhibitor. The initial burst disk assembly was not an elbow joint. After recurring burst disk ruptures at pressures believed to be below 1000 psi, it was conjectured that premature ruptures were being caused by impinging hot aluminum particles on the surface of the burst disk. Therefore, the elbow modification was made to reduce the probability of hot aluminum particles reaching the surface of the burst disk.

A single pressure port was located in the combustion chamber. The pressure port was connected to a Teledyne 0 - 1000 psi pressure transducer. The voltage signal from the pressure transducer was amplified by a Pacific amplifier with the gain set at 100. The amplified signal was directed to a voltmeter in a HP 3054A Data System and to a DASH-16 Metrabyte Data Acquisition Board in an IBM-AT microcomputer. The pressure signal to the HP 3054A was used as an input to the controlling program which was written in HP Basic 5.1, and was run on a HP 9836S microcomputer. The voltage signal to the DASH-16 Metrabyte Board was processed by a commercial IBM compatible software program, LabTech Notebook Version 2.8.

B. LASER LIGHT DIFFRACTION PARTICLE SIZER

The particle sizer used was a commercially produced system by Malvern Instruments. The particular system used was the Malvern 2600c, which is depicted in Figure III.5. A metal casing was built around the system in order to protect the Malvern against possible rocket explosion damage, as well as to provide a means to shield the detector from combustion light. Figure III.6. is a photograph of the encased Malvern 2600c placed in position to make measurements within the NPS two-dimensional rocket motor.

The transmitter unit of the Malvern 2600c contains a 2 mwatt He-Ne laser. The beam is passed through a beam expander to provide a 9 mm diameter collimated analyzer beam. Before reaching the detector, the analyzer beam passes through a Fourier transform range lens. There were three range lenses provided with the system having focal lengths of 63, 100, and 300 mm. Table III.2. shows the detectable particle size classes of each range lens. However, each range lens has a sub-class which extends down to 0.5 microns. The advantage of using a Fourier transform lens to focus the laser light on the detector diode array is that the scattering angle detected will be independent of particle position and velocity in the sample field. Only the particle size will determine the scattering angle. This is depicted in Figure III.7., where

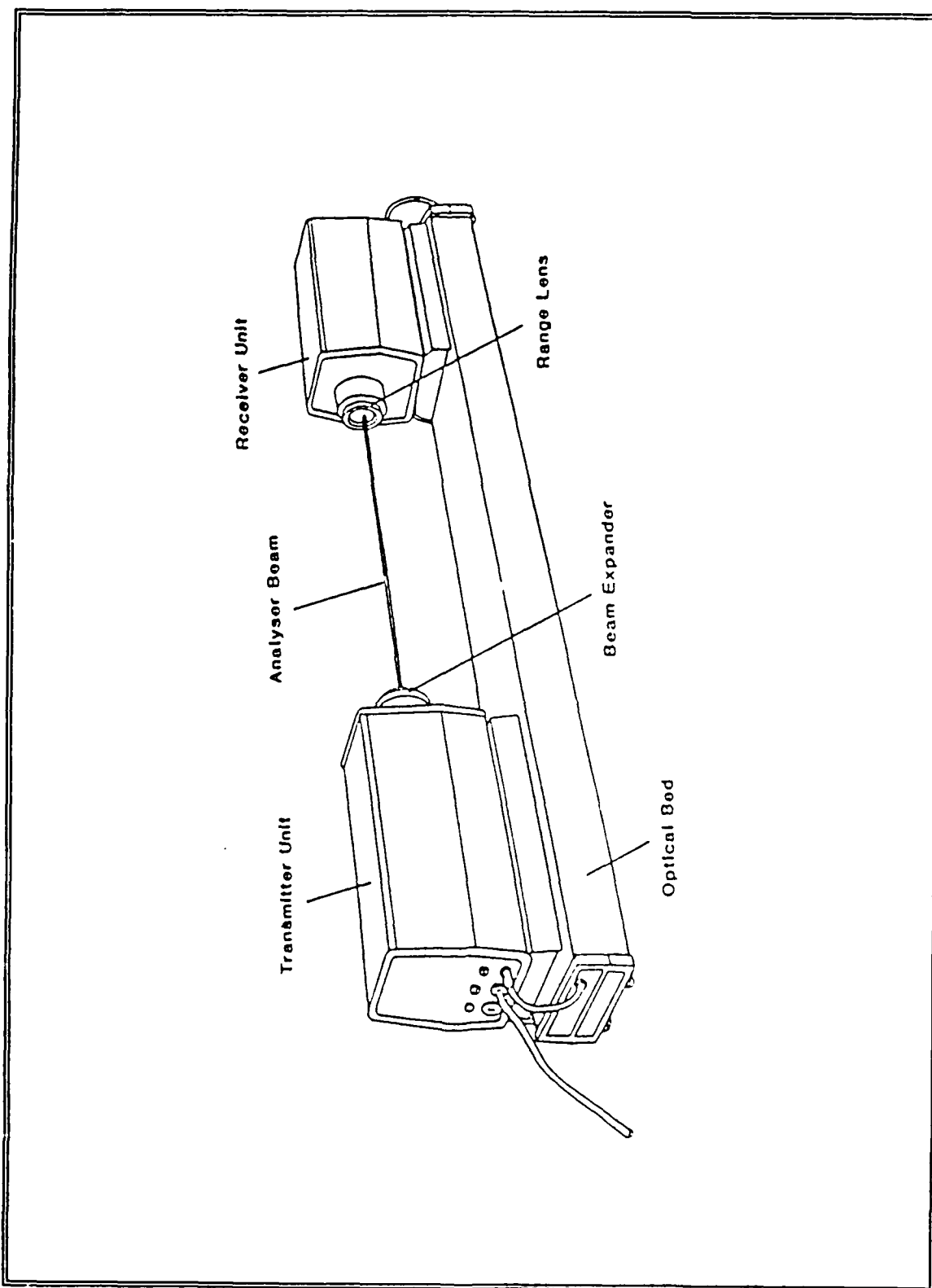


Figure III.5. Malvern 2600c Particle Sizer [Ref. 15].

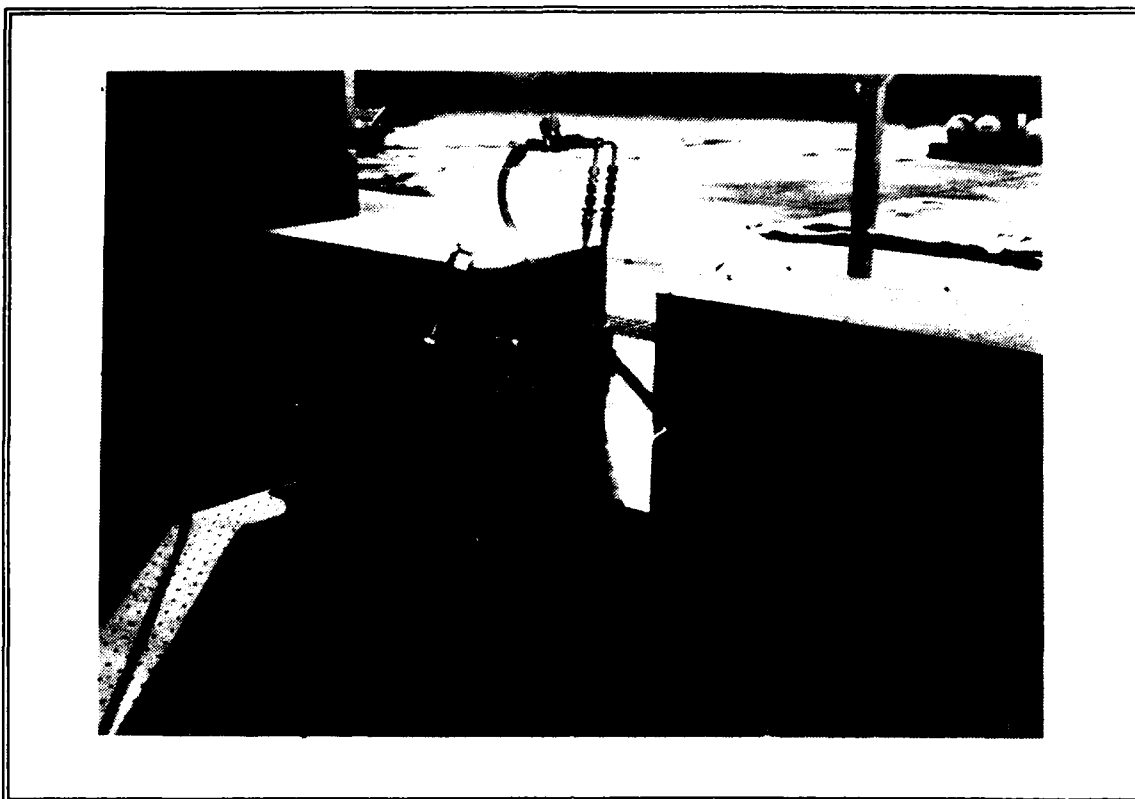


Figure III.6. Encased Malvern 2600c and NPS Two-Dimensional Rocket Motor.

TABLE III.2. MALVERN PARTICLE SIZE CLASSES.

Focal Length (mm)	Size Classes (microns)
63	1.2 - 118
100	1.9 - 188
300	5.8 - 564

it is shown that small particles scatter light at high angles and large particles scatter light at low angles in accordance to Fraunhofer diffraction theory. A disadvantage to this type of detection scheme is that no data can be collected on

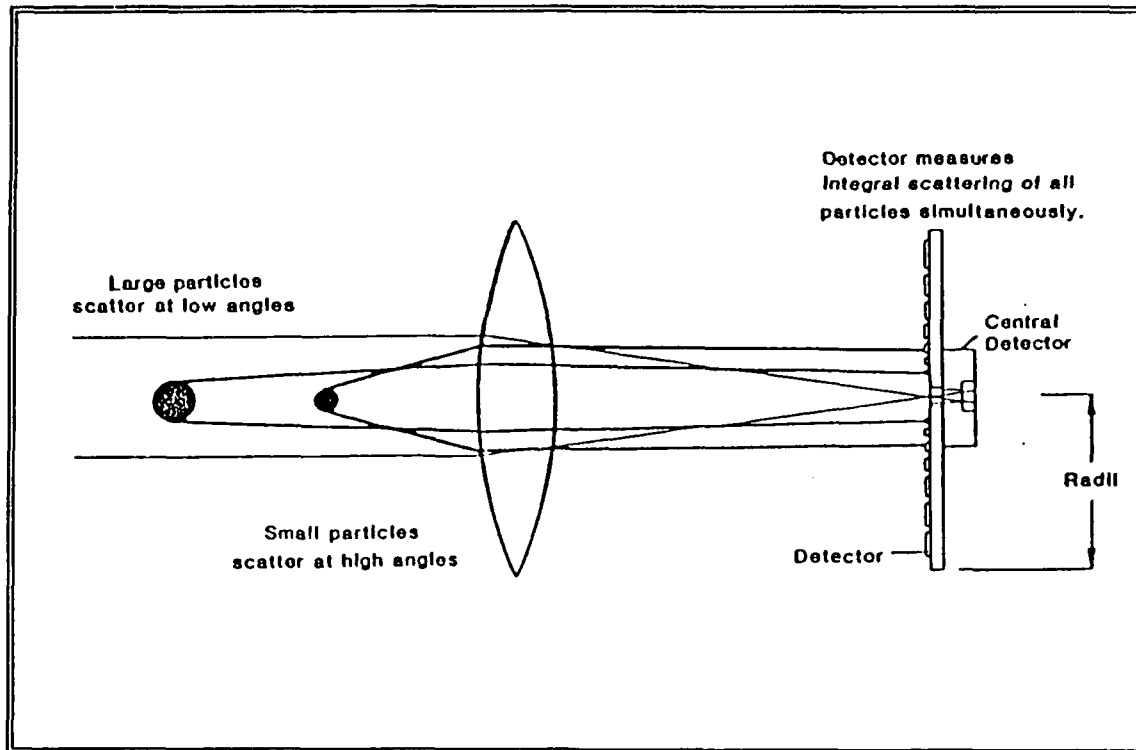


Figure III.7. Large and Small Particle Scattering [Ref. 15].

particle velocity in the flow field and no spatial characteristics are revealed. [Ref. 15]

The 100 mm lens was used for all testing. Although the 63 mm would have been a better match to the expected size range of the combustion particles, vignetting considerations made the 100 mm lens the most suitable choice. Vignetting or lens cut-off occurs when the measurement sample is outside of a specific range from the lens. Typically this range is approximately the focal length of the lens. Figure III.8. depicts vignetting and gives the specific cut-off distances for each of the three available range lenses. Due to the size of the rocket motor and the requirement of the metal casing

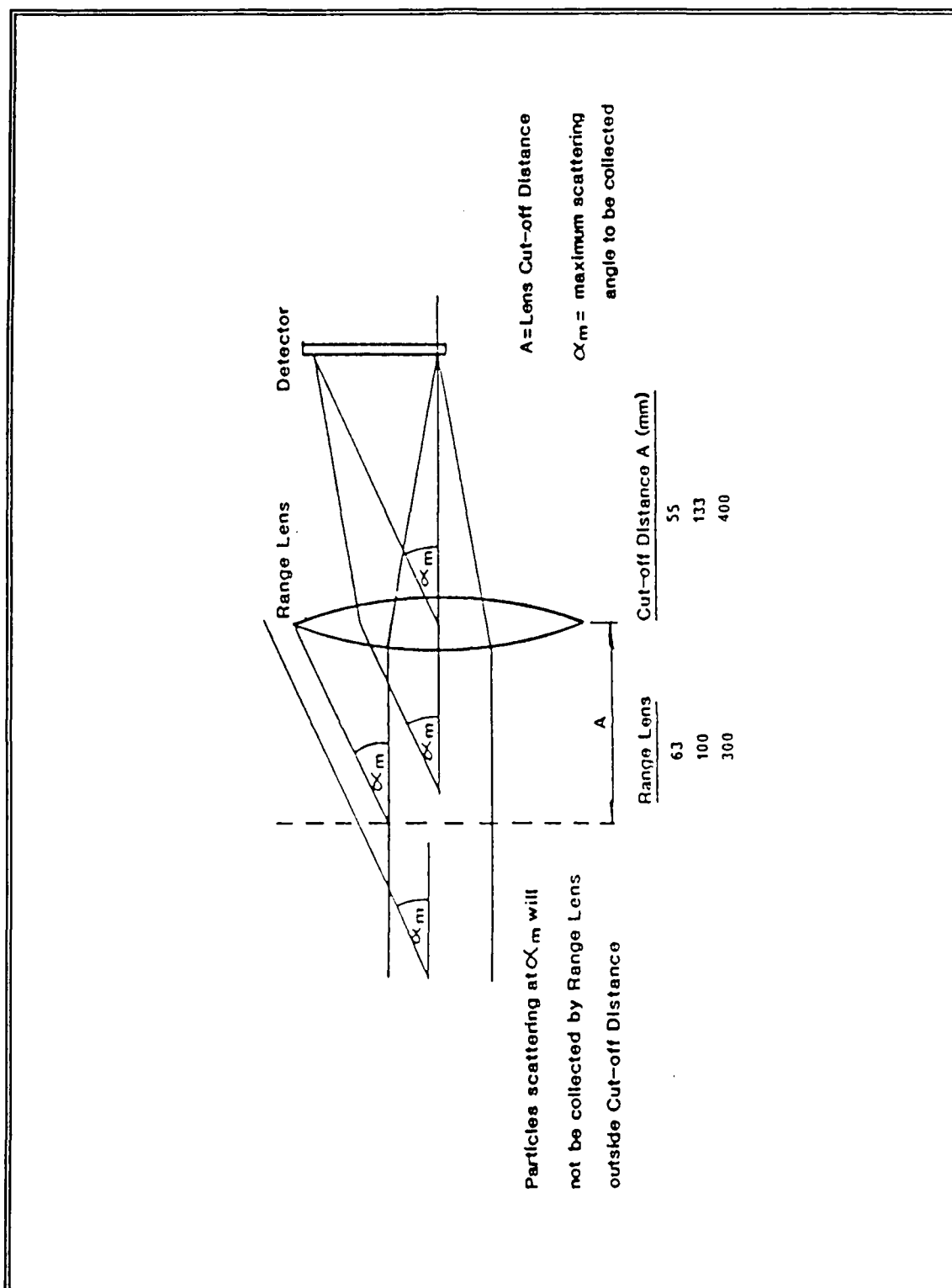


Figure III.8. Vignetting Effect and Lens Cut-Off Distances [Ref. 15].

around the Malvern system, it was not possible to place the sample volume inside the cut-off distance of 55 mm from the 63 mm focal length range lens.

Recognition Systems, Inc. (RSI) designed the monolithic detector. It has 31 semicircular concentric rings which output voltages proportional to the light energy incident on each ring. Each annular ring detector element is of greater thickness as the outside of the ringed detector is approached. Coupled with the increased radius of the outer rings, the areas of the outer rings are much greater than the inner ring areas. This area relationship has the effect of increasing the dynamic range of scattering measurements [Ref. 13]. The particular RSI detector used had a hole in the center of the detector instead of a small circular detector. This was an improved design which decreased possible interference from a strong undiffracted focus spot on the inner rings of the detector [Ref. 16]. The advertised dynamic range of the Malvern 2600c detector is 180:1 [Ref. 15].

A wide band-pass filter was used to help block out combustion light to the detector diode array. The filter was mounted flush over a circular opening in the Malvern metal case just in front of the range lens. Since the Malvern 2600c uses a He-Ne laser, a filter with a pass band centered at 632.8 nm was selected (Figure III.9.).

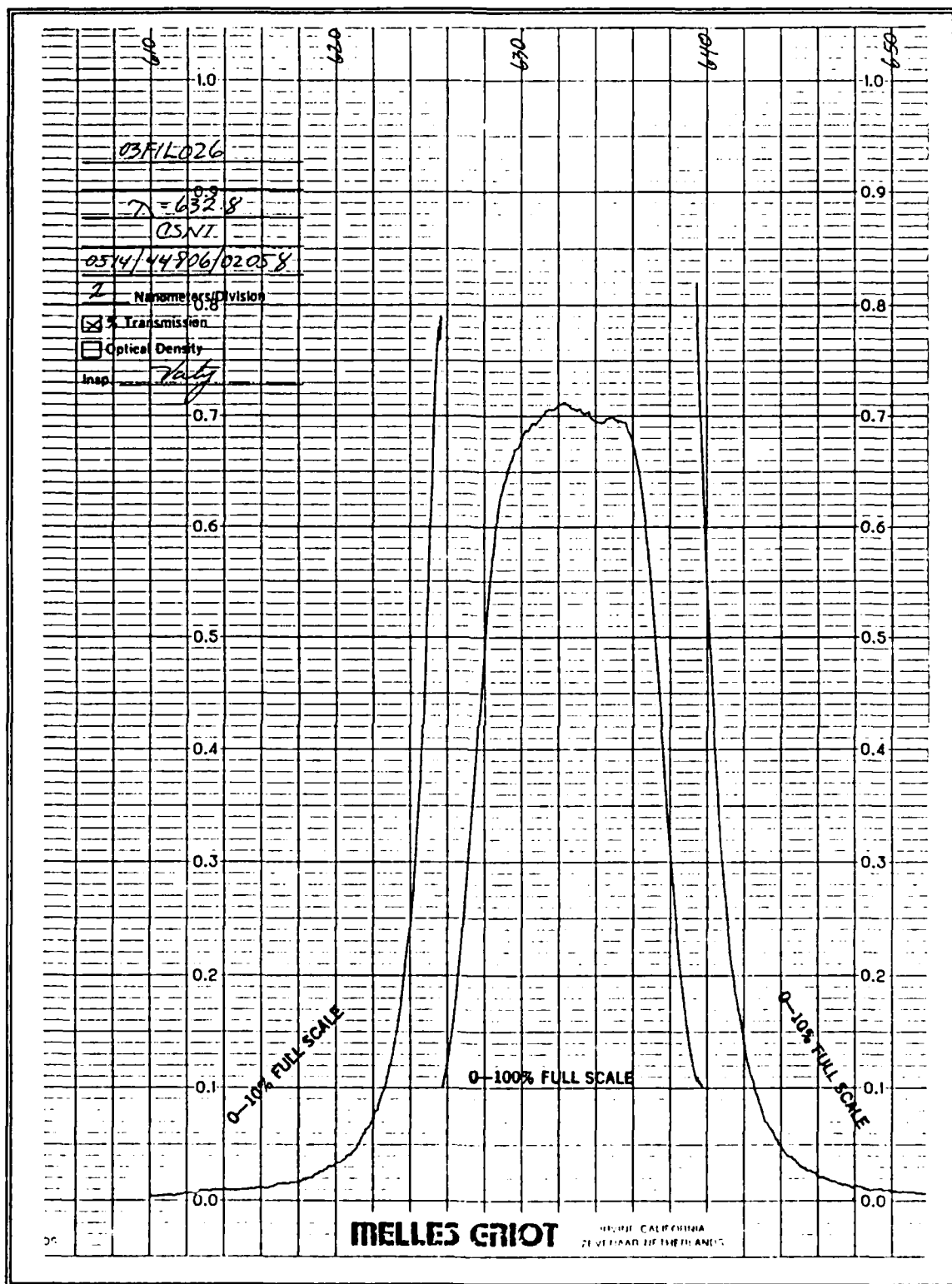


Figure III.9. He-Ne Laser Light Band-Pass Filter Characteristics.

C. DATA ACQUISITION AND CONTROL

Figure III.10. is a schematic of the data acquisition system. At the heart of the system is an HP 9836S microcomputer and an HP 3054A data acquisition and control system. Figure III.11. is a photograph of the two HP systems which are located inside the control room at the NPS Combustion Lab. The controlling software was written in HP Basic 5.1 and was loaded from a 20 megabyte hard disk. The program was adapted from a code previously written by Harris [Ref. 17], and is listed in Appendix A. Inputs to the program include a continuous voltage signal from the rocket motor pressure transducer. Parameters that could be manually set in the program included a constant for the voltage to pressure conversion, a chamber pressure value and subsequent time delay for sending a voltage trigger to the Malvern system. Outputs from the HP computer and controller included a tabular pressure-time printout and switching for the Malvern data trigger circuits. Line 760 of the program gives the instruction to the controller to digitally close switch 11,5 ("DC 11,5"). This completed a circuit which allowed a 5 volt, 100 Hz triangular wave to be sent to the Malvern Spray Synchronizer. This oscillating signal caused the Malvern to trigger at its maximum rate. The trigger or "sweep" rate is the time it takes to store the light intensity information

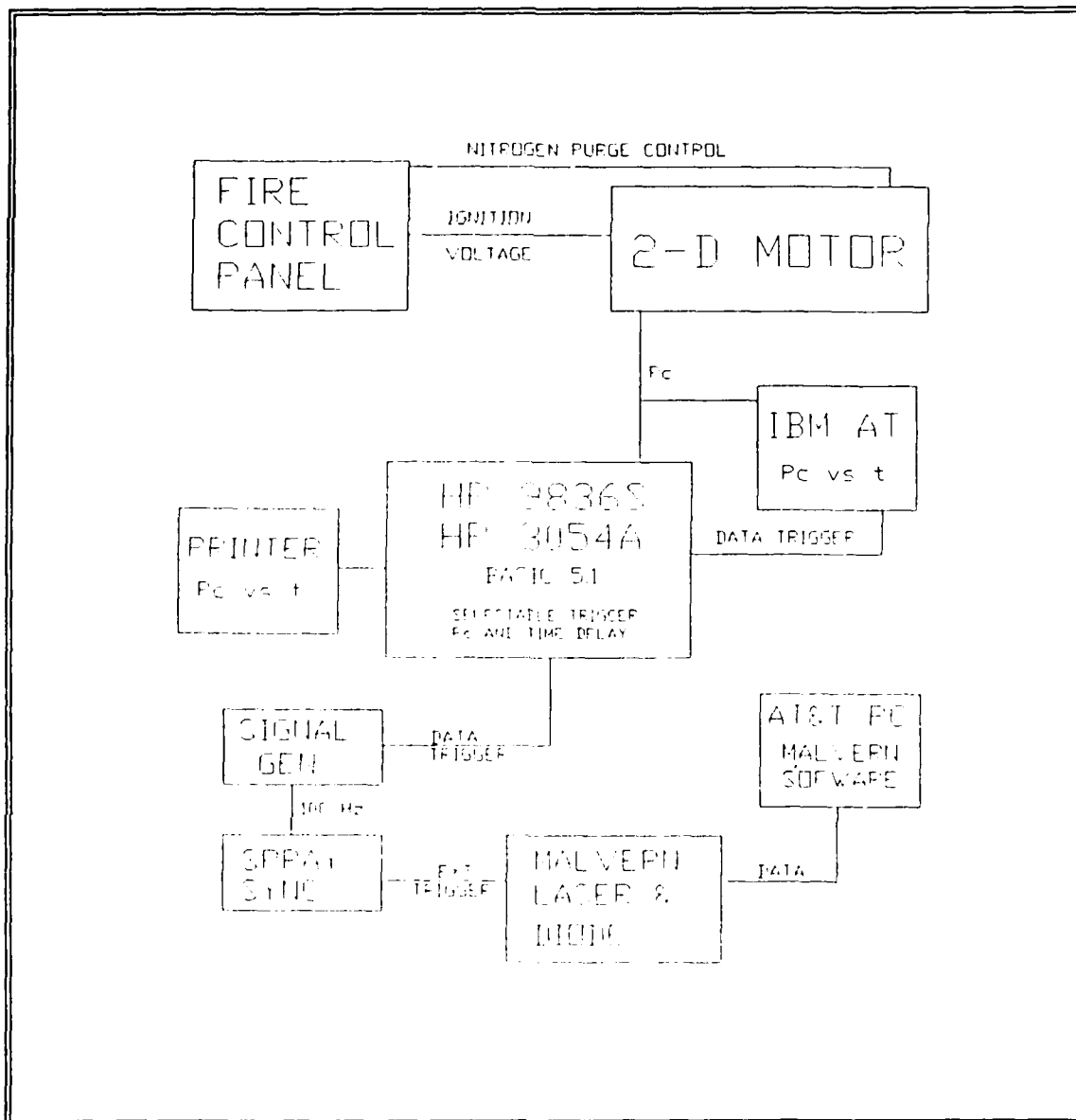


Figure III.10. Schematic of Two-Dimensional Motor Data Acquisition System.

from all 31 diode array rings into the computer's memory. The advertised allowable sweep rate of the Malvern 2600c was 45 Hz. However, the actual allowable sweep rate was measured to be approximately 24 Hz while using the Malvern Master Particle Sizer Version 3.0 software on an AT&T PC6300 computer. The

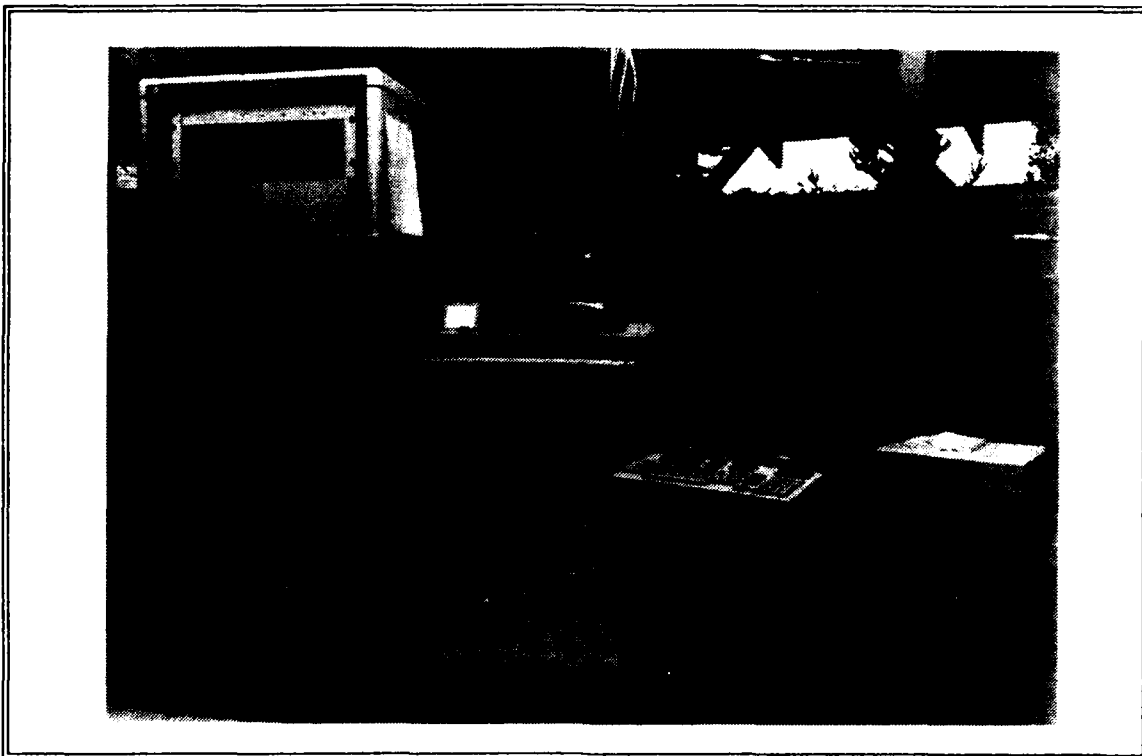


Figure III.11. HP 9836S Microcomputer and HP 3054A Data Acquisition and Control System.

Malvern software allows the desired number of sweeps to be manually set. The light intensity distribution information used by the Malvern to calculate particle size parameters is the average value of all the sweeps. Large total numbers of sweeps are recommended in steady state measurement conditions in order to have high statistical confidence in the Malvern results. The duration of the length of steady state pressure conditions in the NPS two-dimensional motor varied considerably from low pressure to high pressure runs. The total number of sweeps selected was varied from a maximum of 30, which equated to 1.25 seconds of sampling time, to a minimum of 12 sweeps.

Line 770 of the controlling program closes switch 10,8 ("DC 10,8"). This allowed a 1.5 volt signal from a dry cell to be input into the DASH-16 Metrabyte Board on one of the two control room IBM-AT computers. This signal, coupled with the chamber pressure voltage signal, allowed the pressure time trace data and the time of the Malvern initial trigger information to be displayed by the LabTech Notebook Version 2.8 software. The data were stored into a file which were subsequently analyzed and plotted using Lotus 123 Version 2.01 software.

The Fire Control Panel (FCP) provided remote control of nitrogen purge and ignition voltage. The procedures for test firing are listed in checklist form in Appendix B.

D. EXHAUST PARTICLE COLLECTION PROBE

A supersonic shock-swallowing quench probe, designed by Kessel [Ref. 6], was obtained from the Air Force Astronautics Laboratory (AFAL). The probe design objective was to provide a capability for collection of an exhaust particle sample with minimum biasing effects. The principal concern was to ensure that the particle flow did not pass through a strong normal shock. Such an occurrence could tend to breakup larger particles, thereby biasing the collection measurements toward smaller particle size distributions. [Ref. 6]

Figures III.12. and III.13. provide a cut-away sketch and a photo of the collection probe. The tip of the probe is made of tungsten and is removable for cleaning or replacement. The sharp edged tip was designed to capture a stream tube of the supersonic exhaust plume flow at a rate of one gram per second. To ensure that a detached shock does not form, a supply of cold nitrogen gas is introduced inside of the probe, downstream of the tip. The nitrogen flow acts as an ejector which reduces the tip exit pressure to 10 psia. A nitrogen flow rate to exhaust plume flow rate ratio of 14:1 was used to decelerate and quench the hot exhaust plume particles. In the mixing passage, located downstream of where the exhaust flow and nitrogen flow meet, a series of oblique shocks form that slightly lower the Mach Number of the combined flows. The majority of the flow deceleration and cooling is effected in the large diverging section between the mixing passage and the filter paper. The 14:1 flow rate ratio was designed to reduce the exhaust flow temperatures to approximately 270° F in order to prevent burning the filter paper. A static pressure of approximately 30 psia is required to force the flow through the filter paper. [Ref. 6]

The removable 0.025 micron filter paper is capable of collecting up to one gram of particles without creating significant pressure losses. It is expected that the expansion process will scatter particles as a function of

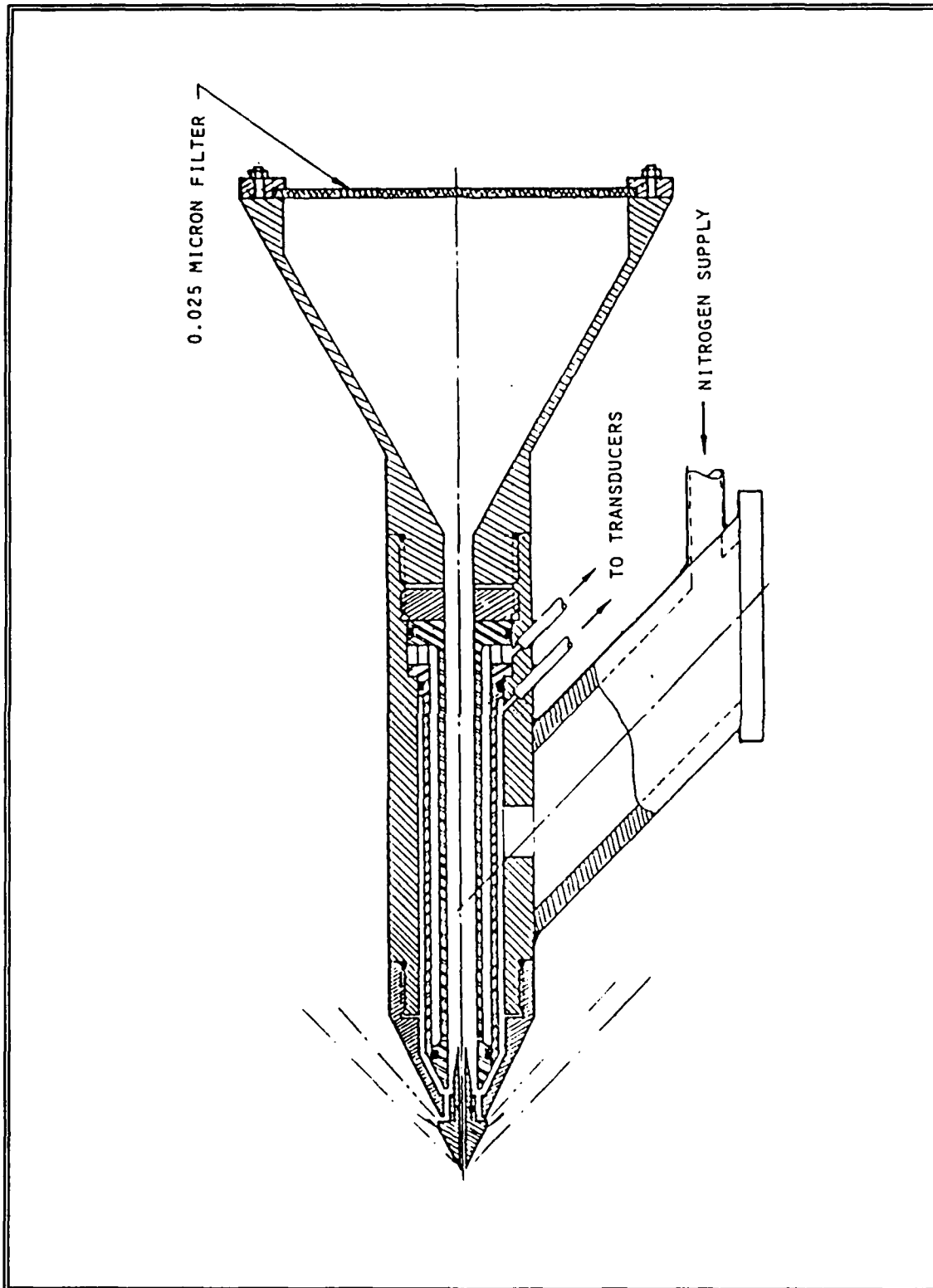


Figure III.12. Schematic of Exhaust Collection Probe [Ref. 6].

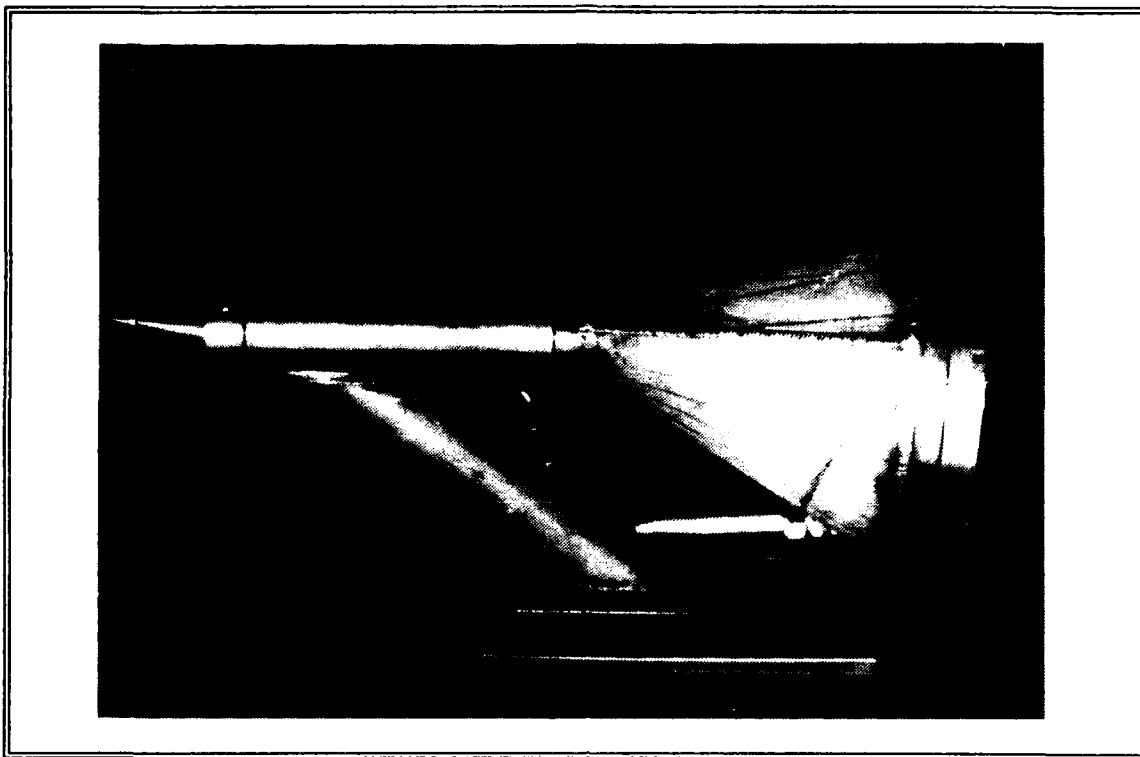


Figure III.13. Photo of Exhaust Collection Probe.

particle diameter, with the smaller particles following the flow and depositing on the outer portion of the filter paper. Therefore, small samples of the filter paper were taken from the center and evenly spaced distances from the center to the outside edge of the paper. These samples were then mounted on posts using double-stick tape and graphite paint. The mounted samples were then gold plated and viewed by a Hitachi S-450 Scanning Electron Microscope (SEM).

IV. RESULTS AND DISCUSSION

A. INTRODUCTION

Over the course of this thesis investigation, thirty-three rocket test firings were conducted. A summary of the firings is included as Appendix C. Eighteen of the test firings yielded useable DD1 and DD5 particle size data. Half of the successful firings were used to collect particle size data in the converging section of the two-dimensional exhaust nozzle and the other half produced exhaust plume particle size information. The collected data fulfilled the specific objective of obtaining particle size information as a function of propellant aluminum content, location in the flow field, and rocket motor chamber pressure. Additionally, the objective of comparing the Malvern 2600c forward light scattering results to the AFAL Probe collection results was met.

The remaining fifteen firings included two firings with zirconium carbide propellant, two DD1 propellant exhaust plume high speed video analysis runs, and 11 unsuccessful data collection attempts. The factors which caused data collection to be unsuccessful can be broken down as follows:

- 5 Burst Disk Ruptures
- 2 Excessively Dirty Windows
- 2 Excessive Data Sweep Time
- 1 Early Data Trigger Signal
- 1 No Data Trigger Signal

The burst disk ruptures were initially thought to be caused to occur prematurely at low pressures due to hot aluminum particles impinging on the burst disk surface. This reasoning led to redesigning the burst disk assembly into an elbow joint which served to reduce the probability of hot particles reaching the burst disk. Subsequent burst disk ruptures and post fire examination of the rocket chamber, typified by Figure IV.1., indicated that, more likely, a failure in the 732-RTV self-vulcanizing silicone inhibitor occurred at pressures above approximately 600 psia. This conclusion was reached based on the isolated areas of propellant burn-back noted in the rocket motor chamber. It appeared that the 732-RTV inhibitor was pushed back by the higher pressures, which allowed an abrupt increase in the propellant surface area to be exposed to the hot combustion gases. Such an increase in propellant burning area would in turn produce a sharp pressure spike of a sufficient magnitude to cause rupture of 1000 psi rated burst disks.

The dirty window problems were solved in part by making hardware modifications to the nitrogen purge system. A

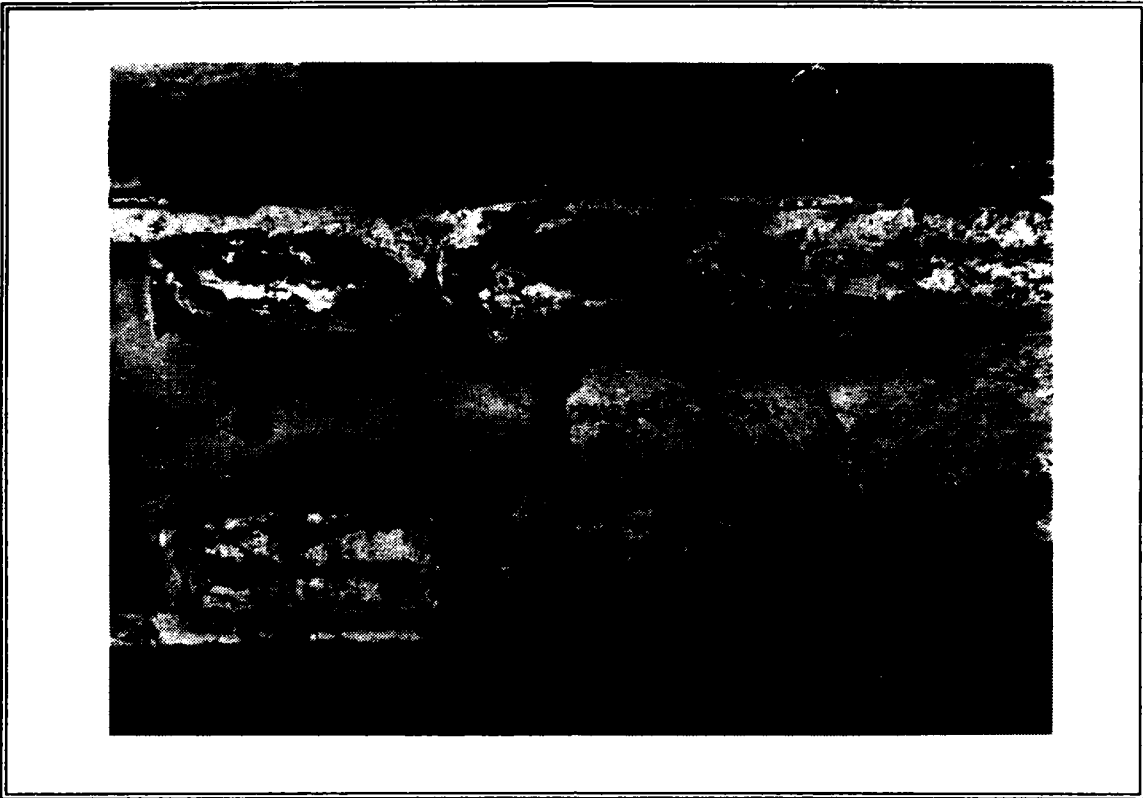


Figure IV.1. Rocket Chamber Residue Following a Ruptured Burst Disk.

pressure dome loader was added between the nitrogen supply bottles and the 0.031 inch sonic chokes. This allowed the mass flow rate to be fixed by adjusting the dome pressure alone. It was also found that it was imperative to keep the sintered bronze diffusers clean. Adequate cleaning of the diffusers was accomplished by using an ultrasonic bath in a soap solution.

Excessive data sweep time became a problem when the chamber pressure was high and the burn time was low. These firings were typically not plateau burns, with little or no steady state time period in which to collect the data. The

initial number of sweeps selected by the Malvern software was 30, which equated to approximately 1.25 seconds on the computer system which was used. Test results were discarded as being invalid on firings where the propellant burn period during the data sweeps was less than 50% of the sweep period. Runs annotated with an asterisk in Appendix C had the propellant burn out during a small portion of the data sweep period. In these cases, the reported pressure for data collection was calculated by taking the average chamber pressure during the propellant burn time only. Data collection pressure calculations made for all other runs were accomplished by averaging the pressure over the entire data sweep period.

The problem of excessive sweep periods described above was handled by reducing the number of sweeps. The adverse side effect of this remedy was that reduction of the number of sweeps below 30 significantly decreases the statistical confidence in the results. Generally, the number of sweeps were reduced only to 24, but on high chamber pressure runs, 12 sweeps were used. Ideally, propellant burn times would have been increased. However, producing plateau burns of at least 1.25 seconds at high pressures was not achievable with the propellant loading configurations used. Future planned computer hardware and software upgrades at the NPS Combustion Lab will increase the data sweep rate by a factor of four.

The two runs which provided high speed video of the DD1 propellant exhaust plume were used to determine the exhaust plume geometry and the location of expansion shock waves in the plume. This information was necessary for determining proper placement of both the Malvern laser beam and the AFAL Probe in the exhaust. In addition, it was apparent from both videos that the exhaust plume was not in steady state. Variations in the size and optical density of the plume were observed and believed to be caused by the shedding of Al_2O_3 slag which had accumulated on the walls of the converging section of the exhaust nozzle. Post-run slag deposits are clearly visible in Figure IV.2. Such an accumulation and shedding process would have served to vary the area ratio of the exhaust nozzle, causing Mach number variations in the converging section. The oscillating phenomena highlights the importance of using sampling periods of the largest possible duration.

Zirconium carbide propellant was used on the two initial rocket test firings conducted in this thesis. This was done in order to provide time to gain familiarization with data collection procedures and techniques as well as to help validate data collected by Youngborg [Ref. 20] and Pruitt [Ref. 5]. One of the two runs was successful and produced an in-motor D_{32} of 68.7 microns at a chamber pressure of 111 psia. Although the test conditions were not identical in terms of

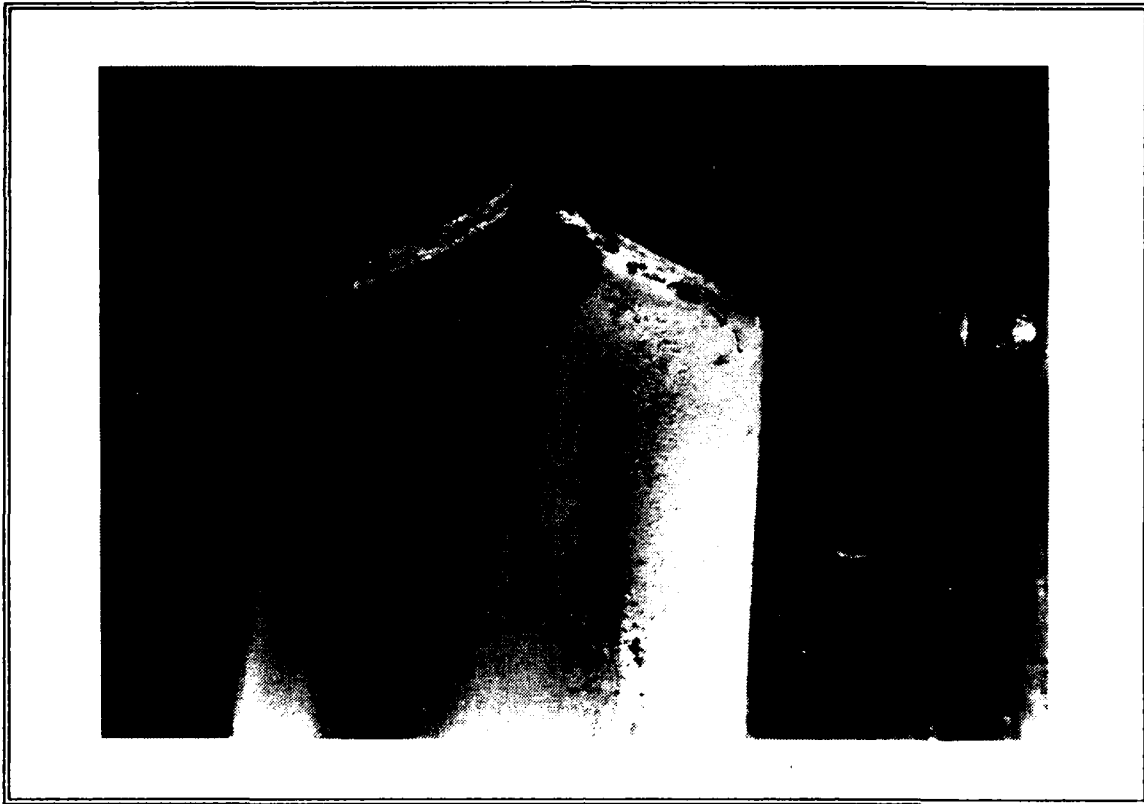


Figure IV.2. Exhaust Nozzle Post Fire Slag Deposits.

the motor used, flow Mach number, and location in the flow, the results compare favorably to Pruitt's [Ref. 5] in-motor result of $D_{32} = 61.8$ microns at a chamber pressure of 134 psia.

B. SYSTEM CALIBRATION

Laser diffraction instruments are typically calibrated by use of calibration reticle or by particle samples of known size distributions which are suspended in liquid. The latter means was used previously by Youngborg [Ref. 20] to calibrate the Malvern 2600c. Polystyrene spheres, glass beads, and aluminum oxide particles were suspended in liquid. Youngborg's results found that the Malvern 2600c could

correctly depict volume distributions from bimodal calibration samples when used in the Model Independent mode. However, it was thought that the Malvern D_{32} calculations underestimated the actual value of D_{32} . [Ref. 20]

In order to increase the confidence in the Malvern 2600c's capability to calculate D_{32} properly, a Laser Electro-Optics Limited Calibration Reticle (#203) was used for calibration purposes. The calibration reticle provided a two-dimensional sample array of approximately 10,000 circular discs of thin chrome film which had been photo-etched on a glass substrate. The discs were randomly positioned on an 8 mm diameter sample area. Twenty-three discrete disc diameters, with one to nearly 3,000 replications of each discrete size, were used to approximate a Rosin-Rammler size distribution. The data sheet for the reticle used is included as Appendix D. [Ref. 18]

Since the calibration reticle which was available contained a Rosin-Rammler distribution, the Rosin-Rammler model was selected in the Malvern 2600c software in order to facilitate a better comparison of results. Ten calibration runs were conducted and the results are listed in Table IV.1. The nominal mean diameter (\bar{X}), the nominal width parameter (N), and D_{32} were all found to agree closely to the published calibration value. The measured value for N indicated a broader distribution range than described by the calibration result, and the D_{32} was larger, but within the published

TABLE IV.1. MALVERN 2600C CALIBRATION USING ROSLIN-RAMMLER MODEL (USING LASER ELCTRO-OPTICS LIMITED CALIBRATION RETICLE #203).

RUN #	XBAR (microns)	N	D ₃₂ (microns)	OBSCUR	LOG DIFF
1	52.02	4.05	42.6	0.22	5.53
2	52.02	3.89	41.8	0.24	5.53
3	52.02	3.77	41.4	0.23	5.44
4	52.02	3.91	41.8	0.23	5.52
5	52.02	3.91	41.8	0.24	5.57
6	50.94	4.05	41.6	0.24	5.57
7	53.26	4.05	43.4	0.24	5.54
8	52.02	3.77	41.4	0.23	5.52
9	53.26	4.05	43.4	0.24	5.56
10	53.26	4.05	43.4	0.24	5.56
AVERAGE	52.284	3.950	42.26	0.235	5.534
STD DEV	0.751	0.116	0.85	0.008	0.038
CAL VALUES	53.0	3.17	40.33*	calibration D ₃₂ accuracy given to be ±2 microns	
DIFFERENCE	-0.716	0.78	1.93		

accuracy tolerance, than the calibration value. The obscuration was measured to be 0.235, which is a typical value which was observed in exhaust plume measurements.

Typically, a specific particle distribution type is not assumed when collecting rocket motor particle distribution data. Therefore, the Model-Independent mode was always

selected for use by the Malvern 2600c. In order to access the ability of the Model-Independent mode to characterize properly a known Rosin-Rammler distribution, the same raw data collected by the ten calibrations readings were reprocessed using the Model-Independent mode. The results are displayed in Table IV.2. It is noteworthy that the Model-Independent D_{32} calculation is within one micron of both the Malvern Rosin-Rammler calculations and the calibration value. This provides strong support that the Malvern 2600c operating in the Model-Independent mode has the capability to accurately calculate the D_{32} particle size parameter.

C. EXHAUST NOZZLE ENTRANCE RESULTS

1. Test Conditions

A series of test firings were conducted using both the DD1 and DD5 propellants over a pressure range of approximately 150 to 450 psia. Data collected correlates to a position within the converging section of the exhaust nozzle where the flow Mach number is approximately 0.1. The location at which the laser beam was passed through the motor in order to collect data was depicted and described in detail in Chapter II. The range of obscurations observed in the tests conducted in the exhaust nozzle were found to be between 0.87 and 0.99. High values of obscuration such as these are outside the prescribed limits of the Malvern 2600c operating range. In

**TABLE IV.2. MALVERN 2600C CALIBRATION USING
MODEL INDEPENDENT MODEL (USING LASER ELECTRO-
OPTICS LIMITED CALIBRATION RETICLE #203).**

RUN #	D ₃₂ (microns)	OBSCUR	LOG DIFF
1	41.6	0.22	5.88
2	41.4	0.24	5.87
3	41.3	0.23	5.76
4	41.0	0.23	5.85
5	41.6	0.24	5.90
6	40.8	0.24	5.91
7	41.5	0.24	5.87
8	41.0	0.23	5.85
9	41.3	0.24	5.88
10	41.6	0.24	5.89
AVERAGE	41.31	0.235	5.866
STD DEV	0.29	0.008	0.042
CALIBRATION VALUE	40.33*	calibration D ₃₂ accuracy given to be ±2 microns	
DIFFERENCE	0.98		

order to compensate for these extreme obscuration values, a correction scheme devised by Gulder [Ref. 19] was employed.

Gulder conducted an experimental study with a Malvern system using multimodal particle distributions over a range of obscurations in order to develop corrective expressions for D₃₂. The need for such expressions stems from the fact that

small interparticle spacing between sample particles causes particle light scattering characteristics to be a function of the relative positions and sizes of surrounding particles. This is termed multiple scattering, which typically occurs at obscuration values above 0.5. Multiple scattering has the effect of reducing the measurement value of D_{32} . The experiments conducted by Gulder were with latex spheres and Al_2O_3 particles in a magnetically stirred liquid sample cell. Corrective schemes were developed for model-independent and bimodal distributions for sample obscurations of 0.50 to 0.98. The empirical expressions developed by regression analysis were:

$$D_{32} \text{ (ADJUSTED)} = D_{32} / C_d$$

$$\text{where } C_d = 1.35e^{(F1 + F2)}$$

$$F1 = -0.1184(D_{32}/100)^2 + 13.122\Phi/D_{32} - 5.7474\Phi/D_{32}^{0.5}$$

$$F2 = 2.2389\Phi^8 - 2.6077\Phi^9$$

$$D_{32} = \text{Malvern } D_{32}$$

$$\Phi = \text{Obscuration}$$

The validity of this correction is for a Malvern calculated D_{32} input ranging from ten to 100 microns and obscuration inputs from 0.5 to 0.98. [Ref. 19]

The Gulder adjustment to D_{32} was only applied to the in-motor data. The Malvern D_{32} values requiring correction for multiple scattering effects ranged from 9.7 to 40.9 microns and the obscurations varied from 0.87 to 0.99.

2. DD1 Results

Table IV.3. lists the exhaust nozzle entrance particle distribution data obtained for the 2.0% aluminum propellant firings. It can be seen that the Gulder multiple scattering correction makes the adjusted D_{32} nearly double that of the uncorrected Malvern D_{32} . Over the range of pressures tested, it was observed that D_{32} decreased as pressure increased. These results are plotted in Figure IV.3. This dependence of D_{32} on motor chamber pressure supports the contention made by Price [Ref. 8] that the particle size distribution should

TABLE IV.3. DD1 IN-MOTOR DATA.

P_C (psia)	OBSCURATION	MALVERN D_{32} (microns)	ADJUSTED D_{32} (microns)
196	0.9828	40.9	72.3
200	0.9860	35.0	63.7
240	0.9866	33.4	61.2
315	0.9891	24.1	45.6
325	0.9792	17.9	32.0
450	0.8723	20.2	26.3

decrease as surface ignition of aluminum particles and agglomerates are enhanced by increased chamber pressure. The dependency of D_{32} on chamber pressure decreased as the pressure became higher. Although higher pressure test firings were not successful due to the burst disk failures described earlier, it appeared as if the D_{32} values would level out at a value between ten and 20 microns as the chamber pressure was further increased. Twenty microns is the mean average size of the

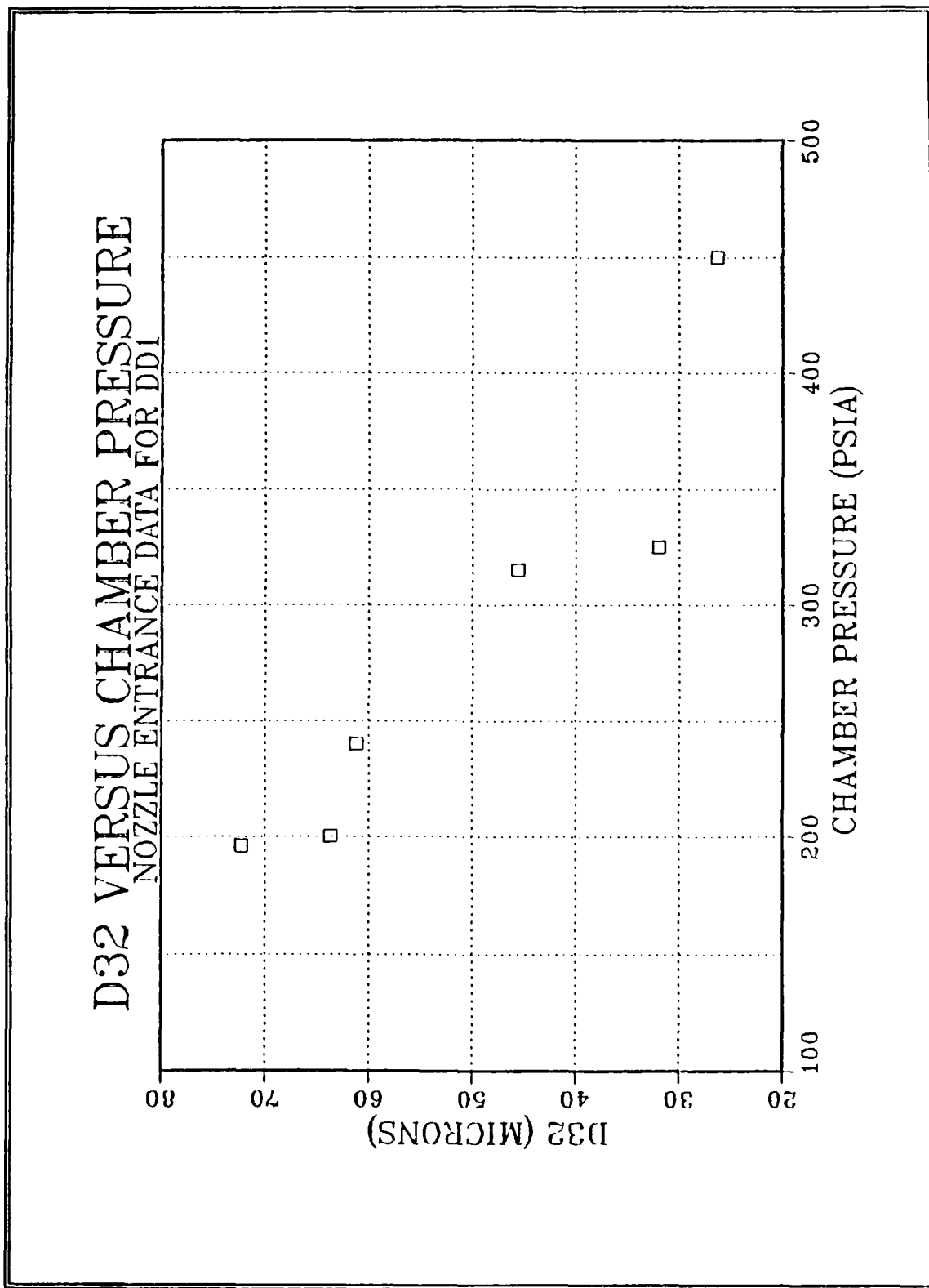


Figure IV.3. DD1 In-Motor D_{32} versus P_c .

aluminum powder particles that make up the propellant matrix. This provides an indication that agglomeration will decrease to insignificant levels at chamber pressures above approximately 600 psia.

Figures IV.4. through IV.8. display the volume distribution data calculated by the Malvern 2600c for the DD1 propellant in-motor data. Due to the high obscurations observed these figures should be shifted to the right. However, the distribution shapes are believed to be accurate.

Figure IV.4. depicts a volume distribution particle size band of 19 to 190 microns, with bimodal peaks at 32 and 45 microns. Figures IV.5. and IV.6. have similar distributions, which was to be expected since the chamber pressure variation was less than 50 psi. These distributions demonstrate the repeatability of the test results. As the chamber pressure was further increased, the volume distribution size bands began to broaden on the low end. Figure IV.7. depicts the volume distribution for a chamber pressure of 325 psia. The main size band was from 11 to 190 microns with a plateau peak ranging from 30 to 60 microns. Additionally, there was evidence of a smaller mode developing in the 2.5 micron range. This gives indication that in terms of numbers, there were many more small particles at the higher chamber pressures. Figure IV.8. is a volume distribution for 450 psia. The main particle size band was even broader, from

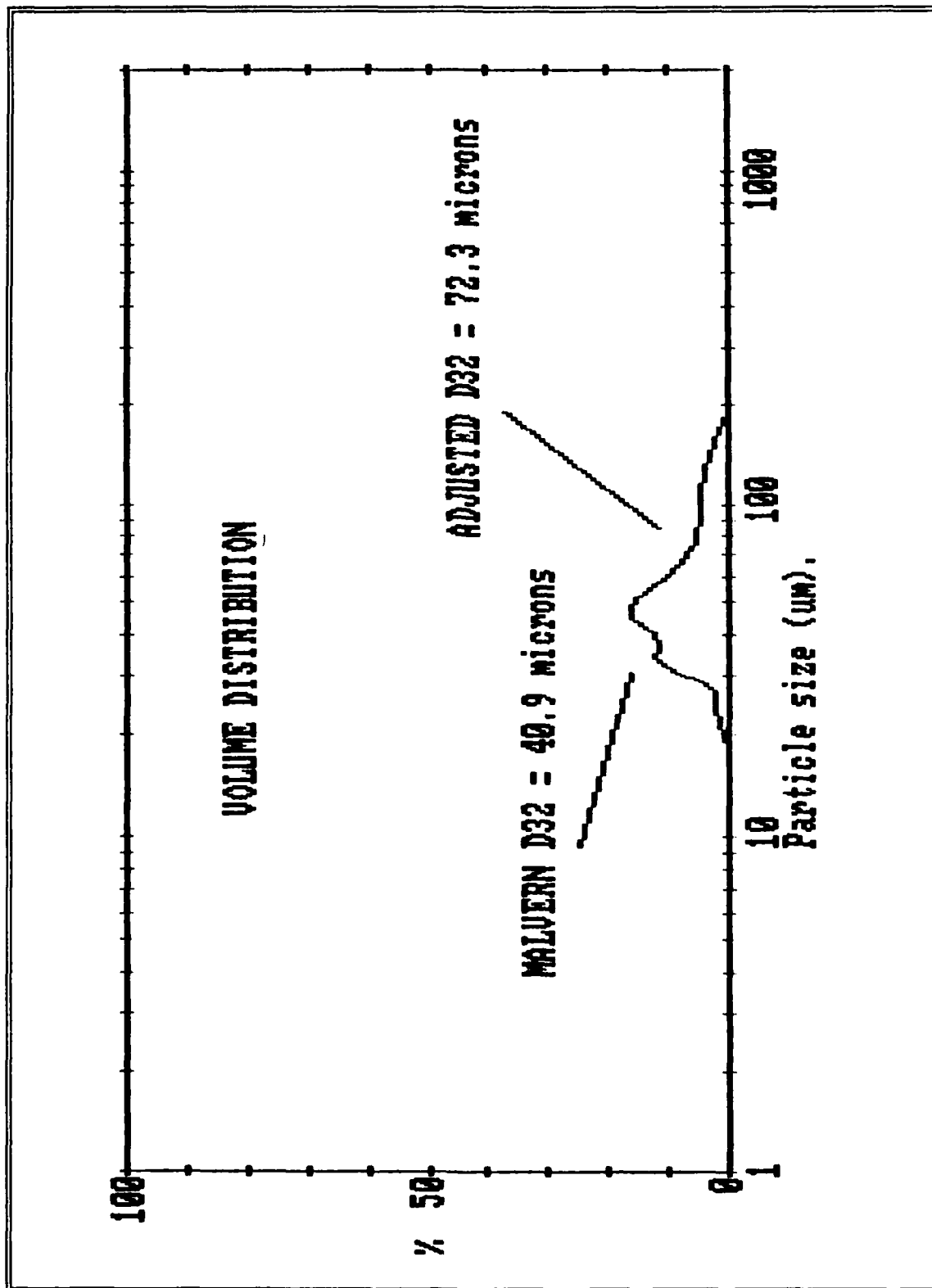


Figure IV.4. DD1 In-Motor Volume Distribution, $P_c = 196$ psia.

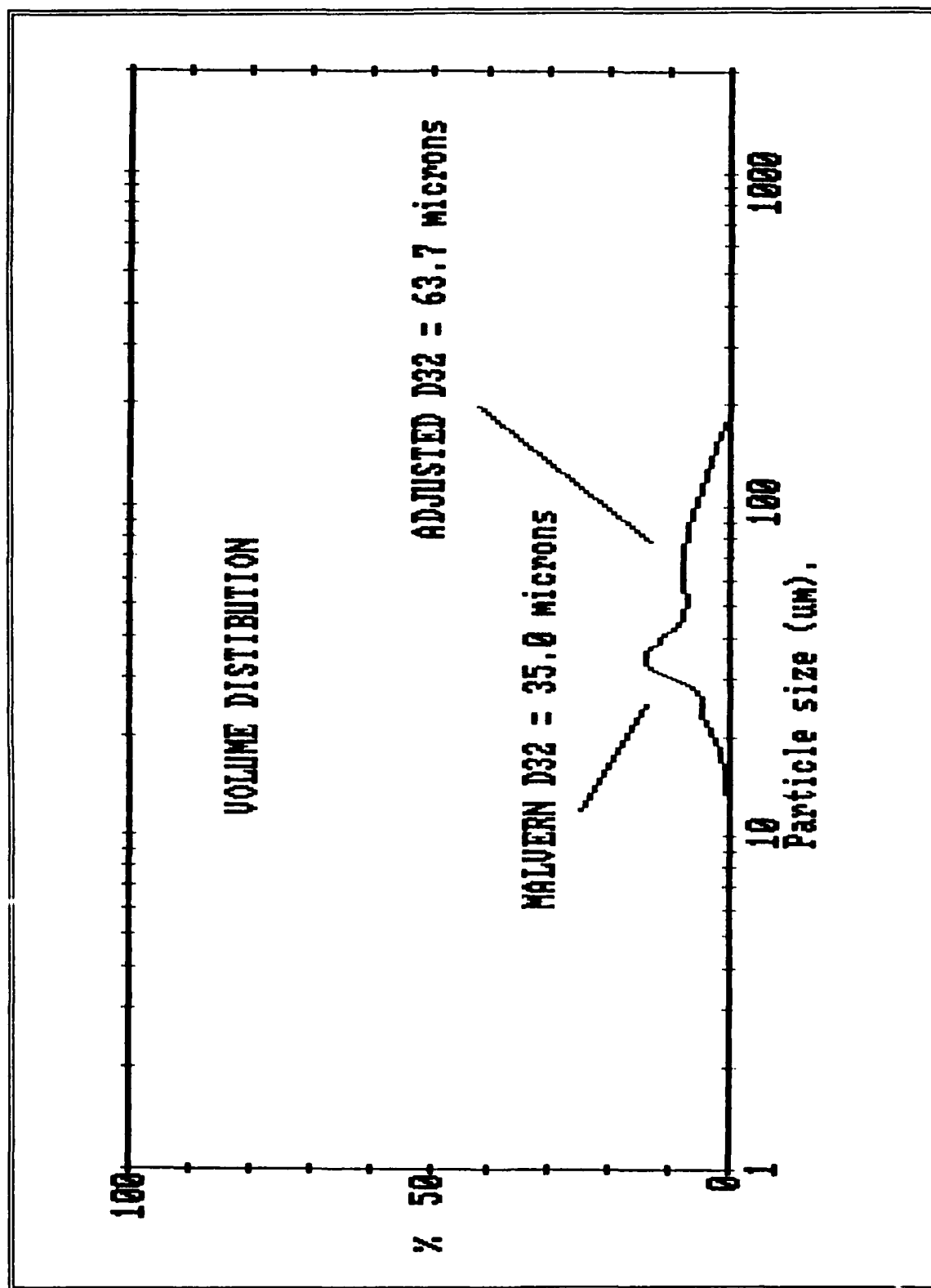


Figure IV.5. DD1 In-Motor Volume Distribution, $P_c = 200$ psia.

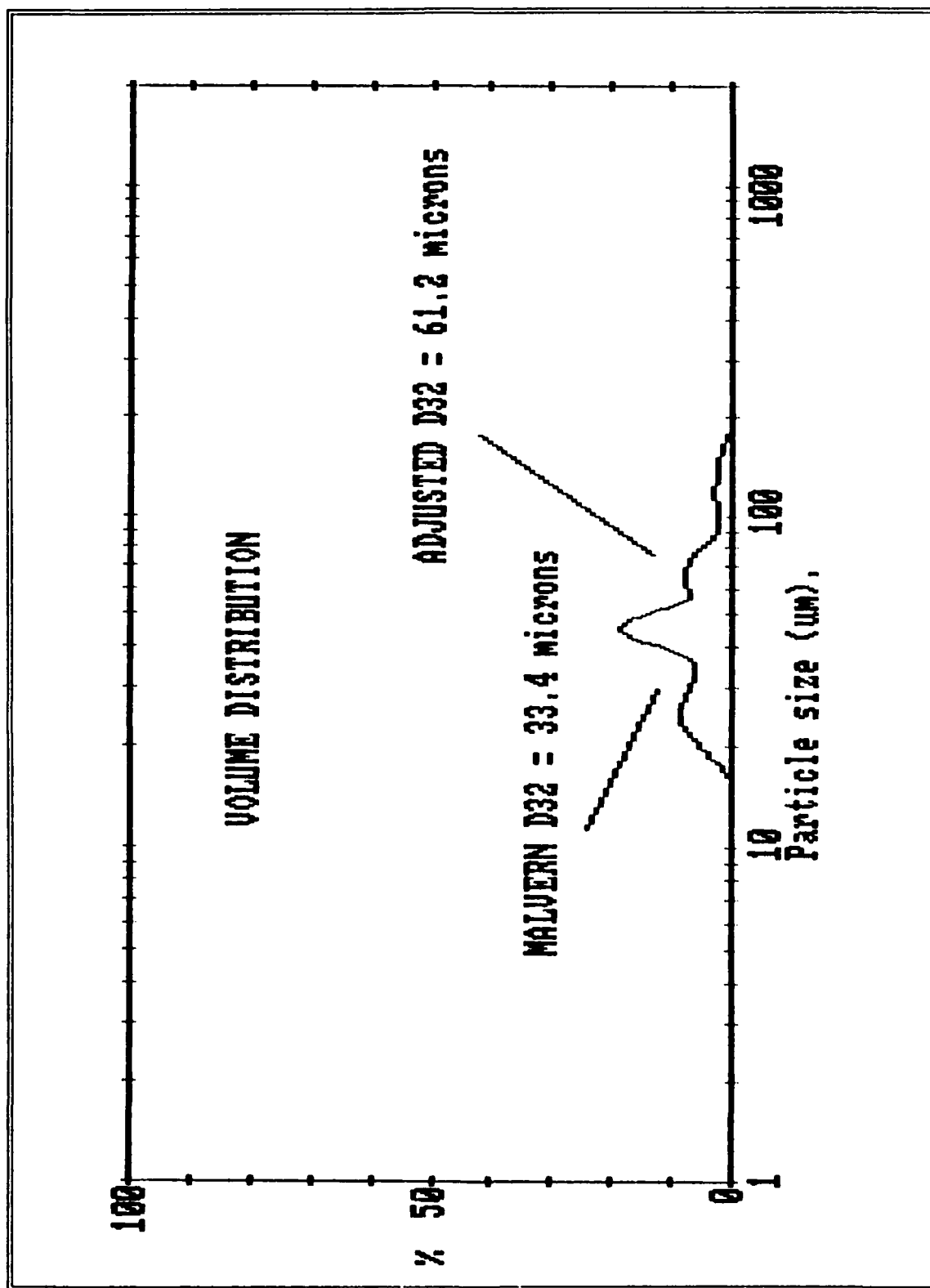


Figure IV.6. DD1 In-Motor Volume Distribution, $P_c = 240$ psia.

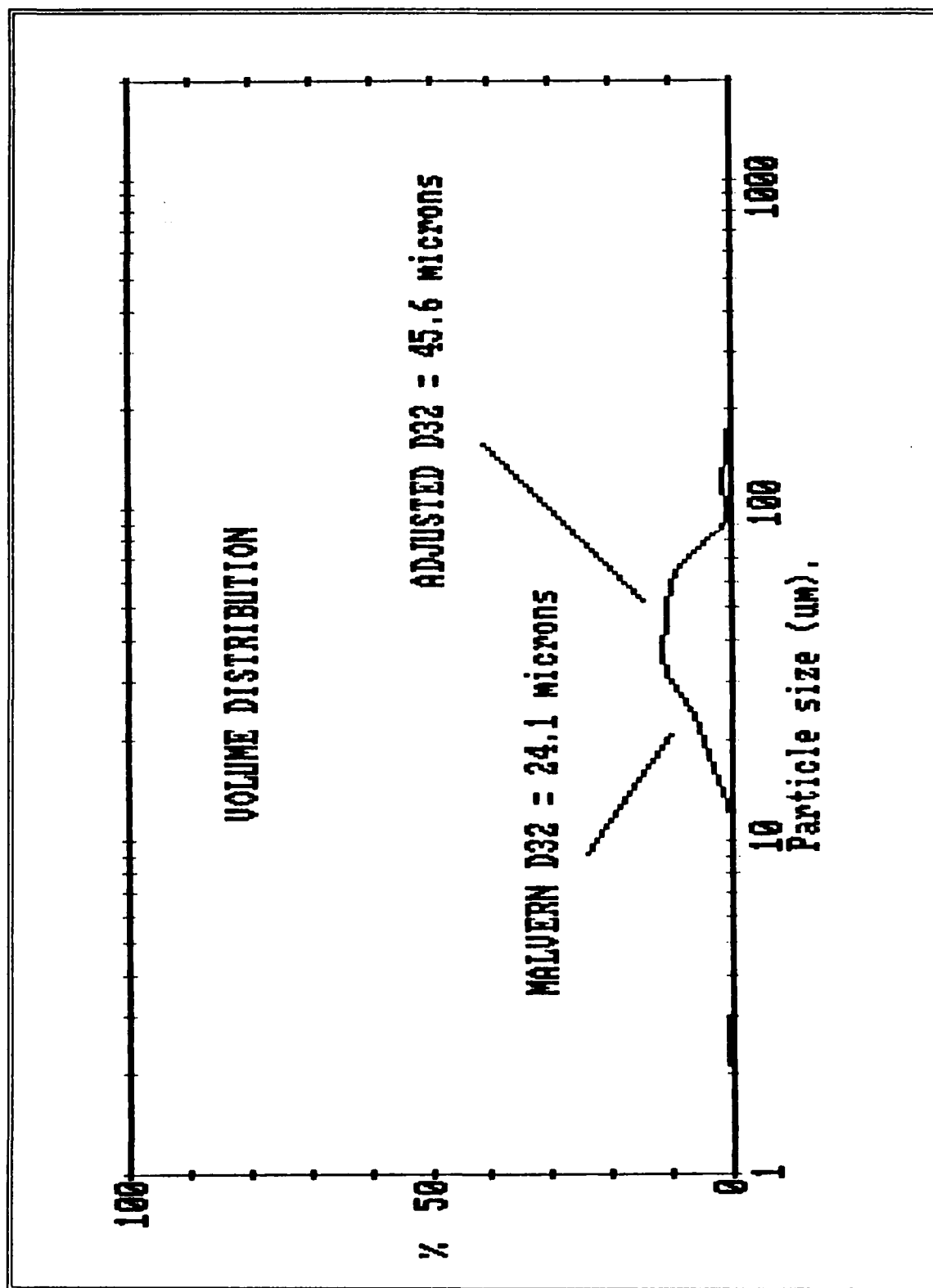


Figure IV.7. DD1 In-Motor Volume Distribution, $P_c = 315$ psia.

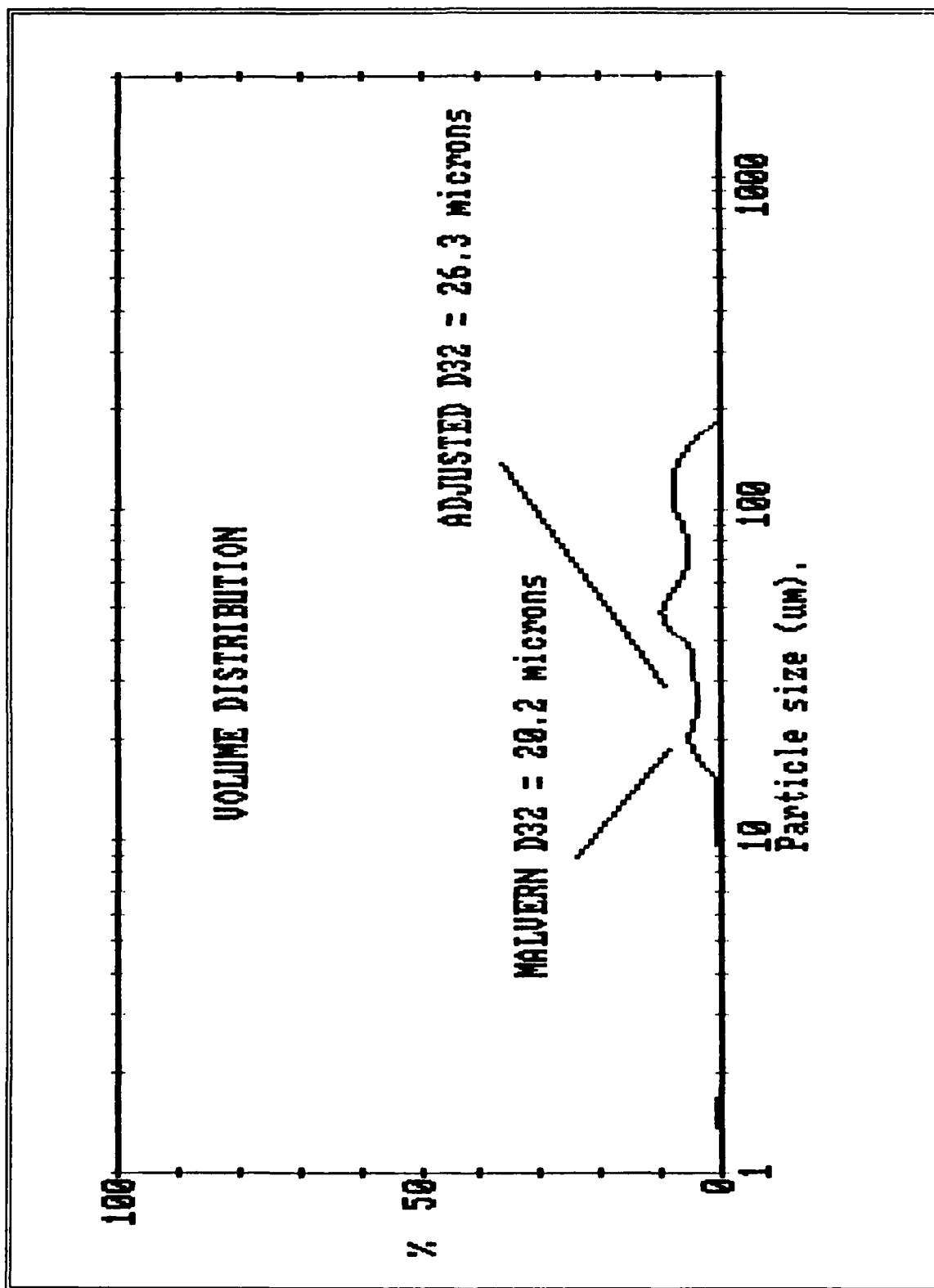


Figure IV.8. DD1 In-Motor Volume Distribution, $P_c = 450$ psia.

9.5 to 195 microns, with a plateau peak from 19 to 130 microns. As in the 325 psia distribution depicted in Figure IV.7., the 450 psia distribution displayed evidence of a small mode at 1.5 microns, below the main size band. Thus, as pressure was increased above approximately 250 to 300 psia, larger quantities of smaller particles were present at the entrance of the exhaust nozzle.

3. DD5 Results

The exhaust nozzle entrance data for the 4.69% aluminum loaded propellant firings are listed in Table IV.4. As with the DD1 firings, the Gulder multiple scattering correction was required and the D_{32} decreased with increasing pressure. The D_{32} dependence on motor chamber pressure is graphically depicted in Figure IV.9. Due to time constraints only three data points were obtained. However, these data were consistent with the DD1 data, indicating a decrease in D_{32} with increasing pressure. A crude extrapolation would suggest a zero slope of the D_{32} curve at approximately ten microns at pressures above 500 psia.

TABLE IV.4. DD5 IN-MOTOR DATA.

P_C (psia)	OBSCURATION	MALVERN D_{32} (microns)	ADJUSTED D_{32} (microns)
166	0.9884	21.7	41.0
265	0.9925	13.2	24.4
410	0.9634	9.7	14.2

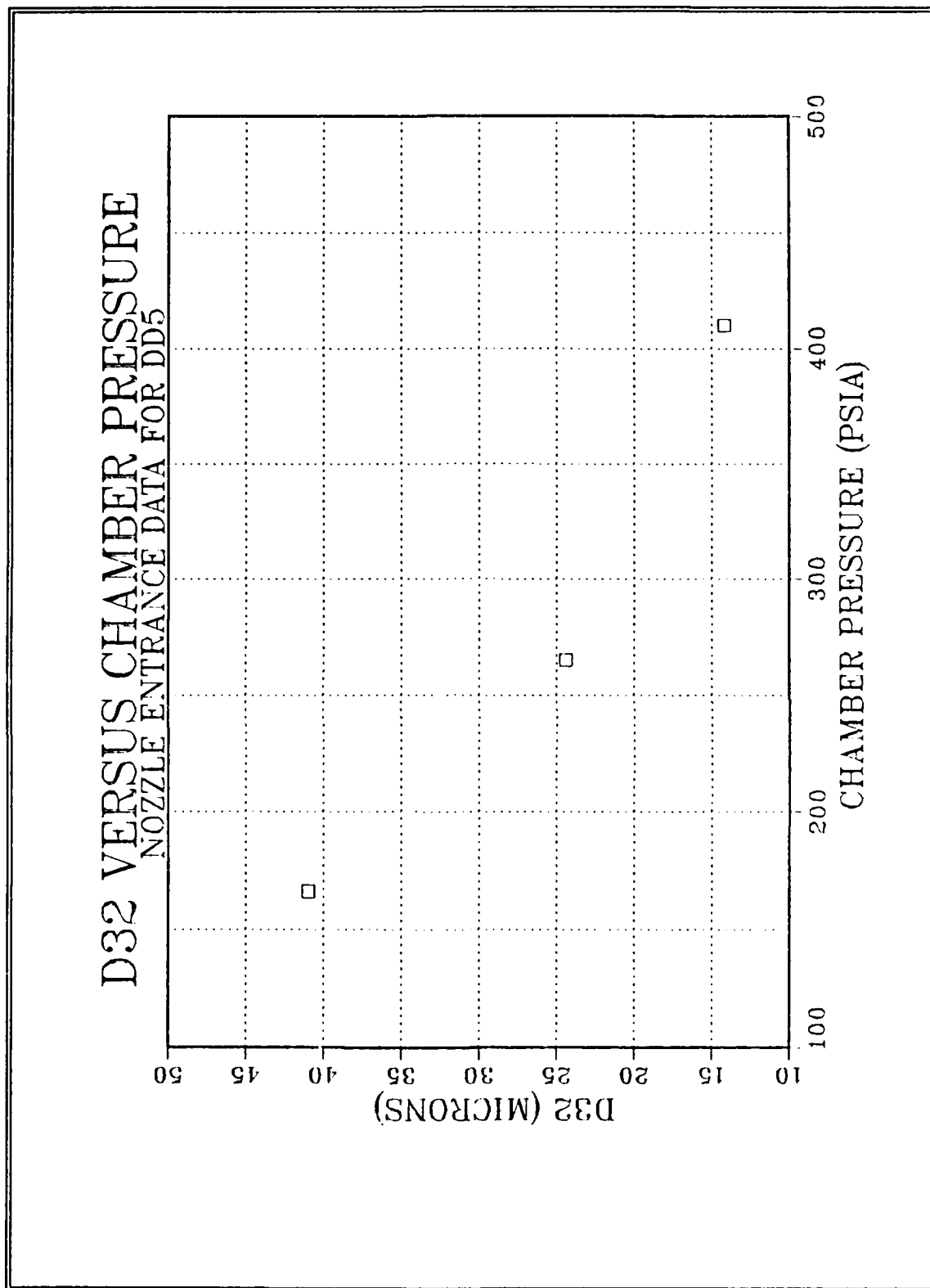


Figure IV.9. DD5 In-Motor D_{32} Versus P_c .

Figure IV.10. presents the volume distribution for the DD5 firing in which the data collection pressure was 166 psia. The main particle size band extended from 22 to 195 microns, with a dominant peak centered at 65 microns. Additionally, there was a significant mode from 2.3 to 4.1 microns with a peak at 3.2 microns. Figure IV.11. displays the volume distribution for the 265 psia DD5 run. The main particle size band was very similar to the 166 psia test firing results. The lower limit of the size band was 19 microns and the upper limit was 190 microns with a band peak at 65 microns. The lower size distribution mode was shifted to the left compared to the lower pressure data. This mode extended from 1.2 to 3.0 microns. Figure IV.12 is the volume distribution for the 410 psia firing. Unlike previous distributions, it was trimodal in nature. The upper two modes extended over the same range, 20 to 190 microns, as did the lower pressure size distributions, but there was an absence of particles in the 40 to 90 micron range. The lower mode was much more predominant, which was to be expected in the higher pressure test firings. This lower mode extended from 1.5 microns to 4.0 microns, with a dominate peak at 2.5 microns.

4. DD1 and DD5 Comparative Results

Figure IV.13. shows a comparison between the D_{32} results obtained from the DD1 and DD5 propellants as a function of motor chamber pressure. Both propellants

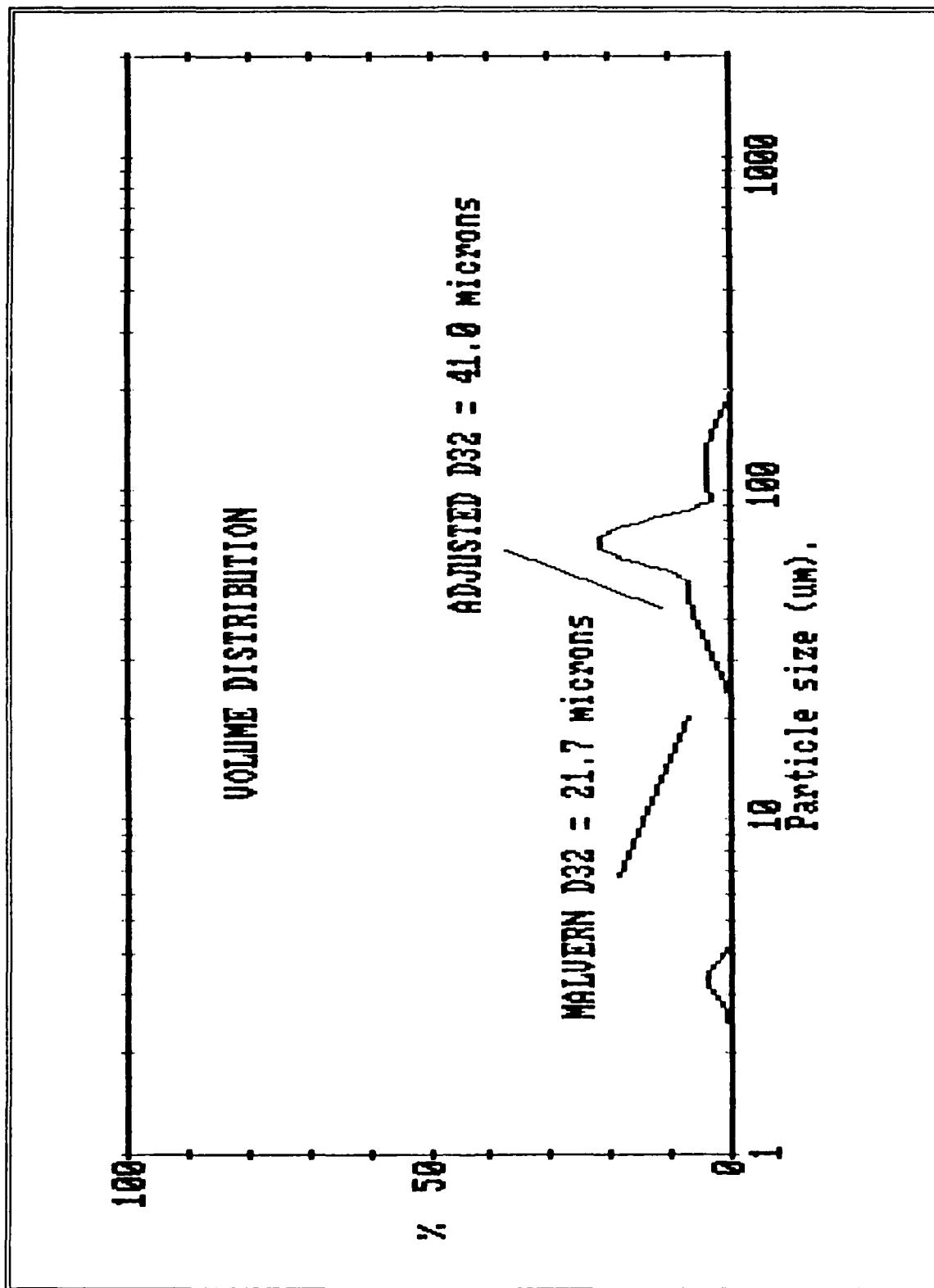


Figure IV.10. DD5 In-Motor Volume Distribution, $P_c = 166$ psia.

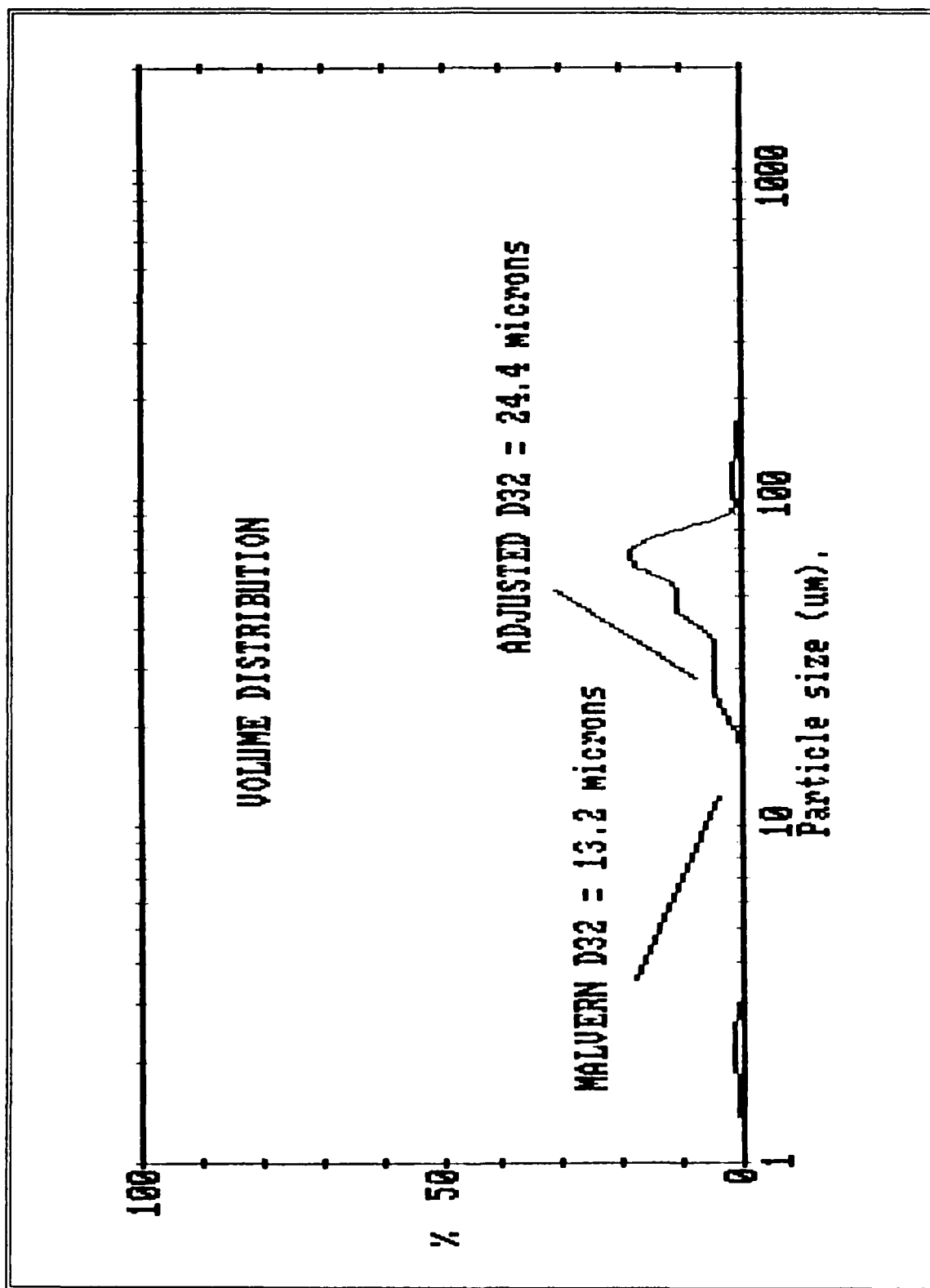


Figure IV.11. DD5 In-Motor Volume Distribution, $P_c = 265$ psia.

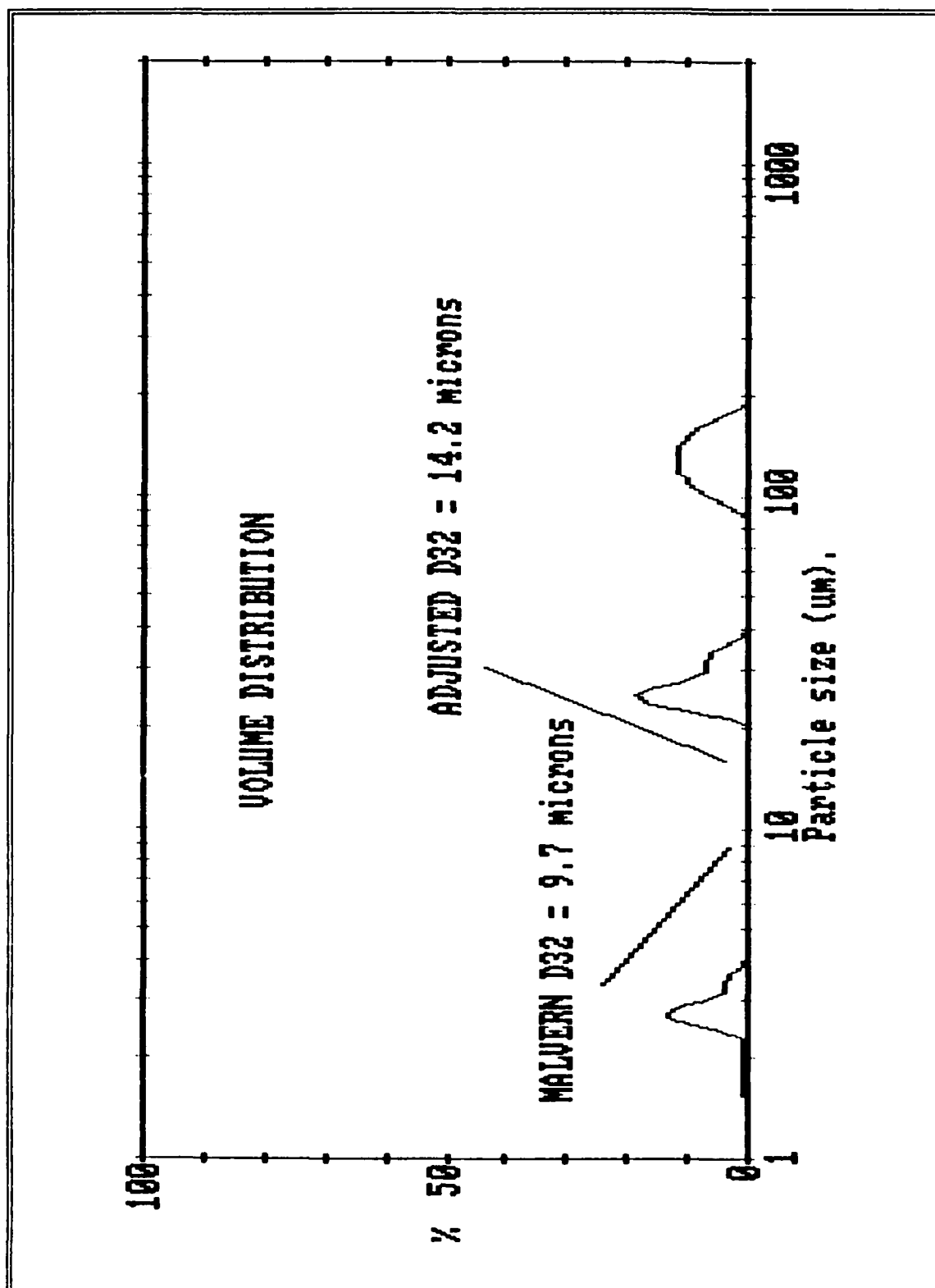


Figure IV.12. DD5 In-Motor Volume Distribution, $P_c = 410$ psia.

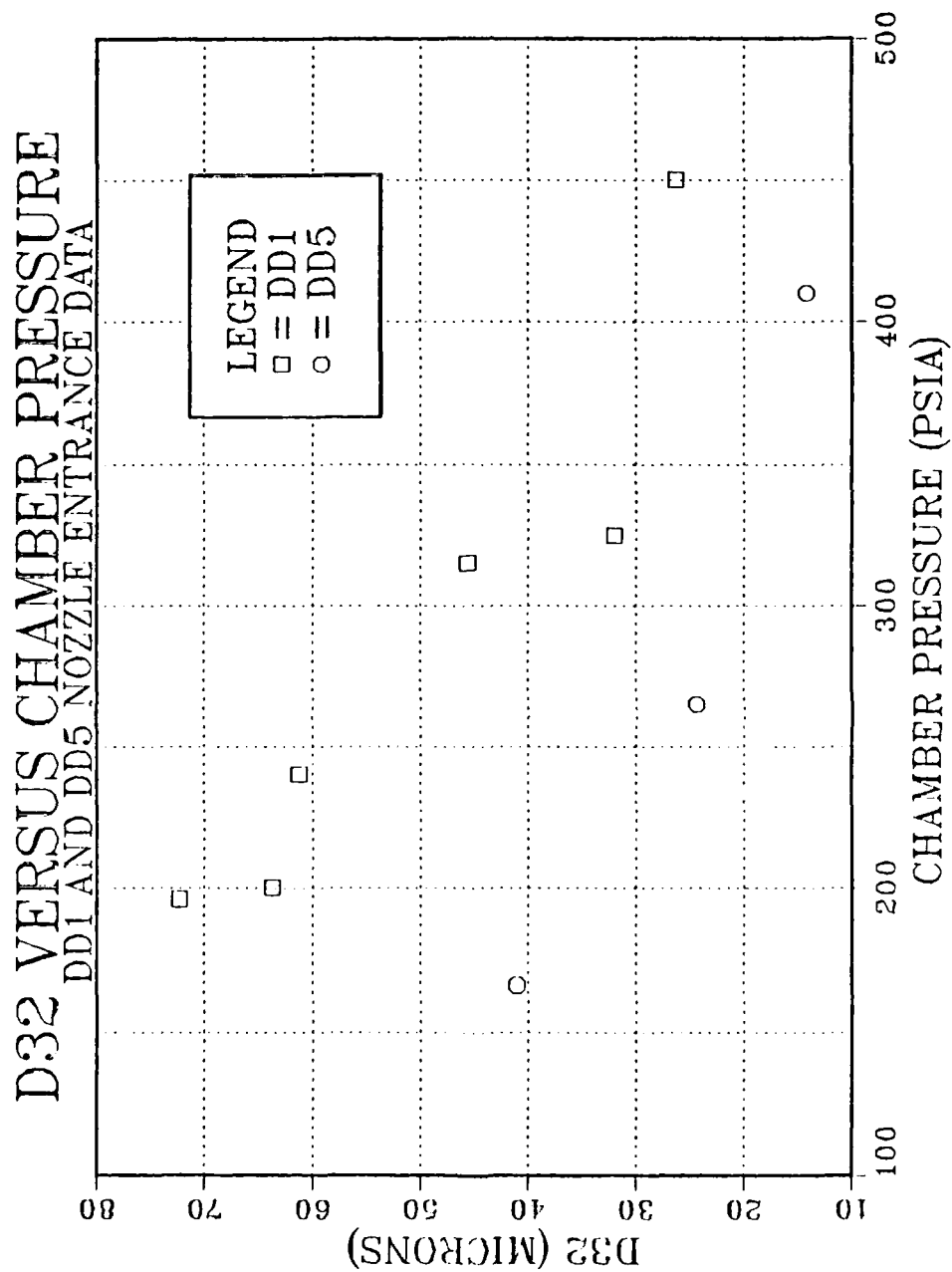


Figure IV.13. DD1 and DD5 In-Motor D_{32} Versus P_c .

displayed a decreasing D_{32} with increasing chamber pressure. The rate of size decrease with pressure was greater for the DD1 propellant. At a given pressure, D_{32} for the DD1 propellant was larger than for the DD5 propellant. Although not confirmed experimentally, it appears from Figure IV.13. that D_{32} for both propellants would have converged to approximately the same value, between ten and 20 microns, as the pressure increased above 500 psia.

The reason the DD1 propellant, which contained the lower amount of aluminum content, yielded a higher D_{32} at lower pressures could possibly be explained by comparison of the matrix structure of the two propellants. Examination of the propellant ingredient breakdown table presented in Chapter III as Table III.1., shows that the increased 20 micron aluminum content in DD5 was at the expense of the 200 micron AP particles and the 25 micron AP particles. Therefore, the DD1 propellant matrix structure was coarser than that of the DD5 propellant matrix. A coarser propellant matrix structure such as the DD1 propellant, would provide larger interstitial "pockets" for the molten aluminum to collect during the agglomeration process described in Chapter II. At the higher pressures the burning rates increase, the AP crystals have less protrusion above the surface, and surface agglomeration would decrease, resulting in similar D_{32} values for the two propellants.

D. MALVERN EXHAUST PLUME RESULTS

1. Test Conditions

Eight test firings were conducted in which the Malvern 2600c was used to collect particle size data in the exhaust plume. Half of the firings were made using the DD1 propellant and half with DD5 propellant. The ranges of motor chamber pressures covered by the DD1 and DD5 firings were 130 to 537 psia and 144 to 568 psia respectively. Use of the Gulder multiple scattering correction was not required since the obscuration values varied from 0.15 to 0.43. The location of the laser beam was kept constant for all of the test firings. The beam was positioned across the centerline of the motor with the most downstream portion of beam positioned at a distance of 0.75 inches from the exhaust nozzle exit plane.

Placement of the laser beam in the exhaust plume was a critical issue due to the nature of the exhaust nozzle design. Making an isentropic flow assumption, and using a gamma of 1.2, it was calculated that the design condition for the exhaust nozzle was for a chamber pressure of approximately 100 psia. Since all of the data of interest were for values above this design pressure, the exit gas from the exhaust nozzle was always in an underexpanded state. Depending upon the degree of underexpansion, it was expected that expansions and shocks would be present in the exhaust plume to return the flow pressure to atmospheric.

A five mwatt laser sheet was used in conjunction with a high speed video camera to detect the location of the expansions and shocks over the range of pressures for which data were desired. This was done with 6.5 inch slabs of DD1 propellant loaded in the rocket motor. The test firing revealed that the first visible shocks occurred at a chamber pressure of 250 psia at a distance of 0.78 inches aft of the exhaust nozzle exit plane. Shock locations were observed to move further aft to a distance of 1.13 inches as the maximum pressure of 1000 psia was approached.

Exhaust plume width was also studied in order to ensure the measurement location chosen for the laser beam would not be such that the laser passed through the boundary between the exhaust plume and the ambient air. This consideration was necessary in order to minimize as much as possible unwanted laser beam steering due to thermal and density gradients. It was determined that locating the downstream edge of the laser beam at a distance of 0.75 inches aft of the exhaust nozzle exit plane would serve this purpose. This position was found to be inside the location of significant shocks in addition to providing a plume width greater than the laser beam.

Despite taking the precautionary measures described above, beam steering was still found to be present. The Malvern software provides the "KILLDATA" command to deal with

this problem [Ref. 15]. Examination of raw data was made after each run in order to access which detection rings were significantly affected by beam steering. Generally, data from six or eight of the inner rings were required to be suppressed by the "KILLDATA" command in order to counter the beam steering effects. This suppression of data from the inner rings should not significantly affect the measured results since the expected particle sizes were small.

2. DD1 Results

Table IV.5. lists the exhaust plume D_{32} data obtained from the 2.0% loaded aluminum propellant test firings. These data points are plotted in Figure IV.14. Over the range of pressures tested, it can be seen that the tendency was for D_{32} to decrease with increasing pressure. However, the pressure dependency was slight, not nearly to the degree noted in the in-motor data.

TABLE IV.5. DD1 EXHAUST PLUME DATA.

P_C (psia)	OBSCURATION	MALVERN D_{32} (microns)	ADJUSTED D_{32} (microns)
130	0.1582	3.3	N/A
208	0.2216	2.7	N/A
337	0.2102	2.8	N/A
537	0.3682	2.0	N/A

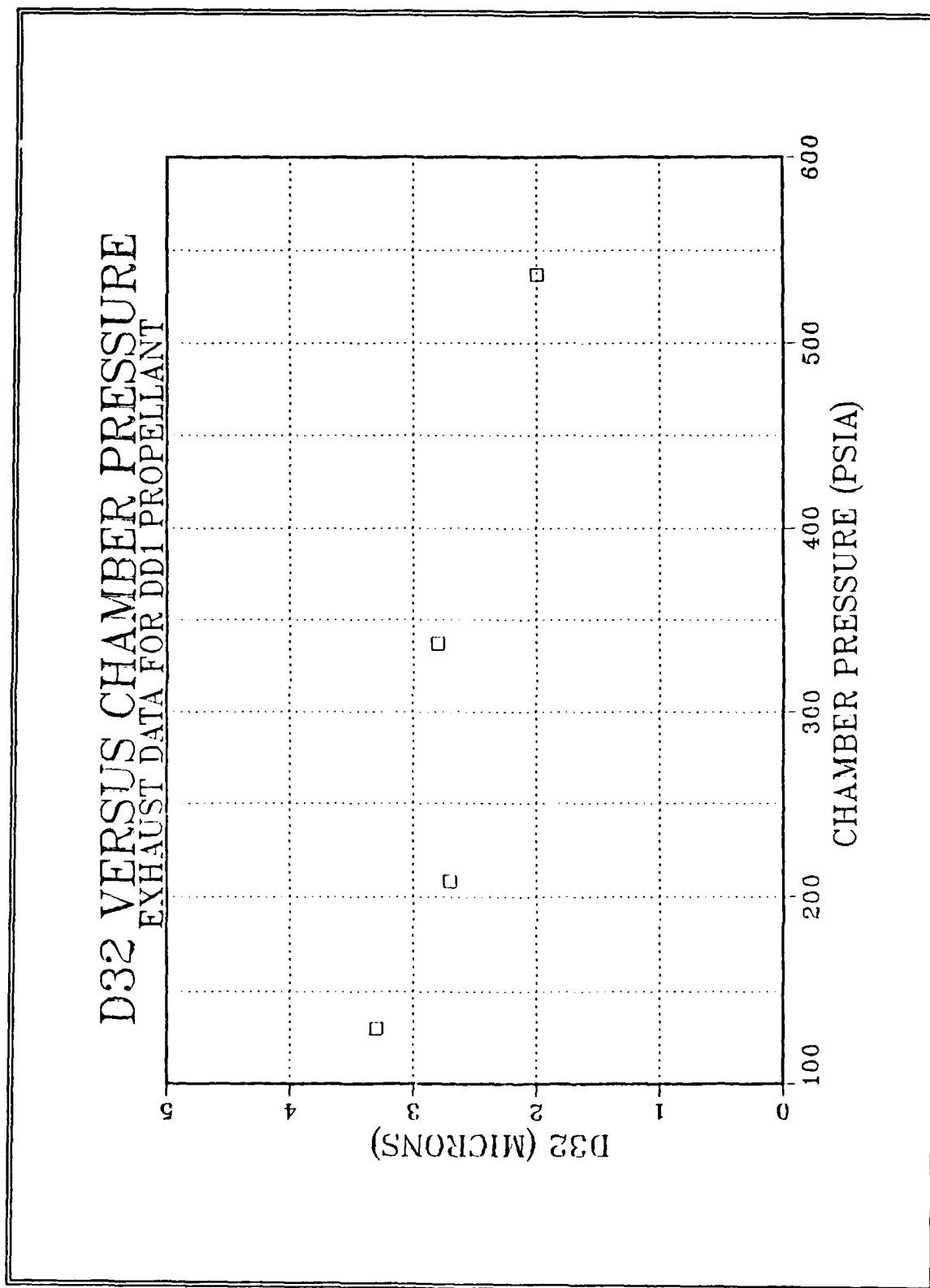


Figure IV.14. DD1 Exhaust Plume D_{32} Versus P_c .

Figure IV.15. shows the DD1 in-motor data and the DD1 exhaust data plotted together. The significant drop in D_{32} between the exhaust nozzle entrance and the exhaust plume supports the critical Weber number breakup theory [Ref. 11]. The low dependence of the exhaust plume D_{32} on chamber pressure was also found by Youngborg [Ref. 20] on tests using a zirconium carbide propellant.

Figures IV.16 through IV.19. are the volume distribution functions for the DD1 exhaust plume data. All distributions were multimodal. The dominant mode for the low pressure firings was centered at 24 microns. This mode gave way to the smaller diameter modes at higher pressures, thereby yielding smaller values of D_{32} .

Review of high speed video of the exhaust plume presented some questions as to the origin of the larger diameter particles. Due to the unsteady exhaust flow presented by the video, it was thought that there may be some biasing towards larger size particles due to slag shedding from the walls of the converging section of the exhaust nozzle. Post fire examination of the rocket exhaust nozzle entrance displayed evidence of slag buildup. It is thought that during the firing there was a slag buildup and shedding cycle, which would account for the observed unsteady flow.

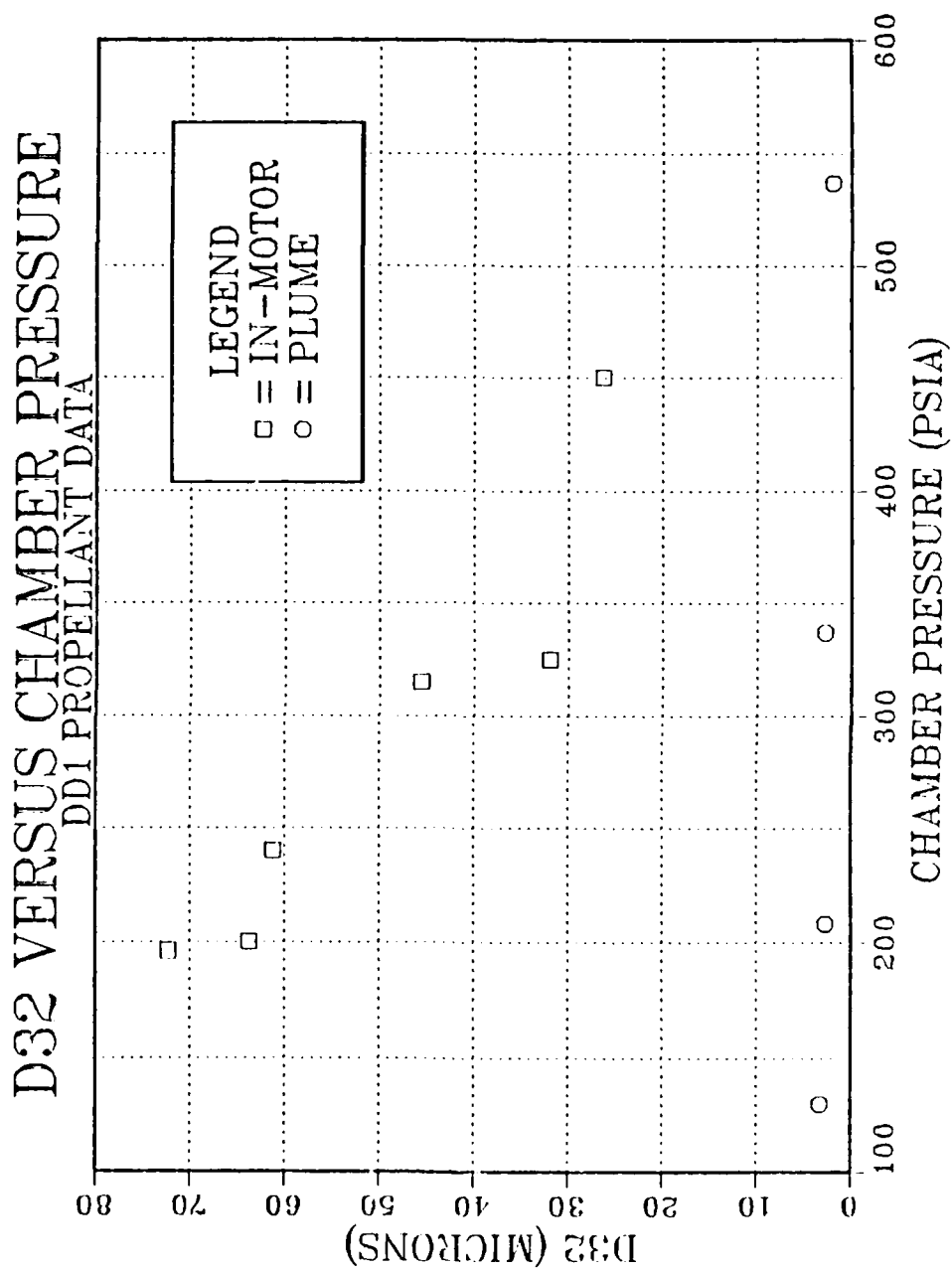


Figure IV.15. DD1 In-Motor and Exhaust Plume D_{32} Versus P_c .

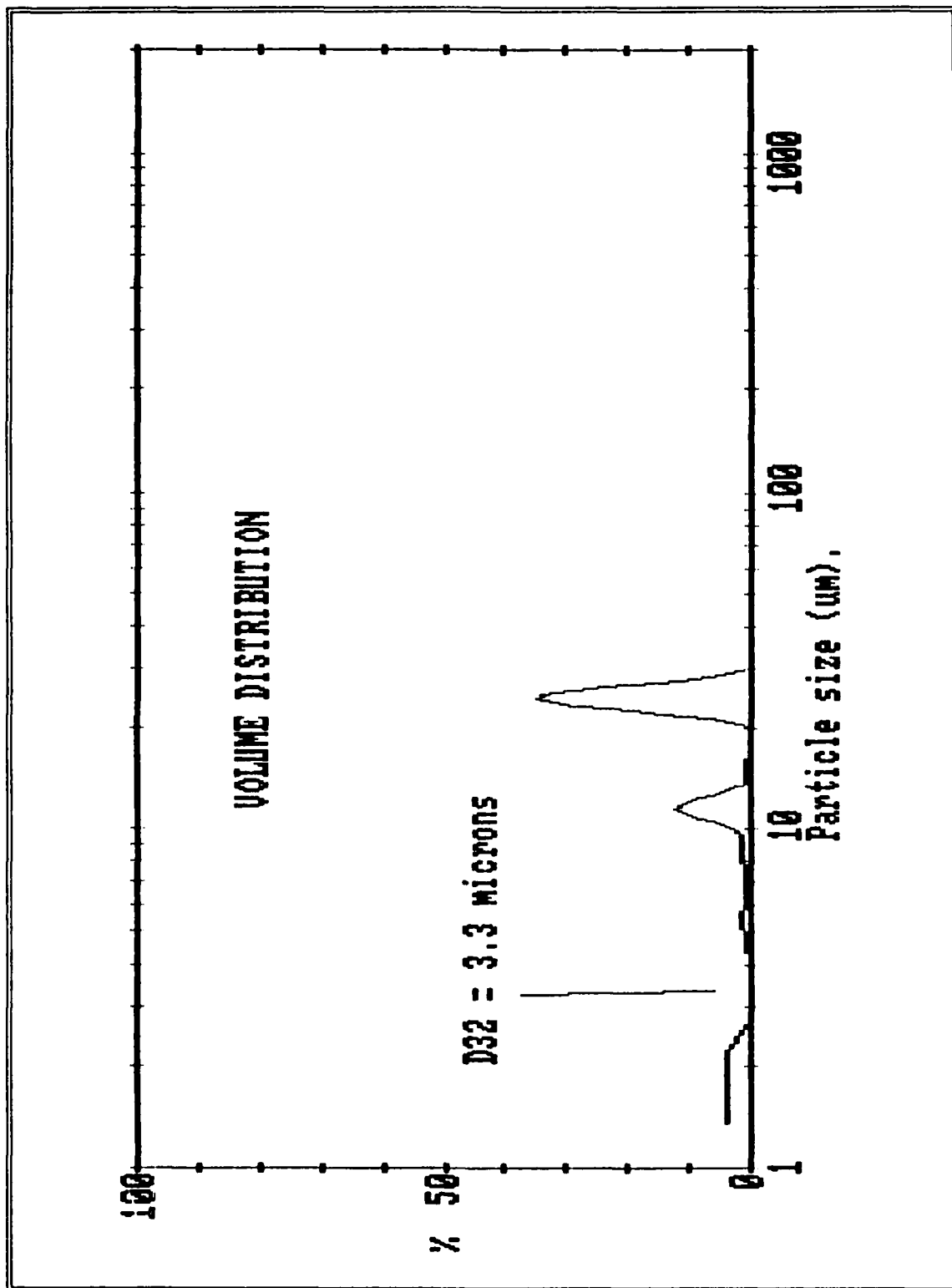


Figure IV.16. DD1 Exhaust Plume Volume Distribution, $P_c = 130$ psia.

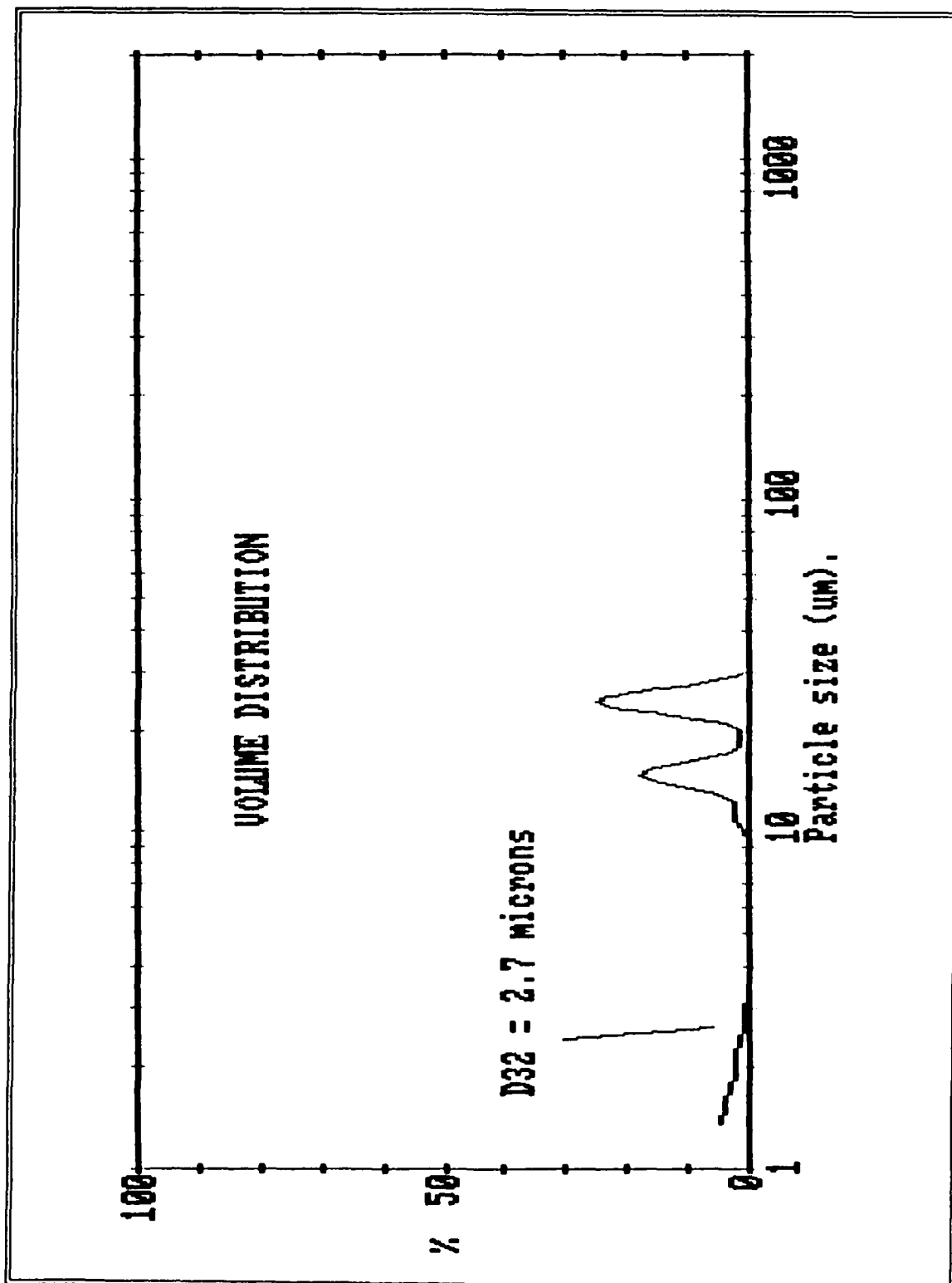


Figure IV.17. DD1 Exhaust Plume Volume Distribution, $P_c = 208$ psia.

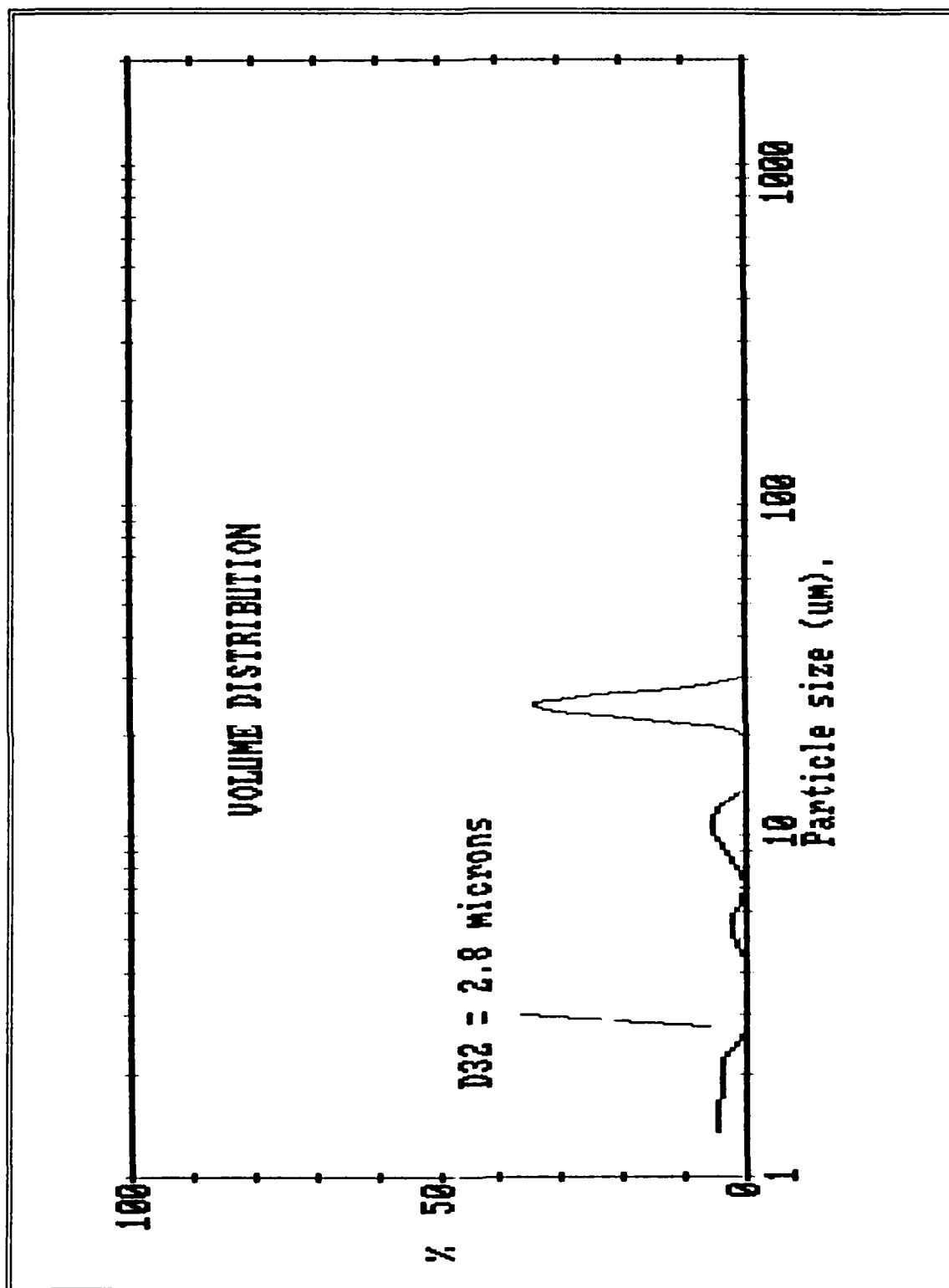


Figure IV.18. DD1 Exhaust Plume Volume Distribution, $P_c = 337$ psia.

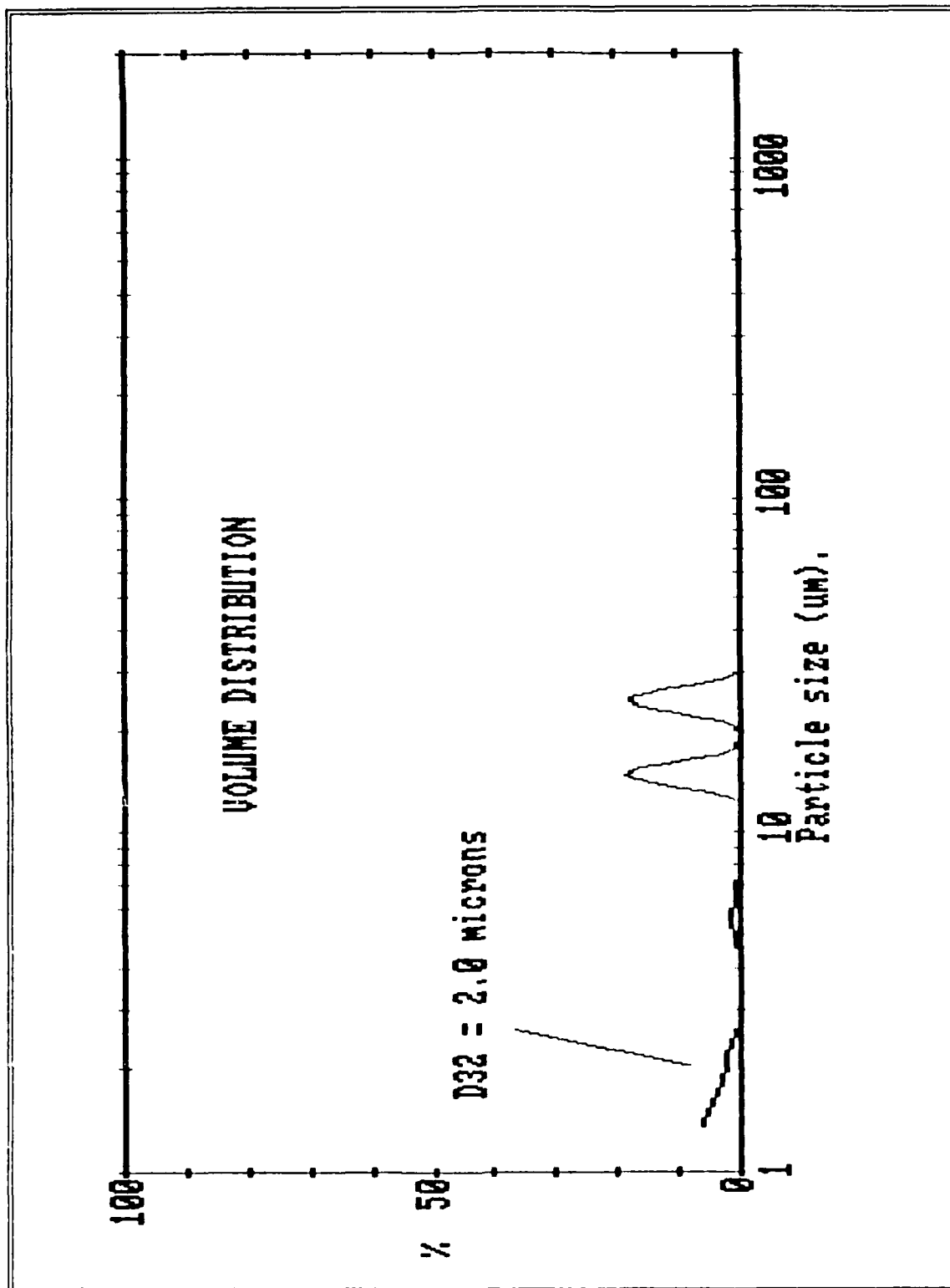


Figure IV.19. DD1 Exhaust Plume Volume Distribution, $P_c = 537$ psia.

In addition to large particle biasing due to slag shedding, it is felt that vignetting effects may have some large particle size parameter bias. However, it should be noted that the inability of the Malvern to detect particles below 0.5 microns would have limited impact on the D_{32} size parameter and even less impact on higher moment size parameters such as D_{43} .

3. DD5 Results

Table IV.6. lists the exhaust plume D_{32} data obtained from the 4.69% loaded aluminum propellant test firings. These data points are plotted along with the DD5 in-motor data points in Figure IV.20. Virtually no D_{32} pressure dependency was noted in the DD5 exhaust plume results. However, it should be noted that the lower limits of the Malvern 2600c measuring capability were approached. As with the DD1 data, particle breakup through the nozzle is supported.

Figures IV.21 through IV.24. are the volume distributions for the DD5 exhaust plume data. All of the distributions were multimodal, with the dominant modes centered at 16 microns and 25 microns. As the chamber pressure was increased, these higher modes became less significant as the lower modes in the region of 1.5 microns and 6.5 microns became more pronounced. As with the DD1 exhaust plume data, it was felt that slag shedding and

TABLE IV.6. DD5 EXHAUST PLUME DATA.

P_c (psia)	OBSCURATION	MALVERN D_{32} (microns)	ADJUSTED D_{32} (microns)
144	0.1486	1.8	N/A
232	0.3128	1.5	N/A
354	0.3608	1.7	N/A
568	0.4251	1.7	N/A

vignetting effects served to bias the size distribution data toward higher D_{32} values.

4. DD1 and DD5 Comparative Results

Figure IV.25. is a plot of the DD1 and DD5 exhaust data. Following the same trend as the in-motor results, D_{32} values for the DD5 propellant were less than for the DD1 propellant. However, the degree to which the DD1 values were larger was not as great. This, coupled with the fact that D_{32} for both propellants in the exhaust plume were much less dependent on chamber pressure, suggests that the size of the particles in the exhaust plume are only slightly dependent upon the size of the particles entering the exhaust nozzle.

E. AFAL PROBE DATA

Since the reason for using the probe was to provide a means to validate the Malvern 2600c exhaust plume data, motor pressure conditions of a previously successful test run were chosen to be repeated. The primary consideration for using

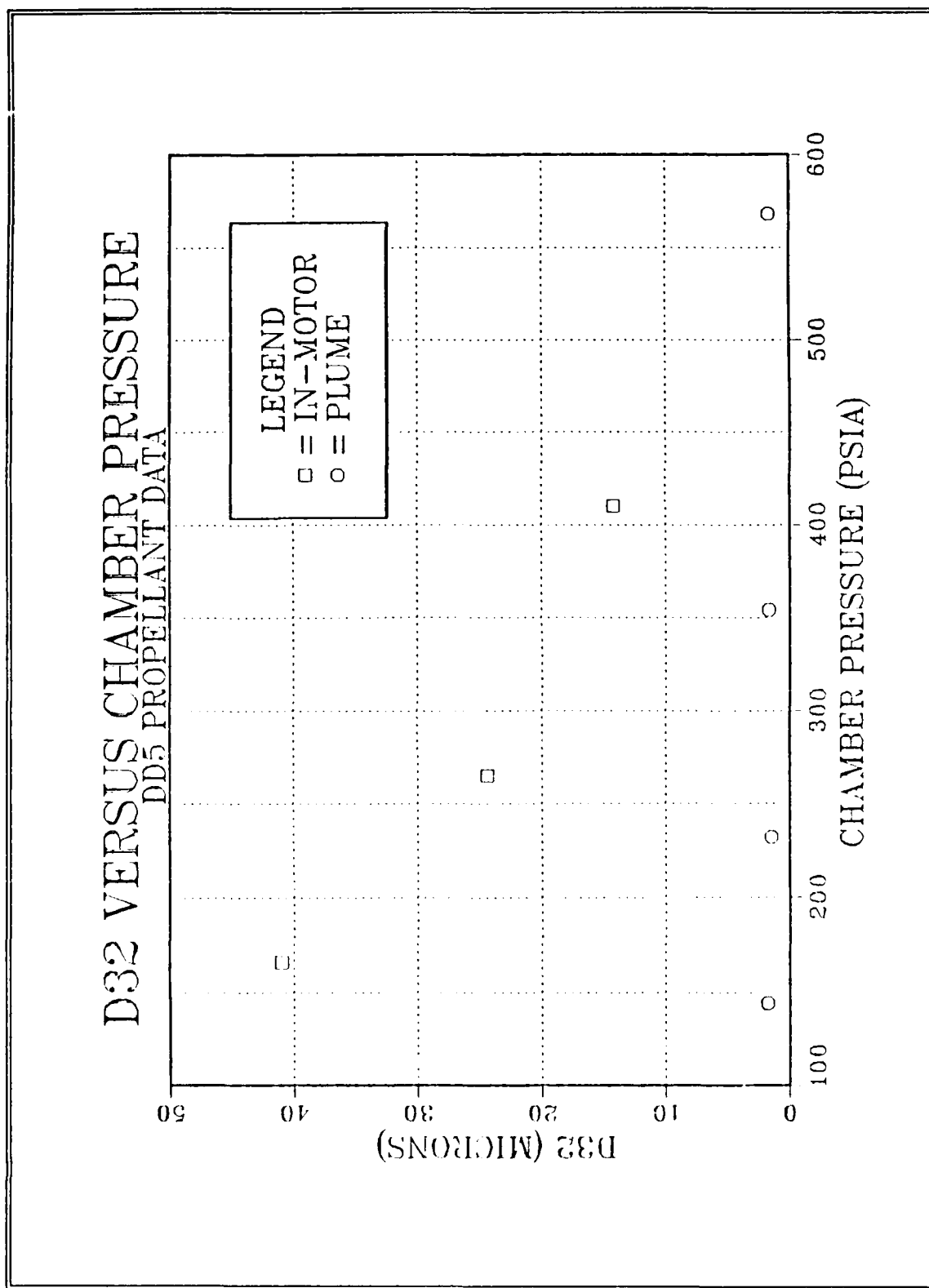


Figure IV.20. DD5 Exhaust Plume and In-Motor D_{32} Versus P_c .

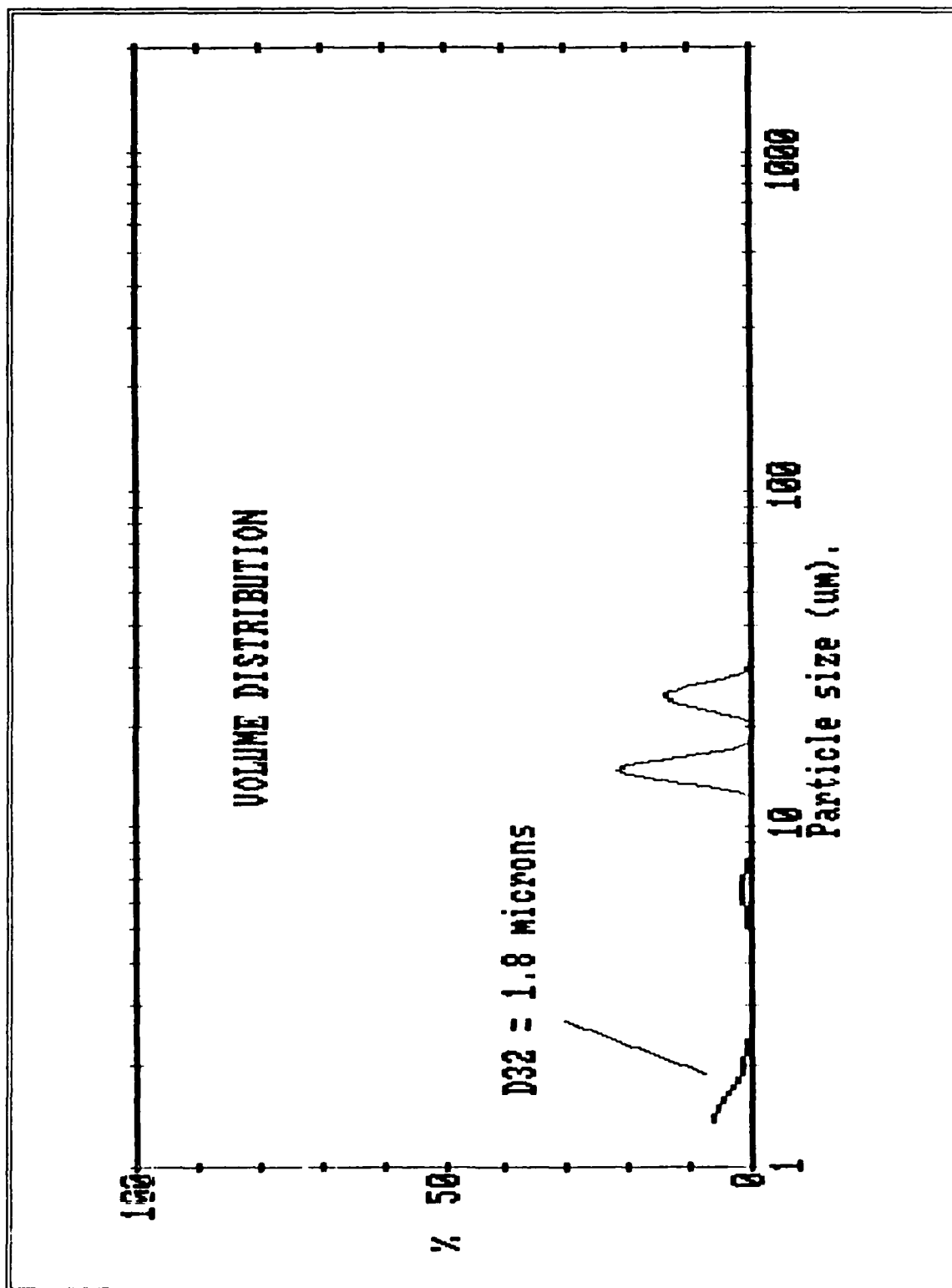


Figure IV.21. DD5 Exhaust Plume Volume Distribution, $P_c = 144$ psia.

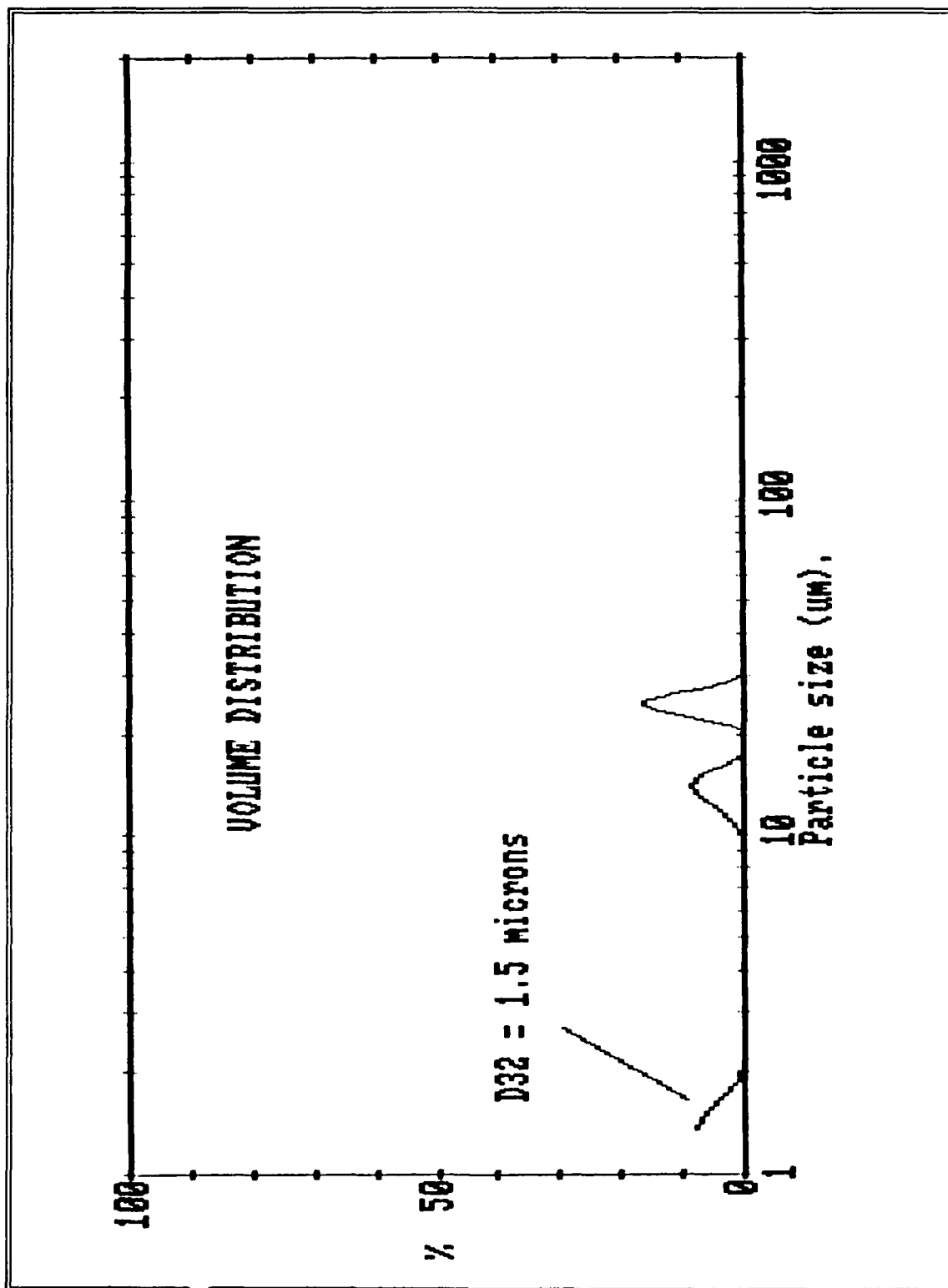


Figure IV.22. DD5 Exhaust Plume Volume Distribution, $P_c = 232$ psia.

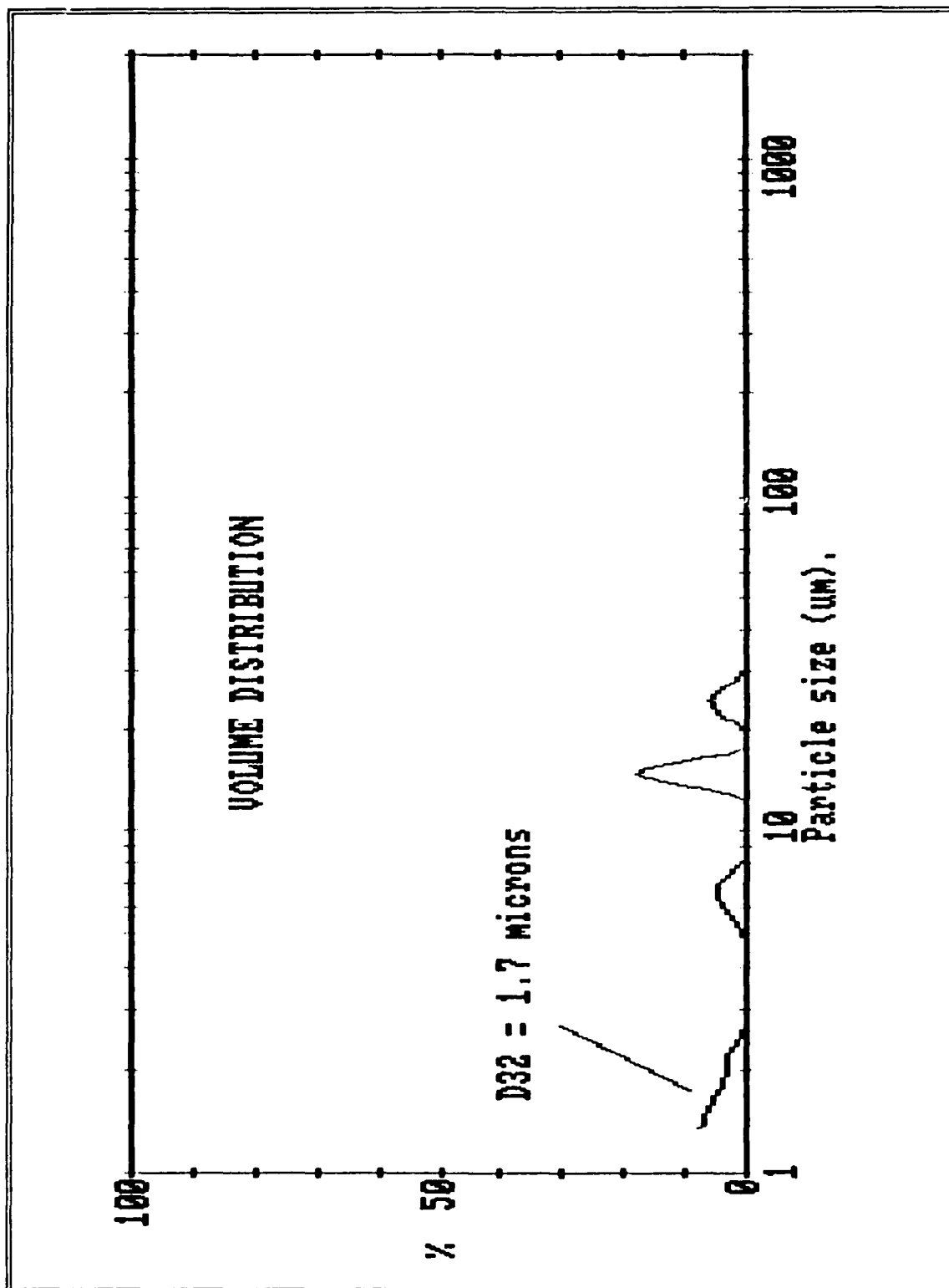


Figure IV.23. DD5 Exhaust Plume Volume Distribution, $P_c = 354$ psia.

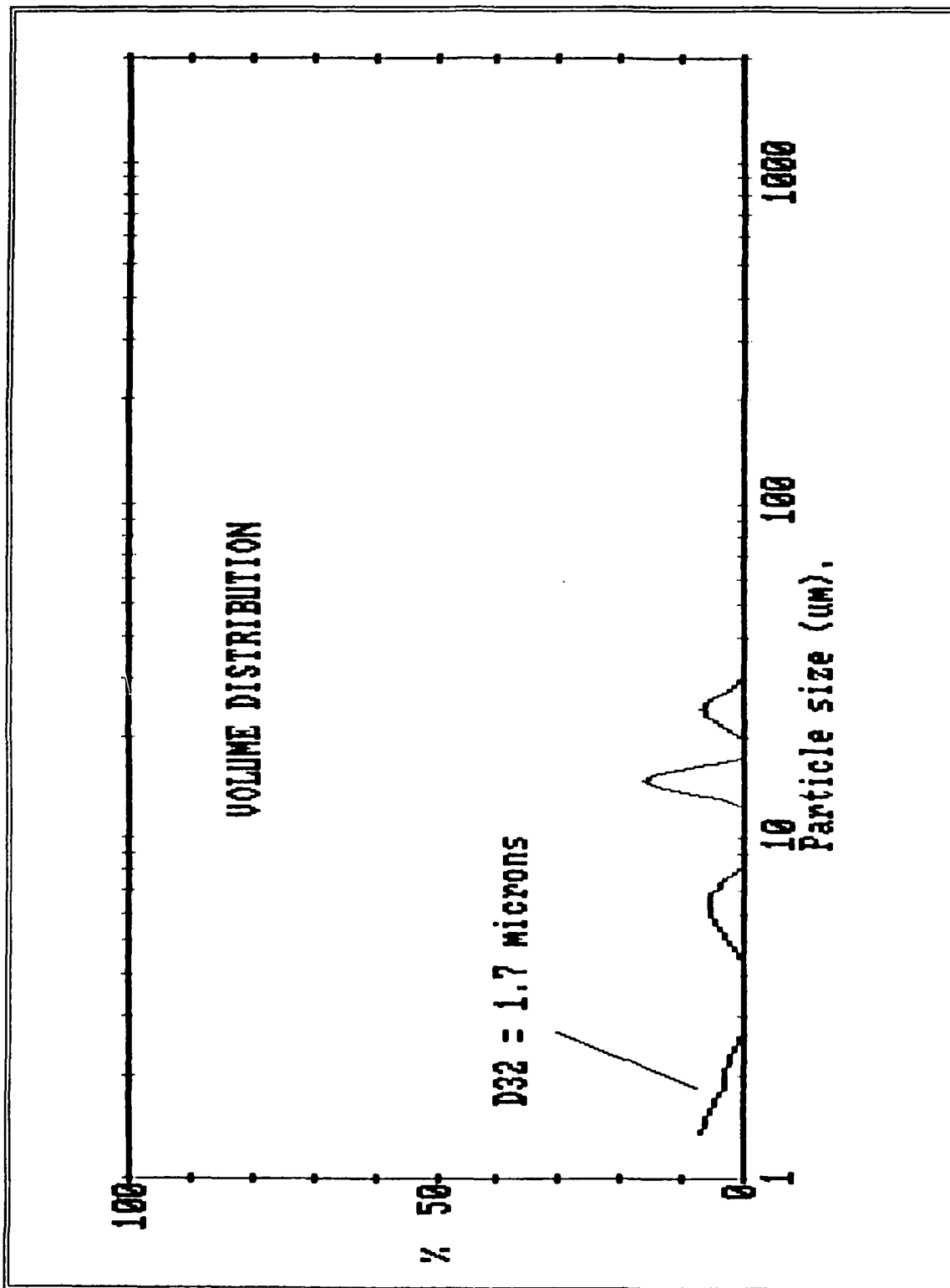


Figure IV.24. DD5 Exhaust Plume Volume Distribution, $P_c = 568$ psia.

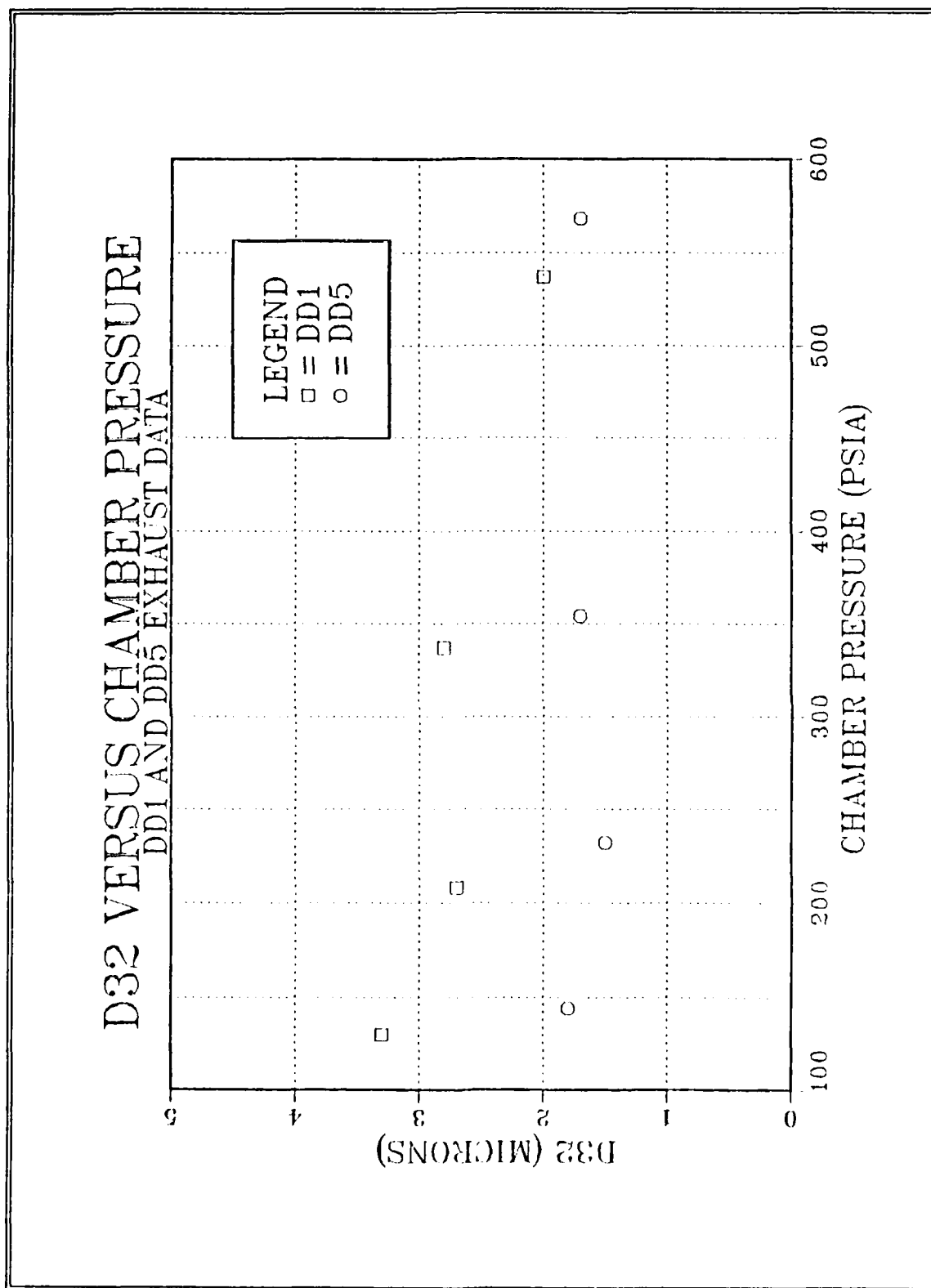


Figure IV.25. DD1 and DD5 Exhaust Plume D_{32} Versus P_c .

the probe was to ensure its design parameter of capturing one gram per second was met during the data collection period. The variables available to meet the probe design requirements were motor chamber pressure and positioning of the probe in the exhaust plume. Calculations based on mass flow rate from the motor exhaust nozzle exit indicated that over the pressure range of interest, the probe would have to be positioned downstream of the expansion shocks. Therefore, it was decided to choose a low pressure run, near the nozzle design condition, in order to eliminate the expansion shocks as a significant factor. Calculations for probe placement were based on a motor chamber pressure of 125 psia. At this pressure the calculated rocket motor mass flow rate was 13.0 grams per second. Based on the observed expansion of previous exhaust plumes, it was calculated that the probe should be positioned 1.64 inches aft of the exhaust nozzle exit plane.

A firing was conducted using two 4.125 inch slabs of DD1 propellant. The maximum chamber pressure during the burn was 147 psia and the average steady state burn pressure was 120 psia. The total burn time was 3.2 seconds.

SEM photographs were taken of representative sample areas from the particle collection filter paper. The filter paper was divided up into seven rings, with ring 0 being the center and rings 1 through 6 being concentric rings equally spaced from the center to the outside edge. Figures IV.26. and

IV.27. are representative SEM photographs of particles collected on the inner and outer rings. Particles greater than 0.5 microns in size were counted from photographs of each of the seven rings. Table IV.7. lists the results from counting 773 particles from the seven SEM photographs. Figure IV.28. is the volume distribution computed from the SEM data. The overall D_{32} , based on all of the counted particles being weighted equally, was computed to be 3.7 microns. When considering the rings individually, the D_{32} computed for each ring ranged from 2.6 microns to 4.4 microns. The average overall D_{32} by weighting the rings equally was 3.56 ± 0.70 microns. These results indicate very little variation in the size parameter values across the filter paper.

The D_{32} values computed by the SEM analysis above compare very favorably with the Malvern 2600c data. The most comparable Malvern DD1 test firing was for a chamber pressure of 130 psia, where the D_{32} was computed to be 3.3 microns. These results provide the initial validation of the Malvern 2600c as an accurate exhaust plume particle sizer. However, more comparison data will be needed to build a reasonable statistical confidence level in the Malvern validation.



Figure IV.26. SEM Photo of DD1 Exhaust Particles, Ring 0.

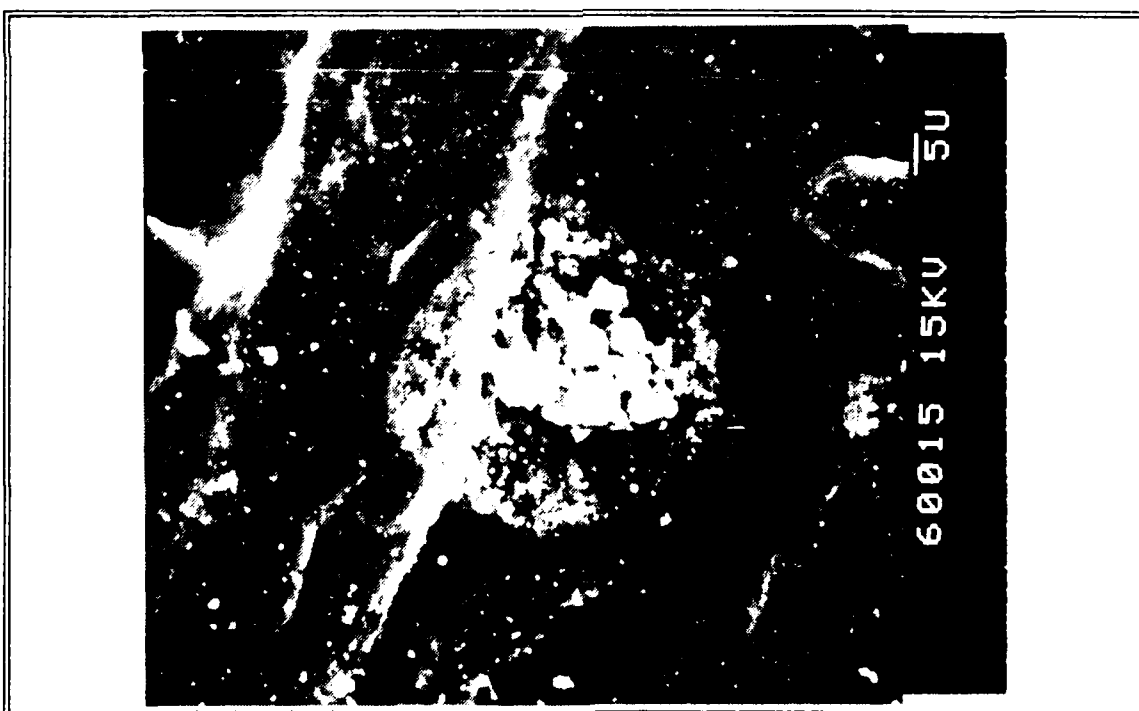


Figure IV.27. SEM Photo of DD1 Exhaust Particles, Ring 6.

TABLE IV.7. AFAL PROBE DD1 EXHAUST PLUME DATA.

DIAMETER (microns)	NUMBER	% NUMBER	% VOLUME
0.5 - 1.0	322	41.65	0.80
1.0 - 1.5	212	27.43	2.68
1.5 - 2.0	60	7.76	2.39
2.0 - 2.5	49	6.34	4.36
2.5 - 3.0	27	3.49	4.81
3.0 - 3.5	40	5.17	12.20
3.5 - 4.0	17	2.20	7.42
4.0 - 4.5	19	2.46	13.05
4.5 - 5.0	12	1.55	12.89
5.0 - 5.5	7	0.91	9.10
5.75	2	0.26	3.69
6.0	3	0.39	6.62
8.5	2	0.26	12.54
9.0	1	0.13	7.54

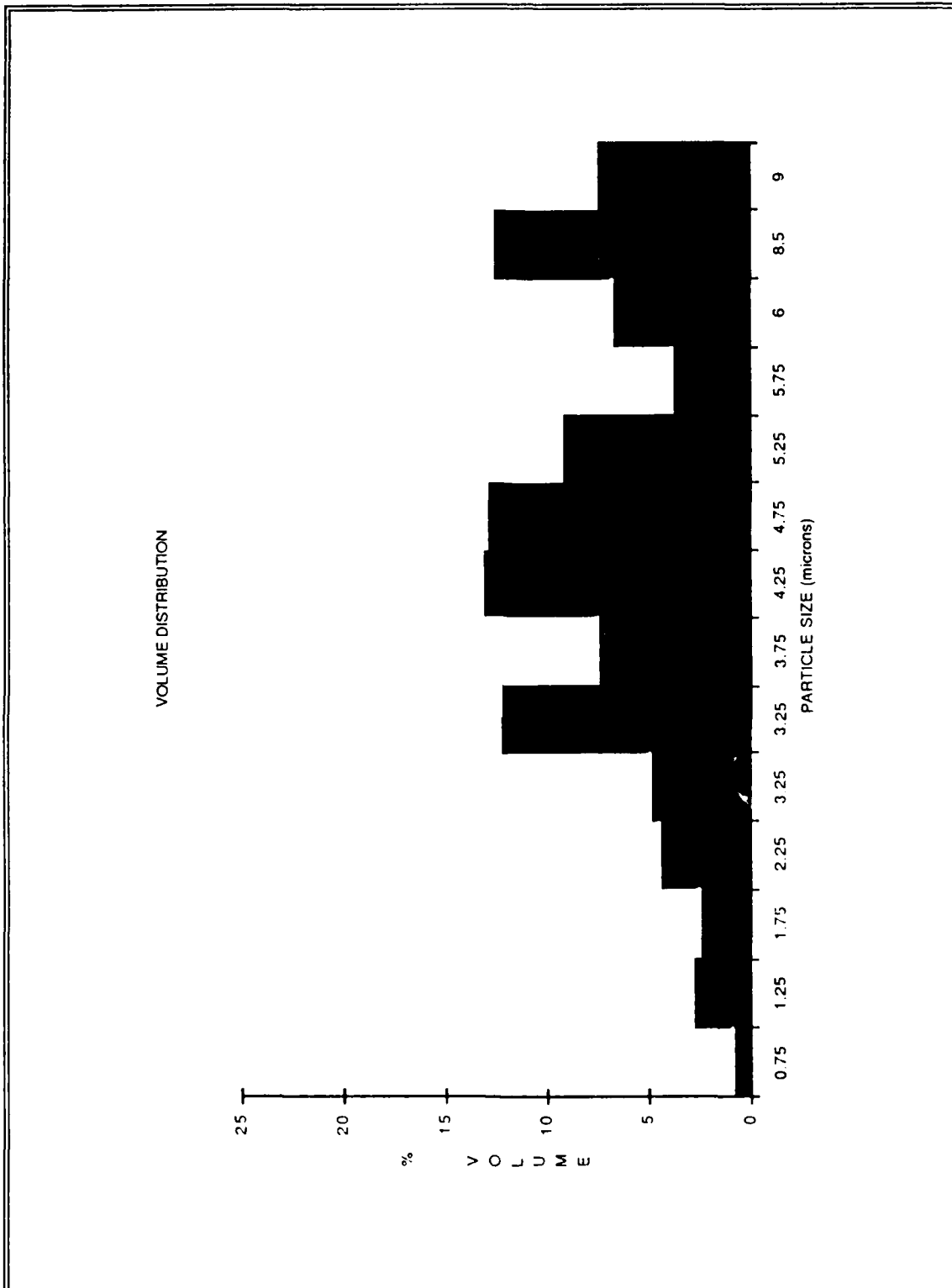


Figure IV.28. AFAL Probe DD1 Exhaust Plume Volume Distribution, $P_c = 120$ psia.

V. CONCLUSIONS AND RECOMMENDATIONS

The experimental results of this thesis investigation provide insight into the behavior of combustion particles in rocket motors loaded with low aluminum content GAP solid propellants. Successful particle size distribution measurements were made by laser light diffraction in the converging section of the motor exhaust nozzle and outside the motor in the exhaust plume. The specific conclusions which were made from the results obtained from the NPS 2-D solid rocket motor firings loaded with 2.0% and 4.69% aluminum content propellants are listed below:

- Particle sizes in the nozzle entrance decreased as surface ignition was enhanced by increased chamber pressures.
- At low pressures the coarser matrix of the 2.0% aluminum content propellant provided larger interstitial "pockets" which enhanced agglomeration more than did the 4.69% aluminum content propellant matrix.
- There was a large increase in quantities of small particles in the exhaust nozzle entrance at chamber pressures above 250 to 300 psia.
- The data indicated that surface agglomeration of aluminum particles will decrease to insignificant levels at chamber pressures above 600 psia.
- At high chamber pressures, where surface agglomeration is minimal, the data indicate that the D_{32} measured in the nozzle entrance should converge to a value between ten and 20 microns for both tested propellants.

- Exhaust plume D_{32} measurements of 1.7 to 3.3 microns, compared against exhaust nozzle entrance D_{32} results of 14.2 to 72.3 microns, support the critical Weber number particle breakup theory [Ref. 11].
- The size of the particles in the exhaust plume was only slightly dependent upon the size of the particles entering the exhaust nozzle.

The confidence in using the Malvern 2600c as a solid propellant rocket motor exhaust plume particle sizer was increased by a successful calibration of the Malvern using a calibration reticle and by favorable comparison with AFAL collection probe results. The calibration reticle provided a check of the Malvern's measurement capability of a sample with an obscuration level typically seen in the exhaust plume measurements. The AFAL collection probe provided D_{32} results that closely correlated to the Malvern results at low chamber pressure conditions. More comparison data should be gathered from higher chamber pressure rocket firings in order to further validate the Malvern 2600c as an accurate exhaust plume particle sizer. This will require that future exhaust nozzle designs have increased pressure expansion capability in the diverging section.

The multiple scattering corrections developed by Gulder [Ref. 19] appeared to be appropriate when applied to the in-motor Malvern D_{32} results. Further validation of the Malvern 2600c D_{32} measurements at high obscurations could be made by acquiring additional calibration reticles and placing them in series along the laser beam path.

Optimal usage of the Malvern 2600c was restricted by the Malvern system data sweep rate and the limited steady state burn period available when the 2-D motor was operated at high pressures. The slow sweep rate was due to processing time required by the Malvern version 3.0 software which was used. A planned near future upgrade of using Malvern version 6.1 software on an IBM-AT computer, modified with Intel 80386 and 80387 microprocessors, will help solve the data sweep restriction.

Overall, the NPS 2-D rocket motor provided an excellent test bed for this thesis investigation. However, encountered shortcomings in the rocket motor included: the propellant displayed progressive burning characteristics at high pressures, successful rocket firings were limited to chamber pressures under 600 psia, in-motor measurements caused high obscurations, and slag shedding was evident in the exhaust plume. The progressive burning problem could possibly be corrected by modification of the propellant slab geometry. Solving the chamber pressure limitation problem will involve either modifying the 732-RTV inhibitor curing procedures or by finding a more suitable inhibitor. The high obscurations and slag shedding problems could possibly be minimized by new nozzle insert designs.

Recommendations for future investigations using the 2-D motor include making measurements further downstream in the

converging section of the exhaust nozzle, at the point where particle breakup is expected to occur. Additionally, the present 2-D motor provides windowing available which could be used to collect particle distribution data near the surface of the propellant.

APPENDIX A

HP BASIC 5.1 DATA ACQUISITION CONTROLLING CODE

```

10 ***** MAL1: FOR 9836S *****
20 ***** TRIGGERS AND ACQUIRES DATA USING THE MALVERN *****
30 ***** DOUG HOVLAND 19 AUG 88 *****
40 ***** REVISION #01 19 OCT 88 *****
50 OPTION BASE 1
60 LOCAL LOCKOUT 7 ! DISABLES FRONT PANELS OF DATA ACQUISITION SYSTEM
70 REMOTE 709 ! COMPUTER CONTROLS THE VOLTMETER
80 OUTPUT 709;"AR" ! ANALOG RESET OPENS ALL CHANNELS
90 REMOTE 722 ! REMOTE IS A LISTEN COMMAND
100 OUTPUT 722;"HSM002S01D1L1Z0F1FL0R11STN.01STI13Q" ! PROGRAMS VOLTMETER
110 ! H homes the DVM (like RESET) SMO02 sets the service request mask to
120 ! tell the computer that a measurement was taken and is ready to be read.
130 ! page 3-20 of DVM MANUAL. S01 means that no reading will be taken until
140 ! the computer receives the one just made (page 3-26). D1 means DISPLAY ON.
150 ! L1 means load the following instructions. Z0 means AUTO ZERO OFF for
160 ! faster but less precise readings. F1 means DC VOLTS measurement.
170 ! FLO means FILTER OFF for faster readings. R1 is AUTO RANGING. 1STN means
180 ! 1 reading will be taken for each trigger. .01ST1---.01powerline cycles
190 ! will be the integration time. T3 is a single trigger. Q means END
200 PRINTER IS 1
210 OUTPUT 1
220 Cal=.002949
230 INPUT "THE PRESSURE CAL IS .002949, DO WISH TO CHANGE IT?(Y/N)",Pc$
240 IF Pc$="N" THEN GOTO 260
250 INPUT "ENTER THE REVISED PRESSURE CAL IN VOLTS/PSI :",Cal
260 PRINT USING "0" ! FORM FEED
270 PRINT "CHECK TO ENSURE THE PRINTER IS 'ON LINE'"
280 PRINT ""
290 INPUT "ENTER THE THRESHOLD PRESSURE TO TRIGGER THE DEVICES (psi)",Pt
300 INPUT "ENTER TIME DELAY FROM THRESHOLD PRESSURE (sec)",T8
310 ! TIMES ARE INTERPRETED BY THE COMPUTER IN SECONDS DOWN TO .001
320 OUTPUT 709;"AC20" ! CHANNEL FOR CHAMBER PRESSURE
330 WAIT .3 ! THIS WAIT IS TO LET VOLTAGES SETTLE DOWN
340 V1=0
350 CLEAR 722 ! THIS DOES NOT ALTER THE INSTRUCTIONS FOR THE VOLTMETER
360 ! IT CLEARS ANY NUMBERS IN THE DISPLAY OR OUTPUT REGISTERS
370 FOR I=1 TO 10
380 OUTPUT 722;"X1" ! TRIGGER VOLTMETER
390 GOSUB Reading ! READ VOLTMETER
400 V1=V1+V
410 NEXT I
420 V1=V1/10 ! THIS AVERAGES READINGS TO GET A ZERO PRESSURE VALUE
430 PRINT USING "40A,D.6D";"ZERO PRESSURE VOLTAGE IS ",V1
440 PRINT ""
450 PRINT "CHECK THE SET-UP IF THIS IS NOT WELL BELOW 0.0001 volts"
460 PRINT ""
470 V1=Pt*Cal ! PSI*VOLTS/PSI TARGET VOLTAGE OF PRESSURE TRANSDUCER
480 PRINT "DATA ACQUISITION BEGINS WHEN VOLTAGE EXCEEDS ",V1
490 PRINT USING "/" ! CARRIAGE RETURN AND A LINE FEED
500 PRINT "BE SURE NITROGEN PURGE IS ON."
510 PRINT "BE SURE VISICORDER IS SET UP TO RUN ON PROPER SCALE WITH LAMP ON."
520 PRINT USING "/"
530 DISP "STANDING BY FOR IGNITION. CHAMBER PRESSURE IS:"
540 PRINT "STANDING BY FOR IGNITION"
550 BEEP 2000,.1
560 OUTPUT 709;"AC20" ! CONNECT PRESSURE XUDUCER TO DVM
570 CLEAR 722
580 WAIT .3

```

```

590 OUTPUT 722;"X1"          ! TRIGGER VOLTMETER
600 GOSUB Reading
610 R9=ABS(V-Vz)             ! THIS IS VOLTAGE CORRESPONDING TO PRESSURE
620 Pz=R9/Cal
630 PRINT Pz
640 IF R9(V) THEN GOTO 590    ! IF PRESSURE IS BELOW THRESHOLD PRESSURE--REPEAT
650 T0=TIMEDATE
660 DISP ""
670 PRINTER IS 701
680 PRINT "TIME ", "PRESSURE"
690 T1=TIMEDATE
700 OUTPUT 722;"X1"
710 GOSUB Reading
720 Pd=ABS(V-Vz)/Cal
730 Tb=ROUND(T1-T0,4)
740 PRINT USING "DD.DD,DDDD.D";Tb,Pd
750 IF Tb(T8 THEN GOTO 690
760 OUTPUT 709;"DC11,5"      ! ACTIVATES THE MALVERN EXT TRIGGER (VOLTS = 5)
770 OUTPUT 709;"DC10,8"      ! SENDS A VOLTAGE SIGNAL TO THE IBM COMPUTER
780 REEP 2000,.1
790 OUTPUT 709;"AC20"
800 OUTPUT 722;"X1"          ! TRIGGERS THE VOLTMETER
810 GOSUB Reading
820 Pd=ABS(V-Vz)/Cal
830 T1=TIMEDATE
840 Tb=ROUND(T1-T0,4)
850 PRINT ""
860 PRINT USING "40A,DDDD.D";" THE DATA PRESSURE IS ",Pd
870 PRINT USING "40A,DD.DD";" BURN TIME (SEC) IS ",Tb
880 PRINT ""
890 PRINT "TIME ", "PRESSURE"
900 T1=TIMEDATE
910 OUTPUT 722;"X1"
920 GOSUB Reading
930 Tb=ROUND(T1-T0,4)
940 Pc=ABS(V-Vz)/Cal
950 PRINT USING "DD.DD,DDDD.D";Tb,Pc
960 IF Tb(5.0 THEN GOTO 900
970 OUTPUT 709;"DU11,5"
980 OUTPUT 709;"DU10,8"
990 PRINT " MALVERN RUN COMPLETED."
1000 PRINTER IS 1
1010 OUTPUT 1
1020 GOSUB End
1030 Reading: !
1040 ENTER 722;V             ! READS VOLTMETER
1050 RETURN
1060 End: END

```

APPENDIX B

2-D ROCKET MOTOR FIRING CHECKLIST

1. HP ACQDATA.....RUN (standing by for ignition)
2. ALARM.....ON
3. LABTECH NOTEBOOK.....GO
4. FCP POWER.....ON
5. PURGE.....ON
6. SHORT PLUG.....IN
7. MALVERN.....F10 (tri ext: mea sam) [enter]
8. REMOTE FIRE BUTTON.....IN
- *****POST IGNITION*****
9. FIRE SWITCH.....OFF
10. SHORT PLUG.....OUT
- *****POST RUN*****
11. PURGE.....OFF
12. FCP POWER.....OFF
13. ALARM.....OFF
14. LABTECH NOTEBOOK.....ANALYZE
15. MALVERN.....pri [enter]
16. MALVERN.....F9 (sav dat #__) [enter]
17. MALVERN.....F4 (tri int: mea bac) [enter]
18. MALVERN.....pri [enter]
19. MALVERN.....dis res: pri [enter]

20. LOTUS123.....COMPUTE ADJUSTED D32
21. MALVERN.....plot freq: art: pri [enter]
22. MOTOR IGN.....DISCONNECT
23. LASER.....OFF
24. SPRAY SYNC.....OFF
25. SIGNAL GEN.....OFF
26. NITROGEN.....CLOSE VALVES
27. HP COMPUTER.....SECURE
28. THREE POWER CBS.....SECURE
29. MALVERN.....end (enter)
30. IBM AT.....BACKUP DATA DISK
31. MOTOR.....DISASSEMBLE & CLEAN

APPENDIX C

2-D MOTOR FIRING SUMMARY

DATE (1988)	PROPELLANT TYPE	SLAB LENGTH (inches)	BURN TIME (sec)	Pc MAX (psia)	Pc DATA (psia)	MEASUREMENT LOCATION	D32 (microns)
28 APR	SW	4.000	7.2	111	111	IN-MOTOR	68.7
3 JUN	SW	9.000	3.9	330		**DIRTY WINDOWS**	
14 JUL	DD1	8.000	-	1000		**BURST DISK RUPTURE**	
20 JUL	DD1	3.000	3.1	320	315	IN-MOTOR	45.6
28 JUL	DD1	3.000	3.3	193		**EARLY TRIGGER**	
19 AUG	DD1	3.000	2.8	219	200	IN-MOTOR	63.7
6 OCT	DD1	5.250	3.0	258		**DIRTY WINDOWS**	
12 OCT	DD1	6.750	-	1000		**BURST DISK RUPTURE**	
14 OCT	DD1	3.500	2.5	240		**DIRTY WINDOWS**	
*19 OCT	DD1	5.375	1.8	389	325	IN-MOTOR	32.0
*21 OCT	DD1	6.500	1.7	563	450	IN-MOTOR	26.3
24 OCT	DD5	3.000	2.9	187	166	IN-MOTOR	41.0
*25 OCT	DD5	5.375	1.9	466	410	IN-MOTOR	14.2
*27 OCT	DD5	4.375	2.1	330	265	IN-MOTOR	24.4
28 OCT	DD1	4.375	2.3	310	240	IN-MOTOR	61.2
31 OCT	DD1	3.938	2.7	299	196	IN-MOTOR	72.3
1 NOV	DD5	5.375	1.5	557		**EXCESSIVE SWEEP PERIOD**	

2-D MOTOR FIRING SUMMARY

DATE (1988)	PROPELLANT TYPE	SLAB LENGTH (inches)	BURN TIME (sec)	Pc MAX (psia)	Pc DATA (psia)	MEASUREMENT LOCATION	D32 (microns)
3 NOV	DD5	6.500	-	1000	**BURST DISK RUPTURE**		
5 NOV	DD1	8.250	-	1000	**BURST DISK RUPTURE**		
7 NOV	DD1	7.000	-	1000	**BURST DISK RUPTURE**		
9 NOV	DD5	5.375	1.7	537.0	**EXCESSIVE SWEEP PERIOD**		
10 NOV	DD1	6.500	-	1000	**EXHAUST PLUME VIDEO DATA**		
11 NOV	DD1	4.160	2.8	230	**EXHAUST PLUME VIDEO DATA**		
14 NOV	DD1	4.160	2.9	137	130	EXHAUST	3.3
15 NOV	DD1	6.000	2.3	396	337	EXHAUST	2.8
16 NOV	DD1	5.000	2.5	221	**NO DATA TRIGGER SIGNAL**		
17 NOV	DD1	5.000	2.5	215	208	EXHAUST	2.7
18 NOV	DD1	7.000	1.8	564	537	EXHAUST	2.0
18 NOV	DD5	4.000	3.0	157	144	EXHAUST	1.8
19 NOV	DD5	7.000	1.8	670	568	EXHAUST	1.7
19 NOV	DD5	5.000	2.0	238	232	EXHAUST	1.5
20 NOV	DD5	5.500	1.9	383	354	EXHAUST	1.7
21 NOV	DD1	4.125	3.4	147	120	EXHAUST	3.7

APPENDIX D

CALIBRATION RETICLE FINAL DATA SHEET

CALIBRATION RETICLE : RR-50-3.0-0.08-102-CF - #203

FINAL DATA SHEET

EFFECTIVE SIZE DISTRIBUTION FOR GAUSSIAN BEAM W = 4.50 MM

	DIAMETER (UM) #	NUMBER	AREA FRACTION	VOLUME FRACTION	CUM VOL FRACTION	DVOL/DD (1/UM)
1	5.33	2904.7	0.015	0.002	1.000	0.0013
2	6.81	783.7	0.006	0.001	0.998	0.0005
3	8.85	892.9	0.012	0.003	0.997	0.0011
4	11.56	1168.6	0.028	0.008	0.994	0.0018
5	17.47	1007.7	0.054	0.024	0.986	0.0049
6	21.38	642.9	0.032	0.028	0.967	0.0087
7	23.91	447.2	0.045	0.027	0.935	0.0097
8	26.87	510.3	0.065	0.043	0.908	0.0126
9	30.75	397.6	0.067	0.051	0.865	0.0140
10	34.13	278.0	0.057	0.048	0.814	0.0152
11	37.14	313.1	0.076	0.070	0.766	0.0217
12	40.62	232.9	0.068	0.063	0.695	0.0244
13	42.78	225.7	0.073	0.078	0.627	0.0227
14	47.40	172.7	0.069	0.081	0.550	0.0213
15	50.41	106.7	0.048	0.060	0.469	0.0240
16	52.41	114.3	0.056	0.072	0.409	0.0239
17	56.42	98.3	0.055	0.077	0.337	0.0182
18	60.89	85.4	0.056	0.085	0.259	0.0157
19	67.17	64.6	0.052	0.086	0.175	0.0136
20	73.48	25.7	0.025	0.045	0.089	0.0066
21	80.73	12.4	0.014	0.029	0.044	0.0041
22	87.34	4.2	0.005	0.012	0.016	0.0020
23	92.78	1.0	0.001	0.003	0.003	0.0006
TOTAL		10490.7	1.000	1.000		

BEST FIT RR PARAMETERS XBAR = 53.0 UM N = 3.17

D10 = 17.96 D20 = 23.21 D21 = 30.00 UM

D30 = 27.91 D31 = 34.79 D32 = 40.23 UM

* DIAMETERS TRACEABLE TO NBS FORT #52577,
ACCURATE TO +/- 2UM (1/- 3% FOR D > 70 UM)

LIST OF REFERENCES

1. Derr, R.L., Mathes, H.B., and Crump, J.E., "Application of Combustion Instability of Solid Propellant Rocket Motor Problems," AGARD Conference Proceedings No. 259, April 1979.
2. Netzer, D.W., "Tactical Missile Propulsion--Design and Applications," Unpublished Course Notes, Naval Postgraduate School, 1988.
3. Edwards, T.D., et al., Measurements of Particulates in Solid Propellant Rocket Motors, AFAL TR-87-029, Air Force Astronautics Laboratory, Edwards AFB, October 1987.
4. Walker, J.D., Holographic Investigation of Metalized Solid Propellant Combustion in Two Dimensional and Three Dimensional Rocket Motors, Master's Thesis, Naval Postgraduate School, Monterey, California, September 1987.
5. Pruitt, T.E., Measurement of Particle Size Distribution in a Solid Propellant Rocket Motor Using Light Scattering, Master's Thesis, Naval Postgraduate School, Monterey, California, June 1987.
6. Misener, J.A., and Kessel, P.A., "Current AFRPL Measurements and Characterization of Particulates in Solid Rocket Motor Plumes," 15th JANNAF Plume Technology Meeting, CPIA Publication 426, May 1985.
7. Gany, A., and Caveny, L.H., "Agglomeration and Ignition Mechanism of Aluminum Particles in Solid Propellants," Volume of the 17th Symposium (International) on Combustion, The Combustion Institute, 1978.
8. Price, E.W., "Combustion of Metalized Propellants," Progress in Astronautics and Aeronautics, v. 90, pp. 479-505, 1984.
9. Price, E.W., "Combustion of Aluminum in Solid Propellant Flames," AGARD Conference Proceedings No. 259, April 1979.
10. NASA SP-8064, Solid Propellant Selection and Characterization, June 1971.
11. Ganey, A., and Caveny, L.H., "Breakup of Al/Al₂O₃ Agglomerates in Accelerating Flow Fields," 17th Aerospace Sciences Meeting, January 15-17, 1979.

12. Jones, A.R., "Error Contour Charts Relevant to Particle Sizing by Forward-Scattered Lobe Measurements," Letter to the Editor, Journal of Physics, D: Applied Physics, v. 10, 1977.
13. Koo, J.H., and Hirleman, E.D., Comparative Study of Laser Diffraction Analysis Using Integral Transform Techniques: Factors Affecting the Reconstruction of Droplet Size Distributions, Arizona State University Laser Diagnostics Laboratory Paper No. 86-18, Joint Meeting of Canadian and Western State Sections of The Combustion Institute, April 28-30, 1986.
14. Malvern Instruments Inc., "Definition of Particle Size," unpublished notes.
15. 2600 Particle Sizer User's Manual, Spring Lane, MALVERN, Worcestershire, WR141AQ, England, Manual Version 2.1, 30 September 1985.
16. Hirleman, E.D., On-Line Calibration Technique for Laser Diffraction Droplet Sizing Investments, ASME 83-GT-232.
17. Harris, R.K., An Apparatus for Sizing Particulate Matter in Solid Rocket Motors, Master's Thesis, Naval Postgraduate School, Monterey, California, June 1984.
18. Calibration Standard Reticles for Particle Sizing Instruments, Laser Electro-Optics Limited Product Description, January 1984.
19. Gulder, O., Multiple Scattering Effects in Drop Sizing of Dense Fuel Sprays by Laser Diffraction, PEP Paper 70-7, AGARD 70th Symposium of the Propulsion and Energetics Panel on Combustion and Fuels in Gas Turbine Engines, October 1987.
20. Youngborg, E.D., Application of Laser Diffraction Techniques to Particle Sizing in Solid Propellant Rocket Motors, Master's Thesis, Naval Postgraduate School, Monterey, California, December 1987.

INITIAL DISTRIBUTION LIST

	No. Copies
1. Defense Technical Information Center Cameron Station Alexandria, Virginia 22304-6145	2
2. Library, Code 0142 Naval Postgraduate School Monterey, California 93943-5002	2
3. Department Chairman, Code 67 Department of Aeronautics and Astronautics Naval Postgraduate School Monterey, California 93943-5004	1
4. Professor D. W. Netzer, Code 67Nt Department of Aeronautics and Astronautics Naval Postgraduate School Monterey, California 93943-5004	2
5. Professor R. Howard, Code 67Ho Department of Aeronautics and Astronautics Naval Postgraduate School Monterey, California 93943-5004	1
6. LCDR D. L. Hovland 4676 Marjorie Drive Murrysville, Pennsylvania 15668	2